Novel approaches to the calculation of the electronic structure and dynamics of excited states : application to trans-di-imide and ethylene

Novel Approaches to the Calculation of the Electronic Structure and Dynamics of Excited States

Application to *Trans*-di-imide and Ethylene

G.C. Groenenboom

Novel Approaches to the Calculation of the Electronic Structure and Dynamics of Excited States

Application to *Trans*-di-imide and Ethylene

Proefschrift

ter verkrijging van de graad van doctor aan de Technische Universiteit Eindhoven, op gezag van de Rector Magnificus, prof. dr. J.H. van Lint, voor een commissie aangewezen door het College van Dekanen in het openbaar te verdedigen op vrijdag 15 maart 1991 om 16.00 uur

door

Gerrit Cornelis Groenenboom

Geboren te Leeuwarden

druk: wibro dissertatiedrukkerij, helmond.

Dit proefschrift is goedgekeurd door de promotoren:

prof. dr. R. A. van Santen
en
prof. dr. ir. A. van der Avoird

Copromotor: dr. J. H. van Lenthe

Aan mijn broer

Contents

Chapter 1

Introduction

A common statement among theorists is "we do not merely want to reproduce experimental data". However, that will be the main purpose of this thesis. When it comes to calculating energy differences to "chemical accuracy" (about 1 kcal/mol), a recent review article of Bauschlicher *et al.* [1] gives a good impression of the state of the art: most of the systems considered are two- or three-atom molecules with up to about 14 electrons (e.g., CH_2 and N_2). For this kind of systems the essentially exact so-called "full Configuration Interaction" (FCI) calculations have recently become possible (see references in [1]). This thesis will focus on methods that are applicable to slightly more complicated systems: excited states of polyatomic molecules of a size that prohibits the FCI approach.

The idea of this work originates from previous work on photochemical *cis-trans* isomerization of small polyenes [2]. Upon electronic excitation, a double bond may start twisting. The system can return to the electronic ground state *via* emission of a photon or radiationless, *via* nonadiabatic interactions. If the intramolecular vibrational relaxation is slow, the molecule can be expected to perform several internal rotations and end up in the *cis-* or the *trans*-conformation with 50% probability, regardless of the initial conformation. If, however, the vibrational relaxation is fast one can expect a *cis-trans* isomerization to occur with a quantum yield higher than 0.5. This is what happens in rhodopsin, which absorbs the light in the primary step of the vision process [3]. To allow the energy to dissipate out of the reaction mode, this mode should be coupled to others, so in this work we have chosen problems which involve a few coupled modes.

The methods developed are of a "first principles nature" and relevant to a wide area of applications in photochemistry and spectroscopy, e.g., atmospheric chemistry [4], astrophysics [5], and laser technology [6]. A rather active field which benefits much from excited state calculations is the fundamental study of photodissociation reactions [7]. However, in this work we will restrict ourselves to spectroscopic problems, in particular to UV-absorption spectra, since this allows for the easiest and most direct comparison between theory and experiment. Since we are interested in developing methods that are not merely suitable for equilibrium

properties, we selected spectroscopic problems in which the spectra reveal large-amplitude excited state motions.

Before giving a (historical) introduction into the theory of molecular spectroscopy, we want to make a few remarks concerning the apparent compelling strive for accuracy throughout this work. This is not just a matter of keeping supercomputers from idling. One should realize that the experimental resolution of gas phase UV-absorption spectra is often in the order of wave numbers (cm^{-1}), while the accuracy attainable in molecular beam experiments can be many orders of magnitude higher. Computationally, however, it is a major job to get excitation energies with an accuracy of, say, one thousand wave numbers (2.9 kcal/mol) and such an accuracy might be required to answer "qualitative questions" such as those concerning the ordering of states or the vibrational assignments.

1.1 Vibrational structure of electronic spectra

Already in the days of the Old Quantum Theory (before 1926) it was noted that a molecule can sometimes absorb a photon of many times its dissociation energy, without dissociating. This was explained by assuming that "the excitation energy is primarily employed for raising the electron system to a higher quantum state". This led Franck [8] to postulate in 1925 his idea of the "vertical excitation", i.e., the idea that the nuclear conformation remains unchanged *during* an electronic excitation. In 1926 Condon extended the rule by postulating that not only the *positions* of the nuclei remain unchanged during the electronic excitation, but also their *momenta* [9]. This makes the theory applicable to electronic excitations from vibrationally excited electronic ground states. In the same year Schrödinger formulated the theory of Quantum Mechanics [10] and very soon after that Condon presented the quantum mechanical version of his theory, which is generally referred to as the Franck-Condon principle ([11], Figure 1).

In 1927 Born and Oppenheimer showed, using perturbation theory, how the large ratio between the nuclear mass and the electron mass justifies the separation of motion of the nuclei and the electrons [12]. In fact their work gives a general recipe for solving molecular problems. First, the Schrödinger equation has to be solved for the motion of the electrons at fixed positions of the nuclei. The resulting energy serves as a potential in the Schrödinger equation for the nuclear motion. The first job is usually referred to as the "electronic structure problem" and the second as the "dynamical problem". Even in cases where this approximation breaks down, because of nonadiabatic interactions, it usually still serves

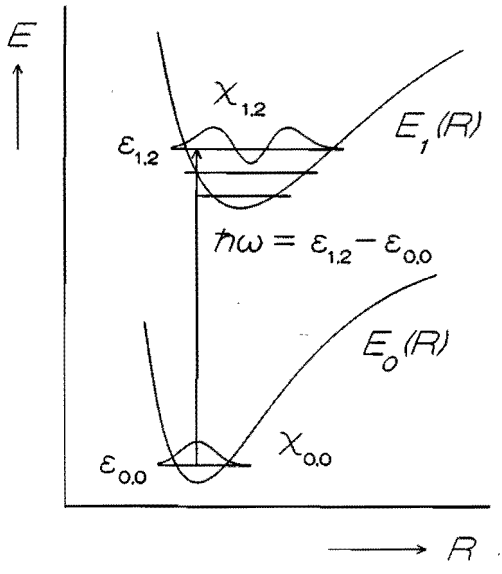

Electronic wave function (r denotes all electronic coordinates $\mathbf{r}_p$):

$$\{H^{\text{electronic}} - E_K(R)\}\psi_K(r;R) = 0\ ;\quad K = 0,1,\ldots \tag{1.1}$$

Nuclear wave function:

$$\{T^{\text{nuclear}} + E_K(R) - \epsilon_{K,i}\}\chi_{K,i}(R) = 0 \tag{1.2}$$

Electronic transition dipole moment:

$$\vec{\mu}_{K,L}(R) = <\psi_K| - e\sum_p \mathbf{r}_p|\psi_L>_r \tag{1.3}$$

The intensity of the electronic transition $|K,i> \rightarrow |L,j>$ is proportional to:

$$F_{K,i\rightarrow L,j} = |\ <\chi_{K,i}|\vec{\mu}_{K,L}(R)|\chi_{L,j}>_R\ |^2 \tag{1.4}$$

Figure 1. The Franck-Condon principle. Usually, the term Franck-Condon transition is used if $\vec{\mu}_{K,L}(R)$ is assumed to be independent of the R. In that case $\vec{\mu}_{K,L}(R_0)$ can be taken out of the integration (Eq. 1.4).

as a starting point for the solution. Before we discuss the computational methods to solve electronic structure and dynamical problems we will digress in some detail on the physical reality of a "vertical transition".

1.2 Heller's time-dependent formulation

In this section we will start with the quantum mechanical description of a Franck-Condon spectrum (Figure 1) and try to get back at Franck's original classical picture [8].

Suppose we have measured an excited state vibrational frequency of 1000 cm^{-1} with an accuracy of 1 cm^{-1}. Now Heisenberg's time-energy uncertainty relation [13] tells us that our measurement - the time the molecule has spent in the field of the photon - must have lasted for at least a thousand vibrational periods! So at first sight one might have expected a classical picture in which the ground state potential energy surface (PES) slowly changes into the excited state PES. However, this would mean that the nuclei will not be vibrationally excited by an electronic transition, which is not in accordance with the experiment. But why then does Franck's "vertical excitation" model work so well? A clue can also be found in Heller's time-dependent formulation of Franck-Condon spectra [14].

It is fairly simple to rewrite Condon's time-independent formula for the transition intensity (Eq. 1.4) as a Fourier transform:

$$\epsilon(\omega) = C\omega \int_{-\infty}^{+\infty} <\phi_0|\phi(t)> e^{i(\omega+E_{K,i})t} dt \tag{1.5}$$

Here ϕ_0 is the ground-state vibrational wave function times (a component of) the electronic transition dipole moment:

$$\phi_0(R) = \mu_{K,L}(R)\chi_{K,i}(R) \tag{1.6}$$

and $\phi(t)$ is its time development if it is lifted instantaneously to the excited state PES at $t = 0$:

$$\phi(t) = \sum_j <\chi_{L,j}|\phi_0> \chi_{L,j} e^{-iE_{L,j}t} \tag{1.7}$$

Equation (1.5) can be verified by substituting Eqs. (1.6) and (1.7) into Eq. (1.5). This gives:

$$\epsilon(\omega) = C\omega \sum_j | <\chi_{K,i}|\mu_{K,L}|\chi_{L,j}> |^2 \delta(\omega - E_{L,j} + E_{K,i}) \tag{1.8}$$

This equation shows that the spectrum $\epsilon(\omega)$ consists of a sum of delta functions at $\omega = E_{L,j} - E_{K,i}$ with a coefficient equal to the Franck-Condon factor (Eq. 1.4). The factor ω turns the transition probability into an energy and C is a constant [15].

Generally, $\phi(t)$ will not be an eigenstate of the excited state PES, but a wave packet, which is moving around on the excited state surface. We do not want to duplicate Heller's detailed analysis, but with Heisenberg's time-energy uncertainty relation in mind we can imagine how the time development of $\phi(t)$ determines the spectrum. The shortest feature in time, the initial fall off of $<\phi_0|\phi(t)>$, determines the broadest feature in energy, the width of the absorption envelope. The recurrences of $\phi(t)$ to its origin determine the level spacings of the vibrational bands. Finally the disappearance of $\phi(t)$ at large t because of fluorescence, radiationless decay or collisions is related to the width of the vibrational bands.

We can now see why the classical picture of a vertical excitation works so well: Equations (1.5)-(1.7) show that *mathematically* the spectrum is entirely determined by the fate of the vertically lifted wave packet ϕ_0, although this does not mean that physically the excitation does take place instantaneously. The quantum mechanical picture of what "really happens" is, in Heller's words: "while the laser of frequency ω is turned on, 'little pieces' of the ground-state wave function are constantly being brought upstairs (with phase $e^{i\omega t}$) while the pieces already upstairs are functionally just $\phi(t)$ at various times t. As these pieces return to their birth place, new pieces are still coming up, constructively (or destructively) interfering with the old pieces and causing absorption maxima (or minima)".

1.3 Electronic structure calculations

The electronic structure problem has been extensively discussed in the literature. Numerous introductory books exist, of which we only mention the book by Szabo and Ostlund [16]. In this section we call attention to some considerations particularly relevant to the calculation of excited states. The starting point will be the restricted Hartree-Fock (HF) approximation. The main feature of this approximation is that the wave function is described by a single spin adapted configuration. Physically this can be interpreted as electrons moving in orbitals and "feeling" only the average electric field of the other electrons and not their instantaneous positions. Therefore, this wave function is said to be uncorrelated (in fact the antisymmetry of the wave function imposed by the Pauli principle causes electrons of parallel spin to avoid each other; this is called

exchange correlation). A single closed shell (i.e., 2 electrons per orbital) configuration can often successfully describe a ground-state equilibrium structure.

Electron correlation can be accounted for by including other configurations. Let us take H_2 as an example. The HF wave function consists of the $|\sigma_g^2|$ configuration. We can introduce so-called "left-right" correlation by including the $|\sigma_u|^2$ configuration. This gives the wave function the flexibility to move the electrons apart.

If we move the H atoms apart, the energy of the two configurations gets closer and the contribution of $|\sigma_u|^2$ steadily increases. At infinite separation the configurations become degenerate and their contributions to the total wave function become equal. At infinity the two configurations do not describe "true" (often called "dynamical") correlation, since the two electrons move independently at the separate atoms. In this case the two configurations are said to be necessary to solve a "near degeneracy problem" or to get a wave function that describes the dissociation properly. The absence of dynamical correlation at infinite separation can easily be shown by writing the wave function as a single, open shell configuration.

If we denote a configuration by ψ_i we can express a general wave function as a linear combination of configurations as:

$$\Psi = \sum_i c_i \psi_i \tag{1.9}$$

A calculation in which the coefficients c_i are variationally optimized is called a Configuration Interaction (CI) calculation. If for a given set of orbitals all configurations are included (full CI), the result will be invariant under unitary transformations of the orbitals (in fact the FCI wave function is invariant under any nonsingular transformation). However, if we want to include only a few configurations, e.g., because we merely want to solve a near degeneracy effect, it can be advantageous to simultaneously optimize the orbitals that constitute the configurations. This is called the multiconfigurational Self Consistent Field (MCSCF) approach.

We are now in a position to explain why we want to do better than Hartree-Fock for the description of excited states. First of all, one can expect near degeneracies to occur more often for higher energies. Furthermore, the correlation energy, although only a small fraction of the total energy, can be in the order of the excitation energy. This is of little concern if one, for example, wants to optimize a ground state geometry, since the correlation energy can be fairly constant for a small part of the PES. However, to predict excitation energies one must account properly for the difference in correlation energy between two states, which might

be considerable because of the different nature of the electronic structure of these states. Finally, if one considers large-amplitude motion, it is very likely that near degeneracies occur at least at some part of the PES.

Let us suppose that we have a qualitatively correct MCSCF description of some state using, say, one to ten configurations. If we want to assess the dynamical correlation energy in a CI calculation we have to select configurations in some way, assuming that the time needed for a FCI calculation is prohibitive. The simplest form of selection is based on the excitation level, i.e., the number of electrons that is promoted from the occupied orbitals of some *reference* configuration to the unoccupied ones.

Doubly excited configurations (doubles) can be expected to be important, because they have a direct interaction with their reference configuration. Higher excitations contribute only indirectly because the electronic Hamiltonian contains at most two-particle interactions. Some singly excited configurations (singles) [17] do not mix directly with a MCSCF reference function because of Brillouin's theorem, but they do account for orbital relaxation. If the MCSCF function is not optimized for the state in question, Brillouin's theorem does not hold and the singles are more important.

A CI calculation which involves more than one reference configuration is called a multireference CI (MRCI) calculation. MRCI calculations that include singles and doubles are often referred to as MRSDCI. For the problems treated in this thesis (12 electrons correlated) the dimension of this problem is in the order of $10^4 - 10^6$. Such a dimension is prohibitive for a conventional CI program, which starts with the construction of the Hamiltonian matrix, but it can easily be dealt with by the direct CI method [18] which is used in this work.

In a conventional CI calculation the number of configurations has to be reduced further. Usually this is done by selecting those configurations that are expected, on the basis of perturbation theory, to contribute more to the wave function (in terms of energy) than a certain threshold. In the MRDCI program package of Buenker and Peyerimhoff [19], which is currently probably the most popular package for the calculation of excited states, the conventional CI is combined with an extrapolation procedure: The effect of inclusion of all singles and doubles is estimated by repeating the calculation for several thresholds and extrapolating to a zero-threshold. Problems that may arise in this extrapolation were studied by Jackels and Shavitt [20].

However, whether one calculates or estimates the effect of all singles and doubles, the contribution of the higher excitations often appears to be non-negligible. In particular, the larger the system (i.e., the number

of electrons) the more important the higher excitations will be. In other words, a SDCI (singles and doubles CI) calculation gets worse if the size of the system increases. This effect will be discussed in more detail in the next section since it is the key to the development of corrections to the CI method.

1.3.1 The size consistency problem

Physically it is clear that the energy of two molecules at infinite separation is equal to the sum of the energies of the separate molecules. A method that upholds this property is said to be size consistent. A more subtle definition of size consistency is that the energy of a many particle system must be proportional to the number of noninteracting particles (N) if $N \rightarrow \infty$. This definition can also be applied in the case of interacting systems. For example, it says that the energy of a crystal is proportional to the number of constituent molecules.

In terms of wave functions, size consistency means that the total wave function must be the (anti-symmetrized) product of the wave functions of the subsystems. HF, perturbation theory (PT), and full CI fulfil this seemingly modest requirement. However, any form of truncated CI, such as MRSDCI, does not. This can be illustrated by the DCI (doubles CI) calculation of two H_2 molecules. The DCI description of a H_2 molecule contains, by definition, the double excitations. So the product wave function for two H_2 molecules should contain quadruple excitations, which are of cause not included in the DCI function. So the somewhat vague statement "DCI gets worse if the size of the system increases" can be formulated much clearer as "DCI is not size consistent".

The simplest way to obtain approximately size consistent results from a CI calculation is by using a size consistency correction such as the Davidson correction [21]. For a single reference SDCI calculation this formula is:

$$\Delta E_{\text{Davidson}} = (1 - c_0^2)(E_{\text{SDCI}} - E_{\text{SCF}}) \tag{1.10}$$

Here c_0 is the coefficient of the reference configuration in the normalized SDCI function. More complicated formulas exist which contain the number of electron pairs (the Pople correction [22], the Siegbahn correction [23], and others [24]). Several multireference analogues are possible ([19] and Chapter 4, Eq. 4.33).

A rigorous size consistent method is the Coupled Cluster (CC) method [25]. CC is a computationally demanding method, but several approximations to CC are possible, such as the Coupled Electron Pair Approximation (CEPA) [16, 26]. We will shortly discuss CC and show how the CEPA

gives rise to a set of equations that are only slightly different from the CI equations. A multireference version of this method was recently developed and is described in Chapter 4.

1.3.2 The Coupled Cluster method

The size consistency of this method follows directly from the *exponential ansatz*:

$$\Psi_{CC} = e^T \Psi_0 \tag{1.11}$$

Here Ψ_0 is a (HF) reference configuration and T is an excitation operator. The exponential is defined by its Taylor expansion. If T consists of only double excitations we arrive at the CCD (Coupled Cluster Doubles) method. In that case we can write T as:

$$T = \sum_{pqrs} t_{pqrs} \tau_{pq,rs} \tag{1.12}$$

The coefficients t_{pqrs} are called the cluster amplitudes and the operators $\tau_{pq,rs}$ generate all double excitations. In this notation the DCI function is written as:

$$\Psi_{DCI} = (1 + T)\Psi_0 \tag{1.13}$$

The size consistency of the CC wave function follows easily if we localize the orbitals on the fragments A and B of a supermolecule AB. If the HF reference function is written as a product and the excitation operators (T) are divided into operators (T_A) working on fragment A and operators (T_B) working on fragment B, i.e., the commutator of T_A and T_B is zero ($[T_A, T_B] = 0$), then we can write the CC function as a product:

$$\Psi_{CC}^{AB} = e^{T_A + T_B} \Psi_0^A \Psi_0^B = (e^{T_A} \Psi_0^A)(e^{T_B} \Psi_0^B) = \Psi_{CC}^A \Psi_{CC}^B \tag{1.14}$$

Variational optimization of the CC function is awfully complicated [26] and therefore the CC equations are derived by projecting the following expression

$$(H - E)e^T \Psi_0 \tag{1.15}$$

to Ψ_0 and all double excitations $\tau\Psi_0$:

$$< \Psi_0 | (H - E) e^T | \Psi_0 > \; = \; 0 \tag{1.16}$$

$$< \Psi_0 | \tau^\dagger (H - E) e^T | \Psi_0 > \; = \; 0 \,, \quad \text{for all } \tau \tag{1.17}$$

Note that the number of unknowns (E, t_{pqrs}) is equal to the number of equations. We will not discuss how this set of nonlinear equations can be

tackled [25], but rewrite it in a form which allows for certain approximations.

By expanding the exponential and taking into account that there are at most two-particle interactions we can rewrite Eq. (1.17) as:

$$<\Psi_0|\tau^\dagger(H-E+\Delta E_\tau)(1+T)|\Psi_0> \tag{1.18}$$

Here ΔE_τ, the so-called diagonal shift, is given by:

$$\Delta E_\tau = \frac{1}{2}\frac{<\Psi_0|\tau^\dagger H T^2|\Psi_0>}{t_\tau} \tag{1.19}$$

where t_τ denotes the cluster amplitude for the double excitation τ. The shifts can now be said to account for all higher excitations that consist of combinations of doubles. The calculation of these shifts is rather troublesome, since the interactions between all doubles and all quadruples are involved in Eq. (1.19). Several approximations are possible, leading to several CEPA versions, referred to as CEPA(0), CEPA(1), CEPA(2) etc. [26]. The CEPA(0) is the starting point for our MRCEPA and it involves two approximations in the expression for the shifts.

1.3.3 CEPA(0)

The first approximation, the direct term approximation, amounts to selecting only those quadruple excitations in Eq. (1.19) that can be written as $\tau'\tau|\Psi_0>$, where τ is the excitation operator for which the shift ΔE_τ is being calculated.

The second approximation, referred to as the H-matrix equivalence, is that we use:

$$<\Psi_0|\tau^\dagger H\tau'\tau|\Psi_0>=<\Psi_0|H\tau'|\Psi_0> \tag{1.20}$$

which is strictly correct only if τ and τ' have no orbital indices in common.

The result of these approximations is that all double excitations get the same shift. The MRCEPA described in Chapter 4[1] is slightly more discriminating in the sense that the excitations are divided into classes and that each class gets its own diagonal shift. To define an excitation class, the orbitals are divided into inactive, active, and virtual, depending on whether they have two, a variable number, or no electrons in the reference configurations. The number of electrons a configuration has in each of these orbital spaces determines its excitation class.

[1]The MRCEPA is developed and implemented in the GAMESS/ATMOL packages by P. J. A. Ruttink, J. H. van Lenthe, and R. Zwaans, Rijksuniversiteit Utrecht.

Although the CEPA(0) and MRCEPA equations do not represent an eigenvalue problem, they can be solved using a CI program, if the shifts ΔE_τ are applied to the diagonal elements after every (Davidson) iteration.

1.4 Dynamical methods

Early developments in the description of the dynamics of molecular systems are based on the concept of an "equilibrium structure". In 1936 Wilson and Howard [27] presented a classical Hamiltonian in which a rotating coordinate system is fixed to this equilibrium structure using the Eckart conditions [28]. The vibrations are described in normal coordinates, which separates the problem in the harmonic approximation. Four years later Darling and Dennison [29] gave the correct quantum mechanical version of this Hamiltonian, which was subsequently rearranged in a much simpler form by Watson [30] in 1968. In the traditional approach one starts with an approximate solution based on harmonic vibrations and rigid rotations. Subsequently, perturbation theory is used to deal with the rotation-vibration interactions and anharmonicities [31].

In this work we will concentrate on the vibrational structure of the spectra, since it is very sensitive to the shape of the PES. If the experimental spectrum exhibits rotational structure it can be used to find the experimental equilibrium structure. This kind of calculations is not performed in this work; we will compare the calculated equilibrium structures to the experimental values known from the literature.

Since we are interested in large amplitude motion, perturbation theory may not be the most suitable method [32]. Furthermore, it has been noted that rectilinear normal coordinates may not be the best choice for systems with coupled large amplitude modes [33]. In particular an expression for the PES in internal curvilinear coordinates will be more accurate than an expression in rectilinear coordinates with the same number of variables [33-35]. An alternative for the perturbation theory approach is the variational method [32]. The main problem of this method is that the dimension of the Hamiltonian exponentially increases with the number of coordinates. Another alternative is the use of semiclassical methods. These methods are based on quantization of classical trajectories, which are relative easy to calculate, even for anharmonic PES's and higher dimensions.

We will employ both semiclassical and fully quantum mechanical methods. Here we will introduce those methods and point out the (current) limitations of the semiclassical methods. We will also show how for some problems a fully quantum mechanical method can be made computationally feasible. Starting point of all the methods used is the classical Hamil-

tonian and so we start with a short discussion of classical mechanics [36].

1.4.1 Classical mechanics

If we assume that the potential energy function (V) only depends on some set of generalized coordinates $\mathbf{q}$ (and not on the time derivatives $\dot{\mathbf{q}}$), we have the following recipe to write down the classical Hamiltonian (H). First write down the total energy, in terms of $\mathbf{q}$ and $\dot{\mathbf{q}}$:

$$H(\mathbf{q}, \dot{\mathbf{q}}) = T(\mathbf{q}, \dot{\mathbf{q}}) + V(\mathbf{q}) \tag{1.21}$$

where T is the kinetic energy. Then define the conjugate momenta p_i as:

$$p_i = \frac{\partial T(\mathbf{q}, \dot{\mathbf{q}})}{\partial \dot{q}_i} \tag{1.22}$$

Rewrite the Hamiltonian in terms of $\mathbf{q}$ and $\mathbf{p}$:

$$H(\mathbf{q}, \mathbf{p}) = T(\mathbf{q}, \mathbf{p}) + V(\mathbf{q}) \tag{1.23}$$

The classical Hamiltonian equations of motion are given by:

$$\dot{q}_i = \frac{\partial H}{\partial p_i} \tag{1.24}$$

$$\dot{p}_i = -\frac{\partial H}{\partial q_i} \tag{1.25}$$

If we have N particles and we take $\mathbf{q}$ to be the corresponding $3N$ cartesian coordinates these equations reduce to Newton's equations of motion. However, in Hamilton's formulation one can always choose the most suitable set of coordinates $\mathbf{q}$. Furthermore, the Hamiltonian formulation enables one to impose a constraint on the motion that corresponds to fixing some coordinate q_i by simply dropping the corresponding equation.

We will now apply this method to a nonlinear molecule with zero total linear and angular momentum. Suppose we can express the $3N$ cartesian coordinates x_i, $i = 1 \ldots 3N$ of the N atoms, with masses m_i, in terms of some set of $(3N - 6)$ internal coordinates $\mathbf{q}$. For the sake of convenience we have numbered the coordinates consecutively, so the coordinates of the first atom are (x_1, x_2, x_3) and its mass is $m_1 = m_2 = m_3$, etc. Direct application of the chain rule to the expression of the kinetic energy in cartesian coordinates gives:

$$2T = \sum_{i}^{3N} m_i (\dot{x}_i)^2 = \sum_{j,k}^{3N-6} \dot{q}_j G_{j,k} \dot{q}_k \tag{1.26}$$

where G generally is a function of $\mathbf{q}$:

$$G_{j,k} = \sum_{i}^{3N} m_i \left(\frac{\partial x_i}{\partial q_j}\right)\left(\frac{\partial x_i}{\partial q_k}\right) \tag{1.27}$$

The conjugate momenta can now be defined using Eq. (1.22) and T can be written in vector notation as (see e.g. [37]):

$$2T(\mathbf{q},\mathbf{p}) = \mathbf{p}^{\dagger} G^{-1} \mathbf{p} \tag{1.28}$$

A quantum mechanical version of this procedure is used in Chapter 5 for three internal coordinates of ethylene. In that particular case it is very simple to define a set of coordinates that leave the total angular momentum of the molecule equal to zero. In general it is not possible to express the cartesian coordinates in the internal coordinates so that the total angular momentum is automatically equal to zero. The reason is that the zero total angular momentum requirement does not forbid a certain conformation of a molecule to assume different orientations in time. This problem can also be formulated as: In general it is not possible to separate the rotation and the vibration of a molecule globally.

Usually, this separation is made approximately using the Eckart conditions [28]. To employ the Eckart conditions one must describe the vibrations as deviations from an "equilibrium structure". If the Eckart conditions are used to define the G-matrix, with the instantaneous positions of the atoms as the "equilibrium structure", the classical kinetic energy expression given above will be exact for a molecule with a zero total angular momentum. This has been worked out for many types of internal coordinates (such as stretching, bending and torsion coordinates) and tables exist with formulas for the inverse kinetic energy matrix [37, 38](Note that often the G-matrix is defined as the inverse of ours). The well known Wilson-GF matrix method for the harmonic approximation boils down to finding a linear transformation which diagonalizes $G^{-1}F$ for the equilibrium geometry, where F is the Hessian matrix of the potential:

$$F_{i,j} = \frac{\partial^2 V}{\partial q_i \partial q_j} \tag{1.29}$$

The eigenvalues of $G^{-1}F$ are the squares of the vibrational frequencies and the eigenvectors define the normal coordinates.

1.4.2 Semiclassical methods

It was the idea of the Old Quantum Theory that the discrete energy levels of bound states can be found by quantization of classical trajectories.

In 1913 Bohr [39] postulated that it is the action integral that is to be quantized. This led to the Bohr-Sommerfeld quantization rules:

$$\oint p\,dq = \begin{cases} (n+\frac{1}{2})h & \text{for vibrations} \\ nh & \text{for rotations} \end{cases} \tag{1.30}$$

where the integration has to be done for one complete oscillation. It can be verified easily that this gives the exact levels of a one-dimensional harmonic oscillator. Ideas of Einstein led to the EBK-quantization rules [40-42] which constitute a generalization of the rule for nonseparable N-dimensional systems:

$$\oint_{C_i} \sum_{k=1}^{N} p_k\,dq_k = (n_i + \frac{1}{2})h\ ; \quad i = 1, \ldots N \tag{1.31}$$

where the $\frac{1}{2}$ is appropriate for nondegenerate oscillators but can be replaced by other (known) values for other kinds of systems, the so-called the Maslov indices [43]. C_i are topologically independent paths on the *invariant tori*. We will explain this concept with a two-dimensional example. For a $2D$ system the *phase space* $(\mathbf{p}, \mathbf{q}) = (p_1, p_2, q_1, q_2)$ is four-dimensional. For a given trajectory the total energy is conserved:

$$H(\mathbf{p}, \mathbf{q}) = E \tag{1.32}$$

This makes the *energetically accessible* region three-dimensional. However, under certain conditions more invariants exist. For separable systems these are simply the energies per mode, which are evidently conserved. This confines the trajectory to a two-dimensional region in phase space called an *invariant torus*. For nonseparable systems the trajectories are also confined to invariant tori in the *regular region* of the phase space. In the irregular region, which usually occurs at higher energies, a trajectory fills the entire energy accessible region. Such trajectories are called chaotic [44] and this will not be further discussed here.

In Figure 2 we schematically show two topologically independent paths on a torus. For EBK quantization considerable freedom exists since the paths for which the action integrals are to be quantized need not be along actual trajectories. The EBK quantization rules may seem unmanageably complicated, even for two-dimensional systems, but in the 1970s the development of practical methods began. The freedom in the choice of the integration path gave rise to a series of methods. For example, Eastus and Marcus [45] presented a method in 1974 in which the integration is performed along the *caustics*, i.e., the multidimensional analogues of the

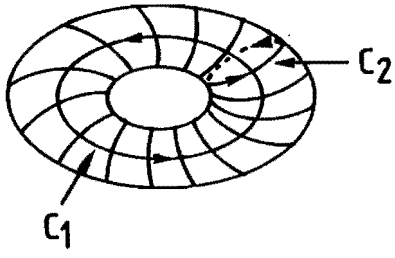

Figure 2. Two topologically independent paths on a torus.

classical turning points. They claimed that this was the first practical method for EBK quantization in a nonseparable system. In 1975 Noid and Marcus used integration along the so-called Poincaré surfaces of section [46]. The method we employed to solve a two-dimensional problem in Chapter 2 is the method of Sorbie [47], where the integration is performed along a trajectory closed in phase space. Some details of this method are given in Chapter 2.

A problem with all of these methods is that they become progressively more cumbersome in higher dimensions, although they have also been applied to three-dimensional cases [48]. For instance, in the Sorbie method finding trajectories that close in phase space with some specified accuracy is the main bottleneck for application to higher dimensions. Another problem is the calculation of Franck-Condon factors. Although in 1985 Gray *et al.* [49] presented a method based on invariant tori which is suitable for the calculation of Franck-Condon factors, it was only worked out for the two-dimensional case. However, the development of semiclassical methods has not stopped and in recent years several promising alternatives were developed [50]. Many relevant references can be found in an extensive review of Reinhardt [51].

The development of a rather different set of semiclassical methods, which do not rely upon the existence of invariant tori, started with the landmark paper of Heller [52] in 1975. In these methods an approximation to the solution of the time-dependent Schrödinger equation is found by calculating the time development of Gaussian wave packets. Heller showed that if the potential, which may be nonseparable, is approximated harmonically around the *instantaneous* position of a wave packet, the center

of this wave packet will follow a classical trajectory. First order differential equations are found to govern the time development of other parameters of a Gaussian wave packet, such as the width and the phase.

It is also possible to represent a wave packet by a linear combination of Gaussians. In that case one may keep the width of the Gaussians fixed in time [53]. This is called the frozen Gaussian approximation (FGA), which we employ in Chapter 2. Since in this way one finds an approximation to the time-dependent wave function, Franck-Condon factors may be obtained easily as was explained in Section 1.2.

1.4.3 Quantum mechanical methods

The semiclassical methods worked rather satisfactorily for our two-dimensional problem in Chapter 2. Still, in the study on the $V \leftarrow N$ band of ethylene in Chapter 5, we applied a fully quantum mechanical method for several reasons. First of all, it is rather difficult to assess the accuracy of semiclassical methods. One has to check a number of parameters, e.g., for the frozen Gaussian approximation the number of Gaussians per coordinate, the width of the Gaussians, and the time step, and still one does not know the error introduced by the semiclassical approximation *an sich*. Secondly, in the ethylene problem two nonadiabatically interacting electronic states are involved. This would require the use of other semiclassical methods, e.g., surface hopping methods [54], which considerably enlarges the problem of assessing the accuracy. This again makes it difficult to draw conclusions on the quality of the PES on the basis of comparison with experiment. Finally, one might argue that a high quality *ab initio* PES is very expensive and it is simply a waste to loose any accuracy in the final step of the calculation of the spectrum.

Conceptually, a fully quantum mechanical method is perhaps the simplest way to calculate bound state vibrational energy levels. The time-independent Schrödinger equation is turned into a matrix eigenvalue problem by introducing a basis set. In p dimensions one chooses n_i one-dimensional functions per dimension and a p-dimensional basis set can be formed by taking the direct or Hartree product of those functions. The problem is evidently the size of the resulting Hamiltonian matrix (N), which grows rapidly if higher energy levels and/or more dimensions are required: $N = n_1 \times n_2 \times \cdots \times n_p$.

If the full Hamiltonian matrix is to be calculated and stored in the core memory of a computer, the maximum size that can be handled conveniently is in the order of $N = 10^3$. However, for Hamiltonians that are sparse, i.e., contain a lot of zero elements, some numerical methods

exist that can deal with sizes several orders of magnitude larger. For sparse matrices with a special structure, e.g., banded matrices, some so-called "direct solvers" exist. Otherwise, iterative methods can be used. For example, if the Hamiltonian is diagonally dominant and only a few eigenvalues are required, the Davidson algorithm [55] is very efficient and so this method is favored in electronic structure calculations. In other cases [56] the Lanczos algorithm (Chapter 3) is more efficient. Such iterative methods essentially only require a routine that calculates the matrix vector product:

$$\psi' = H\psi \tag{1.33}$$

and the memory requirements are only a few times the size of ψ, i.e., a few times (N), or less.

The potential energy part of the Hamiltonian can be made sparse by choosing a specific form of the potential in combination with a proper basis set. For example, one can use a truncated Taylor expansion for the potential in combination with a Harmonic oscillator basis set. For a large amplitude mode, however, one might prefer more flexibility in the choice of the form of the potential, without reducing the sparsity of the matrix. With a grid representation the potential is always diagonal (Chapter 3). Unfortunately, the kinetic energy operator is only diagonal in a Fourier basis. In the Kosloff method [57] the fast Fourier transform (FFT) algorithm is used to switch back and forth between the grid and the Fourier representation, which results in a very efficient implementation of the Hamiltonian. This idea of switching between representations is also used in the Discrete Variable Representation (DVR) of Light and coworkers [58].

In Chapter 3 we present a method which is also based on the grid representation and in which the kinetic energy matrix is made sparse (not diagonal) by using a high (10^{th}) order finite difference formula. This gives rise to a particularly simple implementation of the Hamiltonian since the kinetic energy is represented by only six, problem independent, coefficients. In Chapter 3 we also show how to calculate Franck-Condon factors very efficiently with this method.

A few methods for the calculation of anharmonic vibrations of moderate amplitude are compared in [59].

1.5 Outline of the thesis

In Chapter 2 we describe an exploratory study for which we choose the $\tilde{B}\,^1B_u \leftarrow \tilde{X}$ spectrum of *trans*-di-imide. The $\tilde{B}$ state is of Rydberg char-

acter and can be described by a single reference function. We compare the spectra calculated with the SDCI, SDCI+Pople correction, and single reference CEPA with the experimental spectrum. We also investigate the effect of orbital optimization. Two vibrational modes are included in the study and we employ semiclassical methods to calculate the vibrational structure of the spectra.

In Chapters 3 and 4 we describe the Lanczos/grid method and the MRCEPA method, respectively, and we show the results of some test calculations.

In Chapter 5 these methods are used to study the $V \leftarrow N$ band of ethylene. This problem is chosen because the description of the V state of ethylene really requires a size consistent multireference method and the precise interpretation of the spectrum is still under discussion.

References

[1] C. W. Bauschlicher Jr., S. R. Langhoff, and P. R. Taylor, Adv. Chem. Phys. **77**, 103 (1990).

[2] G. J. M. Dormans, G. C. Groenenboom, and H. M. Buck, J. Chem. Phys. **86**, 4895 (1987).

[3] G. J. M. Dormans, G. C. Groenenboom, W. C. A. van Dorst, and H. M. Buck, J. Am. Chem. Soc. **110**, 1406 (1988).

[4] B. J. Finlayson-Pitts and J. N. Pitts, *Atmospheric Chemistry: fundamentals and experimental techniques* (Wiley, New York, 1986).

[5] E. F. van Dishoeck, *Photodissociation and excitation of interstellar molecules: calculations and astrophysical applications* (Thesis, Rijksuniversiteit Leiden, 1984)

[6] J. O. Hirschfelder, R. E. Wyatt, and R. D. Coalson (Editors), *Lasers, Molecules, and Methods* (Wiley, New York, 1989), Adv. Chem. Phys. **73**.

[7] P. Brumer and M. Shapiro, Adv. Chem. Phys. **60**, 371 (1985) ; G. G. Balint-Kurti and M. Shapiro, Adv. Chem. Phys. **60**, 403 (1985)

[8] J. Franck, Trans. Faraday Soc. **21**, 536 (1925).

[9] E. Condon, Phys. Rev. **28**, 1182 (1926).

[10] E. Schrödinger, Ann. Physik, **79**, 361 (1926).

[11] E. U. Condon, Phys. Rev. **32**, 858 (1928).

[12] M. Born, J. R. Oppenheimer, Ann. Physik, **84**, 457 (1927).

[13] W. Heisenberg, Z. Physik **43**, 172 (1927).

[14] E. J. Heller, Acc. Chem. Res. **14**, 368 (1981).

[15] G. Herzberg, *Molecular spectra and molecular structure*, Part I and III (van Nostrand, New York, 1950).

[16] A. Szabo and N. S. Ostlund, *Modern Quantum Chemistry: Introduction to Advanced Electronic Structure Theory* (McGraw-Hill, New York, 1989).

[17] B. Levy, G. Berthier, Int. J. Quantum Chem. **2**, 307 (1968).

[18] V. R. Saunders and J. H. van Lenthe, Mol. Phys. **48**, 923 (1983).

[19] P. J. Bruna and S. D. Peyerimhoff, Adv. Chem. Phys **67**, 1 (1987).

[20] C. F. Jackels and I. Shavitt, Theoret. Chim. Acta. **58**, 81 (1981).

[21] E. R. Davidson, in: *The world of quantum chemistry*, Eds. R. Daudel and B. Pullman (Reidel, Dordrecht, 1974).

[22] J. A. Pople, R. Seeger, and R. Krishnan, Int. J. Quantum Chem. Symp., **11**, 149 (1977).

[23] P. E. M. Siegbahn, Chem. Phys. Lett. **55**, 386 (1978).

[24] L. Meissner, Chem. Phys. Lett. **146**, 204 (1988).

[25] R. J. Bartlett, Ann. Rev. Phys. Chem. **32**, 359 (1981).

[26] W. Kutzelnigg, in *Methods of Electronic Structure Theory, Modern Theoretical Chemistry*, Part 3, Ed. H. F. Schaefer III (Plenum, New York, 1977).

[27] E. B. Wilson and J. B. Howard, J. Chem. Phys. **4**, 260 (1936).

[28] C. Eckart, Phys. Rev. **47**, 552 (1935).

[29] B. T. Darling and D. M. Dennison, Phys. Rev. **57**, 128 (1940).

[30] J. K. G. Watson, Mol. Phys. **15**, 479 (1968).

[31] D. A. Clabo Jr., W. D. Allen, R. B. Remington, Y. Yamaguchi, H. F. Schaefer III, Chem. Phys. **123**, 187 (1988).

[32] G. D. Carney, L. L. Sprandel, and C. W. Kern, Adv. Chem. Phys. **37**, 305 (1978).

[33] T. Carrington, L. Halonen, and M. Quack, Chem. Phys. Lett. **140**, 512 (1987).

[34] K. M. Dunn, J. E. Boggs, and P. Pulay, J. Chem. Phys. **85**, 5838 (1986).

[35] K. M. Dunn, J. E. Boggs, and P. Pulay, J. Chem. Phys. **86**, 5088 (1987).

[36] H. Goldstein, *Classical Mechanics* (Addison-Wesley, Reading, 1980).

[37] E. B. Wilson, J. C. Decius, and P. C. Cross, *Molecular vibrations* (McGraw-Hill, New York, 1955)

[38] J. C. Decius, J. Chem. Phys. **16**, 1025 (1948).

[39] N. Bohr, Phil. Mag. **26**, 1 (1913).

[40] A. Einstein, Verh. Phys. Ges. **19**, 82 (1917).

[41] L. Brillouin, J. Phys., Paris, **7**, 353 (1926).

[42] J. B. Keller, Ann. Phys. (N.Y.) **4**, 180 (1958).

[43] I. C. Percival, Adv. Chem. Phys. **36**, 1 (1977).

[44] I. C. Percival, J. Phys. B. **6**, L229 (1973).

[45] W. Eastes and R. A. Marcus, J. Chem. Phys. **61**, 4301 (1974).

[46] D. W. Noid and R. A. Marcus, J. Chem. Phys. **62**, 2119 (1975).

[47] K. S. Sorbie, Mol. Phys. **32**, 1577 (1976).

[48] S. M. Colwell and N. C. Handy, Mol. Phys. **35**, 1183 (1978).

[49] S. K. Gray, M. S. Child, and D. W. Noid, Mol. Phys. **54**, 573 (1985).

[50] N. De Leon and M. A. Mehta, Comput. Phys. Rep. **8**, 293 (1988).

[51] W. P. Reinhardt, Adv. Chem. Phys. **73**, 925 (1989).

[52] E. J. Heller, J. Chem. Phys. **62**, 1544 (1975).

[53] E. J. Heller, J. Chem. Phys. **75**, 2923 (1981).

[54] M. Desouter-Lecomte, J. C. Leclerc, and J. C. Lorquet, Chem. Phys. **9**, 147 (1975); M. Desouter-Lecomte and J. C. Lorquet, J. Chem. Phys. **66**, 4006 (1977); C. Galloy and J. C. Lorquet, J. Chem. Phys. **67**, 4672 (1977).

[55] E. R. Davidson, J. Comput. Phys. **17**, 87 (1975); G. Cisneros, M. Berrondo, and C. F. Bunge, Comput. & Chem. **10**, 281 (1986).

[56] R. B. Morgan and D. S. Scott, Adv. Chem. Phys. **73**, 279 (1989).

[57] D. Kosloff and R. Kosloff, J. Comput. Phys. **52**, 35 (1983); R. Kosloff and D. Kosloff, J. Chem. Phys. **79**, 1823 (1983); C. Clay Marston and G. G. Balint-Kurti, J. Chem. Phys. **91**, 3571 (1989).

[58] J. C. Light, I. P. Hamilton, and J. V. Lill, J. Chem. Phys. **82**, 1400 (1985); Z. Bačić, R. M. Whitnell, D. Brown, and J. C. Light, Comput. Phys. Commun. **51**, 35 (1988).

[59] G. E. Quelch, Y. Xie, B. F. Yates, Y. Yamaguchi, and H. F. Schaefer III, Mol. Phys. **68**, 1095 (1989).

Chapter 2

Semiclassical calculation of the vibrational structure of the $\widetilde{B}\,^1B_u$ Rydberg state of *trans*-di-imide from *ab initio* CI potential energy surfaces[1]

Abstract

The applicability of the SDCI and CEPA methods to the excited state of the title molecule is investigated. Two basis sets are used, one of triple zeta quality extended with diffuse functions and another which also contains polarization functions. For the subsequent CI calculations closed shell as well as open shell, molecular orbitals are used. We investigate the Pople correction as a way to obtain size consistent results from the SDCI calculation. For each method, a two-dimensional potential energy surface of the $^1(4a_g, 5b_u)$ Rydberg state of *trans*-di-imide (HNNH) is calculated. The vibrational fine structure in the corresponding $\tilde{B} \leftarrow \tilde{X}$ UV-absorption spectrum is derived from these surfaces and the result is compared with the spectrum measured by Neudorfl *et al.* [P. S. Neudorfl, R. A. Back, and A. E. Douglas, Can. J. Chem. **59**, 506 (1981)]. A semiclassical method [K. S. Sorbie, Mol. Phys. **32**, 1577 (1976)] is used to obtain the vibrational frequencies. A slightly modified version of the Heller frozen Gaussian approximation [E. J. Heller, J. Chem. Phys. **75**, 2923 (1981)] is proposed and used to obtain the intensities of the vibrational bands. We conclude that it is important to use the open shell molecular orbital basis and the SDCI plus Pople correction, or even better, the CEPA. Both methods give good results for the vertical transition energy and excited state geometry. The error in the vibrational frequencies is in the order of 10%, but the NN-stretch mode is best described by the CEPA method.

[1]G. C. Groenenboom, J. H. van Lenthe, and H. M. Buck, J. Chem. Phys. **91**, 3027 (1989).

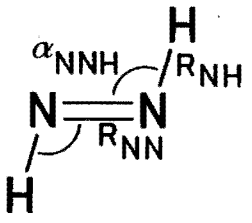

Figure 1. The structure of *trans*-di-imide at the ground state geometry (R_{NN}= 1.252 Å, R_{NH} = 1.028 Å and α_{NNH} = 106.85°).

2.1 Introduction

The common way to calculate excited state potential energy surfaces is due to Buenker and Peyerimhoff [1]. They developed a multireference method in which the choice of the reference space is based on an energy criterium. The single and double excitations from this reference space generate a subspace from which the most important species are selected for inclusion in the final CI expansion. In direct CI methods, all single and double excitations relative to a reference space are used. Evidently this results in large CI spaces, but with present-day programs such as the Saunders-van Lenthe direct CI package [2] calculations involving 10^5 configurations can be handled routinely. Furthermore, the costs of these calculations are approximately linear with the number of configurations. The main drawback of these truncated CI methods is their lack of size consistency; the correlation energy does not scale with the number of electrons (N) but with $N^{\frac{1}{2}}$. Although N does not change in our calculations, the size consistency error may still vary along the PES. Full CI does not suffer from this problem and so increasing the CI space is an effective, but rather expensive remedy. It is also possible, without additional labor, to apply the Davidson or the Pople size consistency correction [3]. Another approach is to use a size consistent method such as the Coupled Electron Pair Approximation (CEPA). Recently a multireference version of the CEPA method became available [4]. In this work we will not exploit the multireference character of this program, but only use the possibility to handle open shell reference functions, which enables us to apply this method to excited states. We have chosen *trans*-di-imide (Figure 1) as a model compound, because there is accurate experimental data to compare with and the vibrational fine structure of its UV-absorption spectrum reveals large-amplitude motion in the $^1(4a_g, 5b_u)$ state.

2.2 Spectroscopy of *trans*-di-imide

Several studies have been performed on the excited states of *trans*-di-imide. *Ab initio* SCF and CI calculations were carried out by Vasudevan *et al.* [5] for a large number of excited states of this molecule. The transition to the first excited singlet state [$^1B_g(n_+, \pi^*)$, at 3.6 eV], which is symmetry forbidden was studied theoretically by Perić *et al.* [6, 7] and observed experimentally by Back *et al.* [8, 9]. The first symmetry allowed transitions are to three $3p$ Rydberg states. Two of these states are of B_u symmetry. The spectrum of the first, the $^1(4a_g, 4b_u)$ state at 6.9 eV, contains only weak and diffuse bands. This paper concentrates on the second, the $\tilde{B}^1B_u(4a_g, 5b_u)$ Rydberg state which has a rotational and vibrational resolved UV-absorption spectrum (measured by Neudorfl *et al.* [10]). *Trans*-di-imide has three totally symmetric vibrations, the NNH bend (ν_2), the NN stretch (ν_3) and the NH stretch (ν_1). The vibrational structure of the spectrum consists of three progressions. The first progression has seven bands resulting from the ν_2 vibration. The other two progressions are assumed to have one and two quanta in ν_3 and consist of, respectively, six and four bands. The first two progressions are about equal in strength and the third progression is much weaker. The NH excited state equilibrium distance is equal to the ground state NH distance and so ν_1 is not excited and will be left out of the calculations.

2.3 Electronic structure calculations

The SCF and CI calculations are performed with the GAMESS [11] and ATMOL [12] program packages. Two different basis sets are employed for the computation of the PES's. The first basis set (labeled TZV+) is the triple-zeta basis set due to Dunning [13] with a $<5s/3s>$ contraction for hydrogen and a $<10s6p/5s3p>$ contraction for nitrogen, augmented with a set of diffuse s and p functions (exponent=0.025 bohr^{-2}) on each nitrogen atom for representing the Rydberg orbitals. The second basis set (TZVP+) is the first (TZV+) augmented with polarization functions, p on hydrogen and d on nitrogen [14]. The TZV+ basis set has 42 basis functions and the TZVP+ 60. In the SDCI calculations, we use the $^1(4a_g, 5b_u)$ single excitation as the only reference configuration, because it is far dominant for all geometries. All single and double excitations are included in the CI list, but the lowest two σ orbitals and their complements are left out, giving the following number of configurations: 11 594 for the TZV+ basis and 27 518 for the TZVP+ basis.

To investigate the effect of the choice of the one-electron basis, both

Table I. The electronic methods used. The code will be used in the other tables: Q, Pople correction; P, polarization functions; O, ROHF. All basis sets are of the triple zeta valence type (TZV) with diffuse functions (+) and some include polarization functions (P). The RHF MO's are the ground state MO's and the ROHF MO's are $^1(4a_g, 4b_u)$ open shell MO's.

	Code	Basis set	MO's	CI
a		TZV+	RHF	SDCI
b	Q	TZV+	RHF	SDCI+Pople
c	P	TZVP+	RHF	SDCI
d	P,Q	TZVP+	RHF	SDCI+Pople
e	P,O	TZVP+	ROHF	SDCI
f	P,O,Q	TZVP+	ROHF	SDCI+Pople
g	P,O,CEPA	TZVP+	ROHF	CEPA

the canonical Hartree-Fock ground state MO's and the $^1(4a_g, 4b_u)$ ROHF MO's are used. Note that neither of these orbital sets are optimized for the state we want to investigate, but an attempt to obtain the $^1(4a_g, 5b_u)$ ROHF orbitals again yielded the $^1(4a_g, 4b_u)$ orbitals. When using the ground state MO's in a calculation with more reference functions and in the CEPA calculations, we found that the $^1(4a_g, 4b_u)$ Rydberg state, which lies just below the $^1(4a_g, 5b_u)$ Rydberg state, starts mixing in. This problem does not occur with the open shell basis. In Table I we give a summary of the different methods.

2.4 The potential energy surface

Although one needs the full six-dimensional potential energy surface for an exact description of the spectrum, we restrict the *ab initio* calculations to the two most important coordinates; α_{NNH} corresponding to ν_2 and R_{NN} corresponding to ν_3. The $2D$ PES is constructed from a 40 point grid with $\alpha_{\mathrm{NNH}} = 90°, 100°, 110°, \ldots, 180°$ and $R_{\mathrm{NN}} = 1.117$, 1.167, 1.217, and 1.267 Å at $R_{\mathrm{NH}} = 1.028$ Å. For every value of α_{NNH} the R_{NN} dependence of the potential is described by a Morse-oscillator, which fits exactly through four points, so we have the following expression for the potential function:

$$V(\alpha, R) = V_\alpha + D_\alpha[1 - e^{-\beta_\alpha(R-R_\alpha)}]^2 \qquad (2.1)$$

The four α-dependent parameters in this function are interpolated by a cubic spline [15]. If the two boundary conditions (the derivatives in the

end points) are used to minimize the norm of the second derivative one obtains the well known minimum energy spline. However, we prefer to minimize the norm of the third derivative. A spline obtained in this way has the property of fitting a parabola exactly, a very desirable feature for the purpose of extracting force constants. Because of symmetry we take the first derivative at $\alpha = 180°$ equal to zero.

The full 10×4 points grid is calculated only for the first four surfaces (Table I). For the other three surfaces only 3×4 points are calculated ($\alpha_{NNH} = 90°$, $130°$, and $170°$) and the *difference* between each surface and surface (c), as a function of α_{NNH}, is fitted with a harmonic function. The surface obtained in this way is added to surface (c) again to get the full 40 point grid to which the original method is applied.

2.5 Dynamical calculations

To derive the vibrational frequencies from the $2D$ PES we use the semiclassical method of Sorbie and the Heller frozen Gaussian approximation (FGA). Although the FGA is known to yield somewhat less accurate frequencies, it gives the relative intensities of the absorptions in the spectrum which is a very sensitive test of the shape of the PES. The two different semiclassical methods are described in detail in the original papers by Sorbie [16] and Heller [17], but we will give a short summary of both methods here. In the Sorbie method a classical trajectory, starting at the minimum of the PES, is run until it closes on itself (in phase space) with some arbitrary accuracy. Along with the trajectory, the classical action integrals are evaluated for each dimension. Now the initial conditions (in two dimensions the total energy and the initial direction) are adjusted to satisfy the semiclassical quantum conditions for every coordinate i:

$$\oint p_i dx_i = N_i(n_i + 0.5)h \tag{2.2}$$

In this equation n_i is the integer quantum number for coordinate i and N_i is the number of circuits (see Sorbie [16] for an explanation of how to count circuits).

To explain the FGA, we consider a molecule after an electronic excitation. Before (radiative) decay to the ground state has taken place such a system can be described, within the Born-Oppenheimer approximation, by a time-dependent nuclear wave function, or wave packet ($|\chi(t)>$), moving around on the excited state potential energy surface. Initially (at $t = 0$) this wave packet is equal to the ground state nuclear wave function at the moment of the excitation (in the Franck-Condon approximation and

if we assume a constant transition dipole moment). In the FGA, the wave packet is described by a linear combination of time-dependent Gaussian functions. In one-dimension the Gaussian has the following form:

$$g(x,t) = \left(\frac{2\alpha}{\pi}\right)^{\frac{1}{4}} e^{-\alpha_t(x-x_t)^2+\frac{i}{\hbar}p_t(x-x_t)+\frac{i}{\hbar}\gamma_t} \tag{2.3}$$

The time-dependent parameters x_t and p_t correspond to the classical position and momentum of the Gaussian, α_t determines the width of the Gaussian and is kept fixed (or frozen, $\alpha_t = \alpha_0$) and γ_t is the phase of the Gaussian, which is essentially the classical action integral along the classical trajectory (x_t, p_t). We made a modification to this integral (for details see the Appendix).

The absorption spectrum can now be obtained by taking the Fourier transform of the autocorrelation function

$$e(\omega) = \int_{-\infty}^{+\infty} e^{i\omega t} < \chi(0)|\chi(t) > dt \tag{2.4}$$

The energies are determined by measuring the positions of the peaks in the spectrum $e(\omega)$. For practical application of this formula, the autocorrelation is cut off with an exponential function with exponent $(-1/T)$, which results in peaks with a Lorentzian line shape and width $(1/T)$. In our calculations, we used 64 Gaussians for the α coordinate and 8 Gaussians for the R_{NN} coordinate (giving 512 trajectories) and the width of the peaks is taken to be 0.0002 a.u.

2.6 Results

2.6.1 MRSDCI, Pople correction, and CEPA

To introduce the different methods used to obtain the correlation energy, we give the results of a series of calculations of the $^1(4a_g, 5b_u)$ state done at the experimental ground state geometry (Figure 1). All these calculations are based on the same $^1(4a_g, 4b_u)$ ROHF/TZVP+ one electron basis. First we do a SDCI $^1(4a_g, 5b_u)$ calculation and we order the CI vector on decreasing magnitude of the coefficients of the configurations. Now we take, respectively, two, three, four, and eight configurations from the top of the list and use these as reference configurations in four additional calculations. The energy as a function of the total number of configurations is given in Figure 2. In the same figure, the energy obtained with the Pople correction is shown. To obtain a Pople correction in the multireference case, we first perform a small CI calculation between the reference

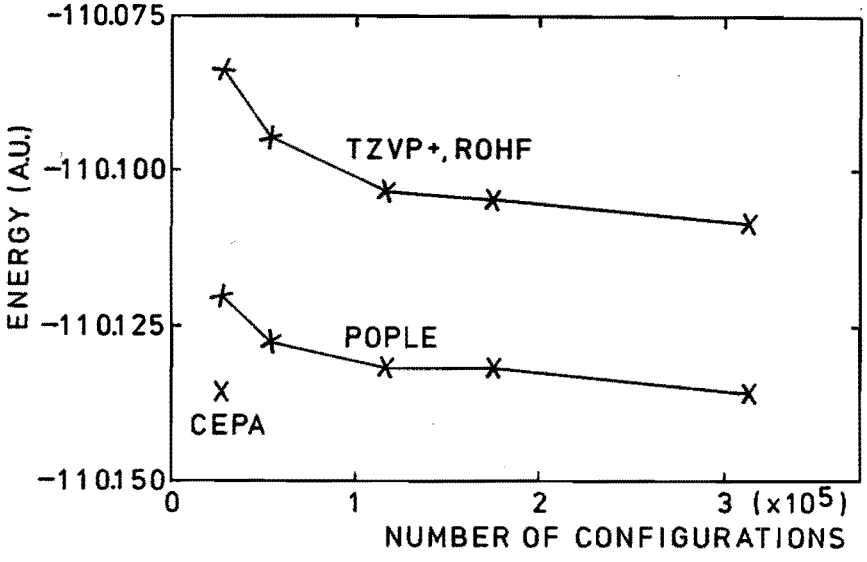

Figure 2. The MRSDCI energy of the $^1(4a_g, 5b_u)$ Rydberg state as a function of the number of configurations. The number of reference functions is, respectively, 1, 2, 3, 4, and 8. The MO's of method (e) are used. The major components of the corresponding CI vectors are given in Table II. The second curve gives the Pople corrected values. The CEPA calculation is based on one reference configuration.

functions, giving an energy E_0 and a wave function $|\Psi_0>$. Now we can use the Pople formula ([3], formula 65), but replace ΔE_{SD} by $E_{MR} - E_0$ and a_0 by $<\Psi_0|\Psi_{MR}>$.

Finally the energy of a CEPA calculation based on one reference function is shown. The energy of the MRSDCI calculations decreases slightly as a function of the number of configurations, but in a way which does not allow for extrapolation. The energy of the MRSDCI+Pople calculations is close to the result of the single reference CEPA calculation. The energy obtained with these methods is much lower, but one should realize that these methods are not variational. Figure 3 gives an analysis of the contribution of the main components of the CI vector and Table II gives the occupation patterns for these configurations. It is clear that the relative importance of the contributions of the configurations to the CI vector strongly depends on the choice of the reference space. The contribution of the main configuration slowly decreases. For the CEPA calculation, this

Table II. The occupation patterns of the six configurations of Figure 3. The excitations patterns are given relative to the $(1a_g^2, 1b_u^2, 2a_g^2, 2b_u^2, 3a_g^2, 3b_u^2, 1a_u^2, 4a_g^2)$-ground state.

1	$4a_g$	$\rightarrow$	$5b_u$
2	$4a_g, 1a_u^2$	$\rightarrow$	$5b_u, 1b_g^2$
3	$1a_u, 3b_u$	$\rightarrow$	$5b_u, 1b_g$
4	$1a_u, 3b_u$	$\rightarrow$	$5b_u, 1b_g$
5	$4a_g, 1a_u^2$	$\rightarrow$	$5b_u, 1b_g, 3b_g$
6	$4a_g$	$\rightarrow$	$6b_u$

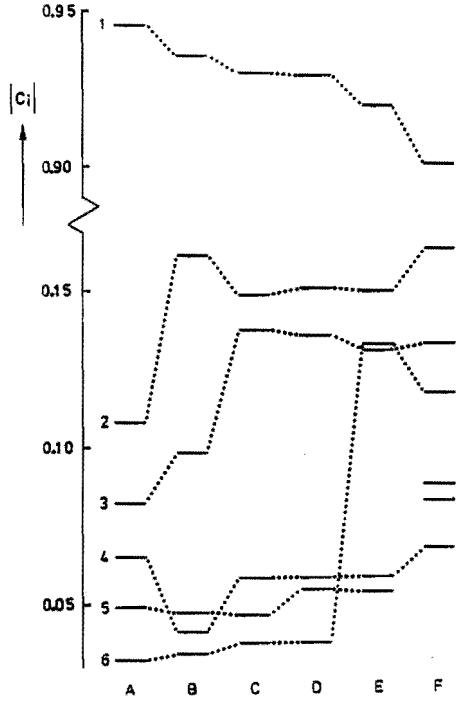

Figure 3. The absolute values of the coefficients of the major configurations (Table II); A–E correspond to the five MRSDCI calculations with increasing numbers of configurations and F corresponds to the CEPA calculation.

Table III. The energies of the ground state ($\widetilde{X}$), the first two Rydberg states [$1B_u = {}^1(4a_g, 4b_u)$, $2B_u = {}^1(4a_g, 5b_u)$], the vertical excitation energies, and the separation of the Rydberg states (Δ).

	$\widetilde{X}$ (a.u.)	$1B_u$ (a.u.)	$2B_u$ (a.u.)	$1B_u$ (eV)	$2B_u$ (eV)	Δ (eV)
Experiment				6.90	7.60	0.70
a	-110.20409	-109.93368	-109.92058	7.36	7.71	0.36
b Q	-110.22526	-109.97888	-109.96333	6.70	7.13	0.42
c P	-110.37122	-110.08576	-110.07721	7.77	8.00	0.23
d P,Q	-110.40388	-110.14244	-110.13197	7.11	7.40	0.28
e P,O	-110.37122	-110.11409	-110.08331	7.00	7.83	0.84
f P,O,Q	-110.40388	-110.15105	-110.12033	6.88	7.72	0.84
g P,O,CEPA	-110.41563	-110.16567	-110.13580	6.80	7.61	0.81

contribution is lower than in the case of the direct CI calculation with eight reference configurations. Evidently this is because the CEPA calculation incorporates the effects of higher excitations. A general rule for the choice of the reference space is that it should give a qualitative description of the surface and since in these calculations the main configuration is far dominant, we see no *a priori* way to choose more reference configurations and all further calculations will be based on one reference function.

2.6.2 Vertical excitation energies

The energies of the ground state and the first two B_u Rydberg states are given in Table III for the seven different methods (see Table I). The vertical excitation energies derived from these data together with the experimental values and the separation of the Rydberg states are also given in Table III.

If we first consider the calculations without the Pople correction (a, c, and e) we find that the excitation energies, which are too high for the TZV+ basis set (a), increase upon adding polarization functions (c). The calculation using the ROHF one electron basis (e) gives much better results. In particular, the separation of the two Rydberg states increases from about 0.2...0.4 to 0.84 eV (experimentally 0.7 eV). Although this might not be surprising since the open shell orbitals are optimized for the lower Rydberg state, note that the Pople correction lowers the excitation energies by about 0.6 eV for the RHF basis (d) and only by about 0.1 eV

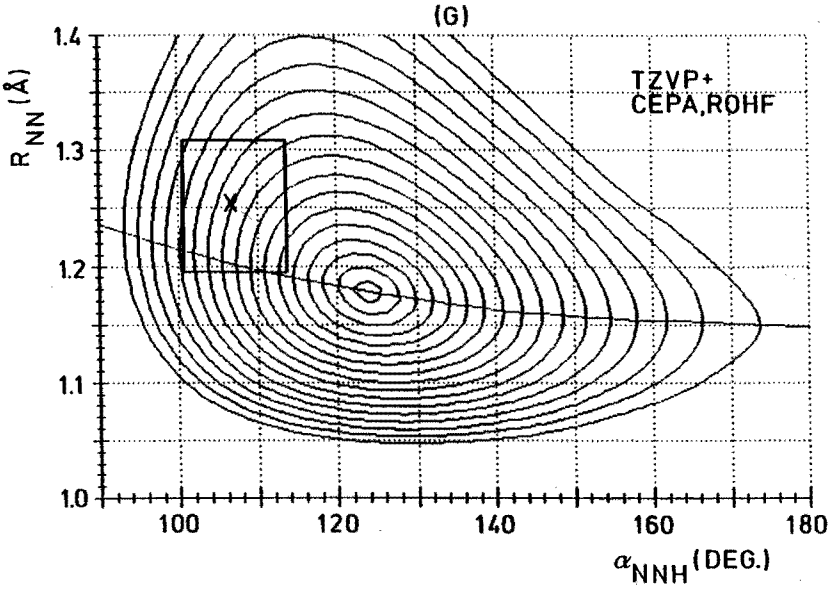

Figure 4. The PES of the $^1(4a_g, 5b_u)$ Rydberg state. The energy of the equipotential curves is $i^2 \times 0.0002$ a.u., relative to the minimum of the surface ($i = 0$). The curve through the minimum of the surface is the R_{NN} equilibrium curve. The cross marks the ground state geometry and the rectangle surrounds the area from which the trajectories used in the FGA start. Only the results of the CEPA calculation [Table I, case (g)] are given here. The results for calculations (a) to (f) are available from the Physics Auxiliary Publication Service [18].

for the ROHF basis (f), for *both* states. The CEPA result is comparable to the ROHF+Pople result and is in very good agreement with experiment (errors less then 0.1 eV).

2.6.3 PES's and spectra

The PES for the CEPA calculation [Table I, case (g)] is shown in Figure 4; the PES's for the other electronic methods are available from the Physics Auxiliary Publication Service [18]. The energy corresponding to the equipotential curve i (start counting from the minimum of the surface) equals $i^2 \times 0.0002$ a.u. The curve through the minimum of the surface gives the equilibrium R_{NN} distance as a function of α_{NNH}. The rectangle identifies the area from which the trajectories (used in the FGA) start and the cross in the center of the rectangle marks the ground state geom-

Table IV. The equilibrium geometry and the harmonic frequencies derived from the PES's in Figure 4. The experimental values for α (in °), R_{NN} (in Å), ν_{NNH} and ν_{NN} (in cm^{-1}) are given, together with the deviations of the different calculations (in %). R_{NH} is kept fixed at the experimental value of 1.028 Å. The experimental values are taken from [10].

		α_{NNH}	R_{NN}	ν_{NNH}	ν_{NN}
Experiment		127.6	1.167	1180.1	1875
a		0.2	0.8	9.5	3.7
b	Q	-0.9	2.3	10.1	-4.3
c	P	-2.4	-1.1	10.4	11.8
d	P,Q	-3.3	0.3	11.2	4.2
e	P,O	-1.9	-0.6	9.6	21.2
f	P,O,Q	-2.4	0.3	9.4	14.1
g	P,O,CEPA	-2.9	0.9	9.5	7.3

etry. The excited state equilibrium geometry and corresponding harmonic frequencies [19] derived from these surfaces are summarized in Table IV.

If we compare (a), (c), and (e) with, respectively, (b), (d), and (f) in Figure 4 and Table IV, we find that the Pople correction lowers the dissociation energy (judged from the number of equipotential curves which reach the R_{NN}=1.4 Å area), increases the R_{NN} equilibrium distance by about 0.9%...1.4% and lowers ν_{NN} by about 8%. The Pople correction has only a small effect on the α_{NNH} angle: the surface is tilted a little toward a smaller α_{NNH}. Considering the CEPA calculation (g), we find the same effects, but somewhat more pronounced. The main effects of extending the basis set with polarization functions [compare (c) with (a)] are: the energy barrier at $\alpha_{NNH} = 180°$ increases, the equilibrium angle α_{NNH} decreases (2.6%), the equilibrium distance R_{NN} decreases (1.9%) and ν_{NN} increases by about 8%. Changing to an open shell basis [compare (e) with (c)] partly cancels these effects except for ν_{NN} which again increases (by about 9%).

The spectra derived from these surfaces are shown in Figure 5. Only the quantum number ν_2 is used to identify the peaks, with no quote for the first progression ($\nu_3 = 0$), one quote for the second progression ($\nu_3 = 1$) and two quotes for the third progression ($\nu_3 = 2$).

Comparing the spectra, we find that the main effect of the Pople correction is to reduce the intensity of the second and - if present at all - the third progression. The relative intensity of the progressions is determined

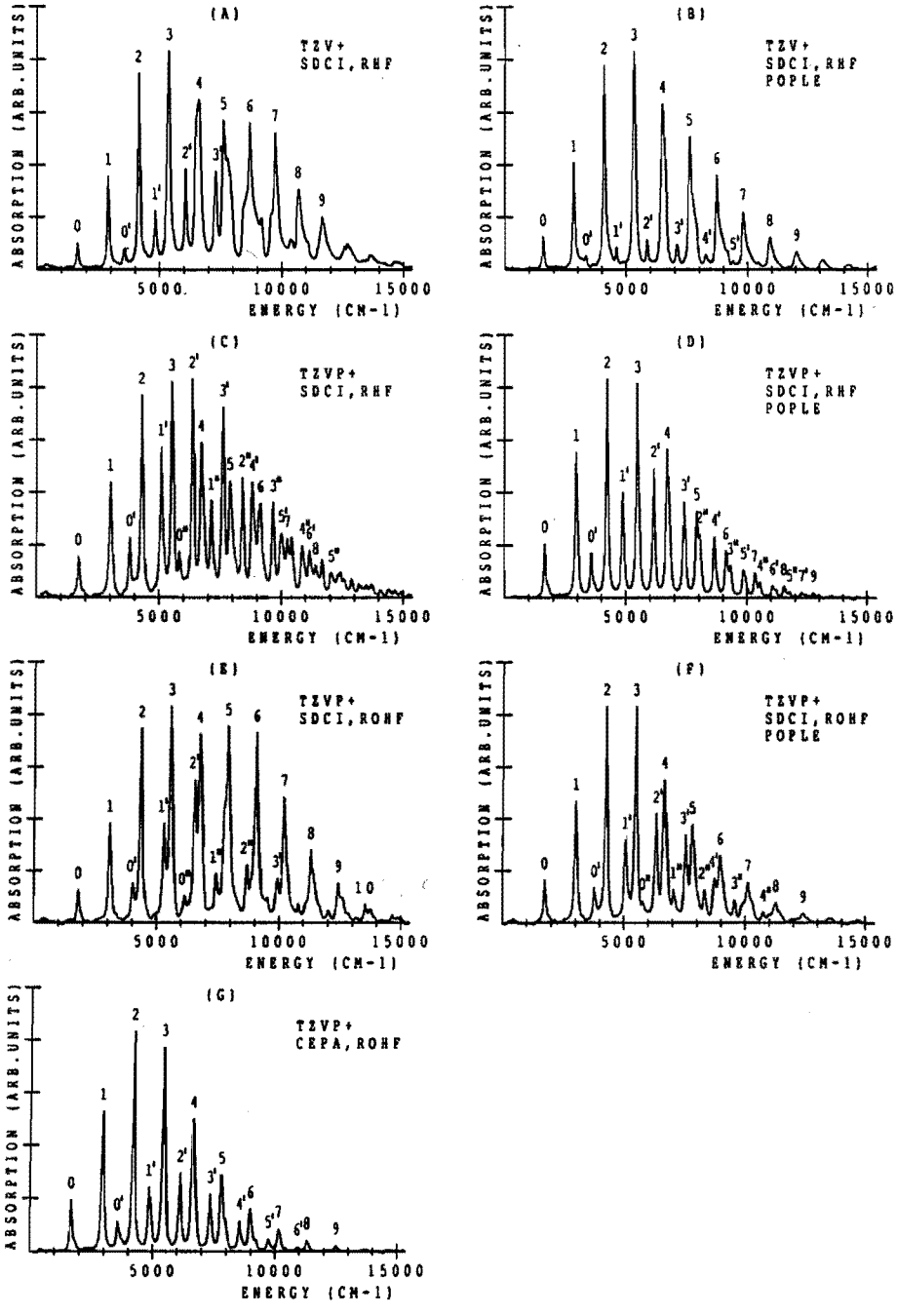

Figure 5. The spectra derived from the seven PES's (Table I and Figure 4). The peaks are labeled with ν_2, with, respectively, 0, 1, or 2 quotes for ν_3=0, 1, or 2.

Table V. The excitation of the R_{NN} stretch. This is the vertical distance between the cross (marking the ground state geometry) and the equilibrium curve in Figure 4.

		Δ (Å)
a		0.041
b	Q	0.019
c	P	0.077
d	P,Q	0.059
e	P,O	0.072
f	P,O,Q	0.060
g	P,O,CEPA	0.050

by the excitation of the R_{NN}-stretch mode, which in turn is related to the vertical distance between the cross (marking the ground state geometry) and the equilibrium curve in Figure 4. These distances are given in Table V.

In the experimental spectrum, we find that the intensity of the absorptions within each progression smoothly increases and decreases as a function of ν_2. This feature is not reproduced bye the first spectrum (a); the absorptions in the first progression between ν_2=5 and ν_2=9 are relative high. Furthermore, the second progression has only four bands and there is no third progression visible. Adding polarization functions (c) seems to resolve these deficiencies, but if an open shell basis is used (e) the spectrum again deteriorates. For the TZV+ basis we see that the Pople correction (b) "smooths" the first progression and increases the number of bands in the second progression, but the α_{NNH}-mode excitation is still too high (absorptions up to ν_2=9 are clearly visible) and the intensity of the second progression is very weak. In the case of the TZVP+ basis, the Pople correction (d) does not improve the spectrum; the main effect is to reduce the intensity of the second and third progressions. Only for the open shell basis does the Pople correction (f) improve the spectrum; the relative high absorption in the first progression at $\nu_2 = 5 \ldots 9$ disappears. In the CEPA calculation (g) we find the same effects as in (f), but again somewhat more pronounced and as a result the third progression completely disappears.

Now that we have discussed qualitatively the shape of the spectra, we will discuss the vibrational frequencies derived from these surfaces by the method of Sorbie (Table VI, again only the results for the CEPA calcula-

Table VI. The vibrational frequencies (in cm^{-1}) calculated by the Sorbie method are labeled by the quantum numbers ν_2 (the α_{NNH}-bending mode) and ν_3 (the R_{NN}-stretching mode). The differences between the frequencies are compared to experiment and the errors are given in % (positive means too high). Only the results of the CEPA calculation [Table I, case (g)] are given here. The results for calculations (a)–(f) are available from the Physics Auxiliary Publication Service [18].

	$\nu_3 = 0$		$\nu_3 = 1$		$\nu_3 = 2$
$\nu_2 = 0$	1641	3 %	3570	0 %	5408
	8 %		10 %		11 %
$\nu_2 = 1$	2920	4 %	4845	1 %	6697
	9 %		10 %		10 %
$\nu_2 = 2$	4177	4 %	6103	1 %	7955
	10 %		11 %		12 %
$\nu_2 = 3$	5416	5 %	7348	2 %	9218
	9 %		9 %		
$\nu_2 = 4$	6636	5 %	8572		10409
	12 %		12 %		
$\nu_2 = 5$	7836	5 %	9766		
	12 %				
$\nu_2 = 6$	9003				

tion are given, the results for the other electronic methods are available from the Physics Auxiliary Publication Service [18]). The vibrational levels are identified by their quantum numbers ν_2 and ν_3. Absolute energies cannot be compared with experiment and so the errors are given (in %) for the *differences* between the energies.

In most cases, the errors increase slightly as a function of the energy, but the variation is always smooth within each mode. In Table VI we find that the error for the α_{NNH}-bending mode varies from 8% ... 12% while the error for the R_{NN}-stretch varies from 0% ... 5%. The error ranges for all seven electronic methods are given in Table VII.

The errors in ν_{NNH} are almost independent of the method. In contrast, the errors in ν_{NN} strongly increase if we add polarization functions to the basis set [compare (c) and (a)], or use an open shell basis (e), and now the Pople correction [compare (b), (d), and (f)] significantly reduces the errors. The CEPA (g) gives the smallest errors for ν_{NN}.

Finally we will compare the frequencies derived directly from the spec-

Table VII. The error ranges for the α_{NNH}-bending mode and the R_{NN}-stretching mode in %, derived from Table VI.

		ν_{NNH}			ν_{NN}		
a		8	...	11	2	...	5
b	Q	8	...	12	−6	...	−4
c	P	9	...	15	11	...	13
d	P,Q	10	...	15	3	...	6
e	P,O	8	...	11	17	...	20
f	P,O,Q	8	...	12	8	...	12
g	P,O,CEPA	8	...	12	0	...	5

tra computed with the FGA, with the results of the Sorbie method. Since the Sorbie method is known to be the more accurate, we use it as a reference. Table VIII gives the deviations of the FGA. The errors range from about +2% in the low energy region to about −2% in the high energy region, so the values are most accurate in region of maximum absorption ($\nu_2 = 2$ or 3), as one would expect.

For one spectrum (c) we also applied the FGA using the unmodified phase integral (see the Appendix). The errors of the frequencies derived from this spectrum are given in Table IX. With this method the errors are much higher and range from +7% in the low energy region to +1% in the high energy region.

2.7 Discussion

Comparing the qualitative shape of the spectra in Figure 5 with experiment, one could draw the conclusion that the SDCI calculation based on the closed shell molecular orbitals with TZVP+ basis set and without the Pople correction (c) gives the best results. This spectrum has three progressions with about the right number of bands and the correct relative intensities. Still we will argue that considering all results in detail reveals that CEPA method, using open shell molecular orbitals and the TZVP+ basis set (g), is superior and that also the Pople correction does give improved results:

(i) Turning from a closed (c) to an open shell (e) basis one would expect better results. Although this is true for some aspects such as the excitation energies, the qualitative shape of the spectrum deteriorates and the error in ν_{NN} increases considerably. But now the Pople correction (f),

Table VIII. The vibrational frequencies derived from the spectra in Figure 5 (the FGA) compared with the Sorbie method (Table VI). The differences are given in %.

	ν_3(a)		ν_3(b)		ν_3(c)			ν_3(d)		
ν_2	0	1	0	1	0	1	2	0	1	2
0	2.4	1.0	2.4	0.8	1.7	0.8	0.2	1.8	0.7	
1	0.6	0.2	0.7	0.3	0.9	0.4	0.0	1.0	0.3	
2	0.0	-0.1	0.3	0.2	0.7	0.4	0.1	0.5	0.4	0.0
3	0.0	-0.1	-0.1	-0.1	-0.1	-0.1	0.0	0.0	-0.1	-0.1
4	0.2		-0.8	-0.7	-0.6	-0.5	-0.3	-0.3	-0.3	-0.4
5	-1.9		-1.6	-1.2	-1.0	-0.7	-0.6	-0.4	-0.3	
6	-2.2		-2.0		-0.3			-0.2	-0.3	
7	-2.5				-0.8			0.0		

	ν_3(e)			ν_3(f)			ν_3(g)	
ν_2	0	1	2	0	1	2	0	1
0	1.8	0.5	-0.1	1.5	0.0	-0.2	1.7	-0.2
1	0.5	0.2	-0.2	0.7	-0.2	-0.3	0.9	-0.1
2	0.4	0.2	-0.2	0.6	0.1	-0.2	0.5	0.1
3	-0.1		0.1	-0.2	-0.2	-0.1	-0.1	-0.3
4	-0.7			-0.8	-0.5	-0.3	-0.4	-0.5
5	-1.1			-1.3			-0.6	-0.5
6				-1.2			-0.4	

Table IX. The same as Table VIII, but now the FGA with the unmodified phase integral (see the Appendix) is used. This is done only for calculation (c).

	$\nu_3(c)$		
ν_2	0	1	2
0	7.4	3.5	2.2
1	4.2	2.6	1.8
2	3.0	2.1	1.5
3	2.5	1.8	1.5
4	2.0	1.4	1.2
5	1.4	1.2	1.0
6	1.2		
7	1.6		

which did not seem to give much improvement in spectrum (d), does give a better spectrum.

(ii) As pointed out in the Introduction, the size consistency error may vary along the PES. From the error ranges for ν_{NN} in Table VII, we conclude that this is indeed the case for the stretching mode, since the Pople correction and the CEPA reduce the errors in ν_{NN} considerably.

(iii) Still remains to be explained why the relative intensity of the progressions in spectrum (c) is much better than in spectrum (g). The relative intensity of the progressions is determined by the energy in the NN-stretch mode which depends on the square of the excitation distance as given in Table V. The difference in excitation between (g) and (c) is only 0.027 Å, but in Table IV we can see that the equilibrium distance of (c) is about 0.013 Å too short, while the equilibrium distance of (g) is about 0.011 Å too long, so in a way the correct relative intensity of the progressions in (c) is accidental. Furthermore, if we compare (c) and (a), we see that extension of the basis set increases the excitation distance which would be favorable to the CEPA calculation (g), but not to the SDCI calculation (c) (the excitation would become too high).

(iv) Concluding these arguments, we note that the vertical excitation energies obtained from the calculations based on the open shell, one electron basis are all much better than the ones based on a closed shell, one electron basis.

If we take the CEPA calculation as the final result we can summarize the accuracies for the different properties: about 0.1 eV for the vertical

excitation energy, 0...5% for ν_{NN}, 8...12% for ν_{NNH}, +1% for R_{NN} and −3% for α_{NNH}. So the errors for the bending mode are higher than for the stretching mode and because the errors do not decrease upon improving the description of the correlation effects (compare the values for α_{NNH} and ν_{NNH} in Table IV), we think that inclusion of *f* functions in the basis set might be needed to reduce those errors.

2.8 Conclusion

Different electronic methods are investigated by comparing the results with experiment. We have shown that when investigating the electron correlation problem it is essential to perform a series of calculations to judge the effect of the basis set incompleteness. The combination with semiclassical dynamical methods to obtain the vibrational fine structure of the spectra appears to be a very fruitful way to test the electronic structure calculations.

We conclude that the direct CI method can be applied successfully to the excited state. In this study we only need one reference function, probably due to the high contribution of this function. The Pople size consistency correction gives an improvement of the description of the stretching mode. Using a CEPA approach and orbitals that are optimized for a nearby open shell Rydberg state seems a good way to obtain reliable results.

Acknowledgements

We would like to thank P. J. A. Ruttink for his work on the MRCEPA program and for reading the manuscript. We also gratefully acknowledge R. Zwaans for implementation of the program and bringing it to my (G. C. G.) attention. The Cyber 205 computer time was financed by the Foundation SURF from the National Fund Supercomputers (NFS).

Appendix: Adaption of the phase integral in the frozen Gaussian approximation.

Heller [17] uses the classical action integral modified by the zero point energy of the frozen Gaussian in each point of the trajectory. Since the width of the Gaussians depends on the initial state, which is determined by the ground state, the vibrational frequencies derived for the excited state by this method depend on the ground state, which is physically

unrealistic. For this part of the phase integral, we use the zero point energy associated with each point of the trajectory and the phase integral becomes independent of the width of the Gaussian.

References

[1] see P. J. Bruna and S. D. Peyerimhoff, Adv. Chem. Phys. **67**, 1 (1987) and references therein.

[2] V. R. Saunders and J. H. van Lenthe, Mol. Phys. **48**, 923 (1983).

[3] J. A. Pople, R. Seeger, and R. Krishnan, Int. J. Quantum Chem. Symp. **11**, 149 (1977).

[4] see Chapter 4 and P. J. A. Ruttink, J. H. van Lenthe, R. Zwaans, and G. C. Groenenboom, J. Chem. Phys. (1991), accepted for publication.

[5] K. Vasudevan, S. D. Peyerimhoff, R. J. Buenker, and W. E. Kammer, Chem. Phys. **7**, 187 (1975).

[6] M. Perić, R. J. Buenker, and S. D. Peyerimhoff, Can. J. Chem. **55**, 1533 (1977).

[7] M. Perić, R. J. Buenker, and S. D. Peyerimhoff, Mol. Phys. **35**, 1495 (1978).

[8] R. A. Back, C. Willis, and D. A. Ramsay, Can. J. Chem. **52**, 1006 (1974).

[9] R. A. Back, C. Willis, and D. A. Ramsay, Can. J. Chem. **56**, 1575 (1978).

[10] P. S. Neudorfl, R. A. Back, and A. E. Douglas, Can. J. Chem. **59**, 506 (1981).

[11] M. Dupuis, D. Spangler, and J. J. Wendoloski, NRCC Program QG01 (Lawrence Berkeley Laboratory, 1980); M. F. Guest, J. Kendrick, *GAMESS User Manual* (Daresbury Laboratory, Daresbury, 1986); M. F. Guest, F. J. Harrison, J. H. van Lenthe, L. C. H. van Corler, Theor. Chim. Acta **71**, 117 (1987).

[12] V. R. Saunders and M.F. Guest, ATMOL3 Part 9, RL-76-106 (1976); M. F. Guest and V. R. Saunders, Mol. Phys. **28**, 819 (1974).

[13] T. H. Dunning Jr., J. Chem. Phys. **55**, 716 (1971).

[14] R. Ahlrichs and P. R. Taylor, J. Chim. Phys. **78**, 315 (1981).

[15] J. Stoer, R. Bulirsch, *Introduction to Numerical Analysis* (Springer, New York, 1980).

[16] K. S. Sorbie, Mol. Phys. **32**, 1577 (1976).

[17] E. J. Heller, J. Chem. Phys. **75**, 2923 (1981).

[18] See AIP document no. PAPS JCPSA-91-3027-10 for 10 pages of in information concerning calculations (a)–(f) (see Table I), the PES's (as in Figure 4) and the vibrational frequencies (as in Table VI). Order by PAPS number and journal reference from American Institute of Physics, Physics Auxiliary Publication Service, 335 East 45th Street, New York, NY 10017. The price is $1.50 for each microfiche (98) pages or $5.00 for photocopies of up to 30 pages, and $0.15 for each additional page over 30 pages. Airmail additional. Make checks payable to the American Institute of Physics.

[19] E. B. Wilson, J. C. Decius, and P. C. Cross, *Molecular Vibrations* (McGraw-Hill, New York, 1955).

Chapter 3

Solving the discretized time-independent Schrödinger equation with the Lanczos procedure[1]

Abstract
A new method is presented to find bound state solutions of the one-, two-, or three-dimensional Schrödinger equation. The equation is turned into a sparse matrix eigenvalue problem by representing the potential energy surface and the wave function on a grid. The Laplacian is represented by a high (10^{th}) order finite difference formula. Eigenvalues are found by the Lanczos procedure [J. Cullum and R. A. Willoughby, J. Comput. Phys. **44**, 329 (1981)] and transition probabilities (Franck-Condon factors) are found by the recursive residue generation method [A. Nauts and R. E. Wyatt, Phys. Rev. Lett. **51**, 2238 (1983)]. Examples are given for the $1D$ Morse-oscillator and the $2D$ Hénon-Heiles potential. Numerical convergence can be checked easily and highly accurate results can be obtained. The algorithm is fast, easy to implement, and vectorizable.

3.1 Introduction

In 1983 Kosloff *et al.* [1, 2] introduced a method to solve the time-dependent Schrödinger equation. This method is based on discretizing space and time on a grid. An initial wave function is represented by its values at the grid points. To perform a time step, the Hamiltonian has to be applied to this wave function. For the potential energy part of the Hamiltonian this simply means a pointwise multiplication of the wave function by the potential energy at the grid points. For the kinetic energy part, the second derivative (or Laplacian) of the wave function at the grid points is needed. Kosloff *et al.* used an N-dimensional fast Fourier transform (FFT), followed by a multiplication with the square of the momentum and an inverse FFT to do this. Even if the Hamiltonian is not explic-

[1] G. C. Groenenboom, H. M. Buck, J. Chem. Phys. **92**, 4374 (1990).

itly time-dependent it can be advantageous to use this method, because energies and transition probabilities can be computed, without the need to compute (and store) eigenfunctions. For example, if the initial wave function is taken to be the lowest vibrational eigenfunction of the electronic ground state of a molecule and the Hamiltonian corresponds to an electronically excited state of this molecule, then the Fourier transform of the autocorrelation function (the overlap between the initial wave function and its time evolution) will give the Franck-Condon spectrum of the corresponding transition [3].

However, we found that for a time-independent problem, a more efficient method to compute eigenvalues and transition probabilities (and, if desired, eigenfunctions) is possible. The key to this method is the Lanczos procedure, introduced by Lanczos [4] in 1950 as a way to recursively generate an orthogonal transformation, which tridiagonalizes a symmetric matrix. The matrix (or the Hamiltonian) enters the formula only through a matrix-vector product, just as in the Kosloff approach. At first the Lanczos procedure seemed to be numerically instable because, due to round-off errors, the orthogonality of the transformation is lost very quickly. Paige [5-7] , however, demonstrated that the spectrum of the tridiagonal matrix contains, amongst others, correct eigenvalues (i.e., good approximations to eigenvalues of the original matrix). Furthermore, it is possible to identify those correct eigenvalues with an ingenious device of Cullum *et al.* [8]. Although the Lanczos procedure is used in numerous applications, work on a completely black-box Lanczos program is still in progress [9] and we will give a short discussion of our implementation in Section 3.3.

If needed, the transition probabilities can be derived from eigenvectors. However, the computation of *one* eigenfunction might take as much computer time as the computation of *all* eigenvalues (see Section 3.5). Fortunately, in 1983 Nauts *et al.* [10, 11] presented the so-called recursive residue generation method (RRGM), a very efficient procedure to calculate transition probabilities, which circumvents the calculation of eigenvectors. A somewhat different approach to the RRGM has been given by Wyatt *et al.* [12].

Before we start a detailed discussion of our method we note that we do not use the Fourier transform technique of Kosloff *et al.* [1, 2] to evaluate the Laplacian, but use a (high-order) finite difference formula instead. The advantage of such a formula is that it is very easy to implement and that only a few additions and multiplications per grid point are needed. Although we did not try the Fourier transform technique, we think that it might be particularly advantageous in the case of periodic boundary conditions.

Finally we note that this method is not variational, i.e., it does not give an upper bound to the energy, but convergence can be checked easily, so that results can be obtained with any desired accuracy.

3.2 The Hamiltonian

3.2.1 The one-dimensional case

We will consider the following $1D$ Hamiltonian (in atomic units, $\hbar = 1$):

$$H = T + V = -\frac{1}{2m}\frac{\partial^2}{\partial x^2} + V(x). \tag{3.1}$$

The wave function $\psi(x)$ is represented on a grid:

$$\psi_i \equiv \psi(x_i);\ x_i = x_0 + i\Delta x;\ i = 0, 1, 2, \ldots, (n_x - 1) \tag{3.2}$$

For the calculation of the eigenvalues $H\psi$ is needed. For the potential energy part we have:

$$V\psi_i \equiv V(x)\psi(x)\mid_{x=x_i} = V_i\psi_i;\ V_i \equiv V(x_i) \tag{3.3}$$

So if the components of ψ_i are arranged as a column vector, then V is a square diagonal matrix with diagonal components V_i.

The simplest finite difference approximation of the Laplacian is the second-order three-point formula:

$$\frac{\partial^2}{\partial x^2}\psi(x)\mid_{x=x_i} = \frac{\psi_{i-1} - 2\psi_i + \psi_{i+1}}{\Delta x^2} + O(\Delta x^2) \tag{3.4}$$

So in matrix notation the kinetic energy operator becomes a tridiagonal matrix:

$$T = -\frac{1}{2m\Delta x^2}\begin{bmatrix} \ddots & & & & & \\ 1 & -2 & 1 & & & \\ & 1 & -2 & 1 & & \\ & & 1 & -2 & 1 & \\ & & & & \ddots \end{bmatrix} \tag{3.5}$$

If the diagonal potential energy matrix is added to this, a tridiagonal Hamiltonian results, which can be diagonalized directly and no Lanczos procedure is needed. This approach can be a convenient tool for one-dimensional potentials.

Table I. The coefficients c_j, used in the $2N^{\text{th}}$ order approximation of the Laplacian (Eq. 6).

N	c_0	c_1	c_2	c_3	c_4	c_5
1	-2	1				
2	$-\frac{5}{2}$	$\frac{4}{3}$	$-\frac{1}{12}$			
3	$-\frac{49}{18}$	$\frac{3}{2}$	$-\frac{3}{20}$	$\frac{1}{90}$		
4	$-\frac{205}{72}$	$\frac{8}{5}$	$-\frac{1}{5}$	$\frac{8}{315}$	$-\frac{1}{560}$	
5	$-\frac{5269}{1800}$	$\frac{5}{3}$	$-\frac{5}{21}$	$\frac{5}{126}$	$-\frac{5}{1008}$	$\frac{1}{3150}$

A higher accuracy can be obtained if a higher-order formula is used (with the same grid constant). The general form of a formula of order $2N$ is

$$\frac{\partial^2}{\partial x^2}\psi(x)|_{x=x_i} = \frac{1}{\Delta x^2}\left[c_0\psi_i + \sum_{j=1}^{N} c_j(\psi_{i-j} + \psi_{i+j})\right] + O(\Delta x^{2N}) \qquad (3.6)$$

The coefficients c_j are obtained by using a Taylor expansion for $\psi_{i\pm j}$:

$$\psi_{i\pm j} = \sum_{k=0}^{\infty} \frac{1}{k!}\psi_i^{(k)}(\pm j\Delta x)^k \qquad (3.7)$$

where

$$\psi_i^{(k)} = \left.\frac{\partial^k \psi(x)}{\partial x^k}\right|_{x=x_i} \qquad (3.8)$$

and substituting this into Eq. (3.6). If terms of the same power in Δx are taken together, a set of linear equations results, from which the coefficients c_j can be derived. For example, for $N = 3$ the equations are (after some rearrangement):

$$\begin{bmatrix} 1 & 2 & 2 & 2 \\ 0 & 1^2 & 2^2 & 3^2 \\ 0 & 1^4 & 2^4 & 3^4 \\ 0 & 1^6 & 2^6 & 3^6 \end{bmatrix} \begin{bmatrix} c_0 \\ c_1 \\ c_2 \\ c_3 \end{bmatrix} = \begin{bmatrix} 0 \\ 1 \\ 0 \\ 0 \end{bmatrix} \qquad (3.9)$$

The results for c_j are given in Table I for $N = 1 \ldots 5$.

Application of these higher-order formula in the $1D$ case will lead to band matrices and the Lanczos procedure can be used to solve the eigenvalue problem. At the boundaries, it is not possible to apply the

central difference formula. We solved this problem by simply putting the wave function equal to zero outside the discretized area, which is a good approximation if the grid is extended far enough into the classically forbidden area for the solution required.

3.2.2 The higher-dimensional case

Extension of this formalism to higher dimensions is very straightforward. As an example we take a $2D$ Hamiltonian:

$$H = -\frac{1}{2m_x}\frac{\partial^2}{\partial x^2} - \frac{1}{2m_y}\frac{\partial^2}{\partial y^2} + V(x,y) \tag{3.10}$$

The wave function (and the potential energy) can again be represented by a single column vector:

$$\psi_{i+jn_x} \equiv \psi(x_i, y_j) \tag{3.11}$$

$$x_i = x_0 + i\Delta x;\ i = 0, 1, 2, \ldots, (n_x - 1) \tag{3.12}$$

$$y_j = y_0 + j\Delta y;\ j = 0, 1, 2, \ldots, (n_y - 1) \tag{3.13}$$

Again the potential energy matrix is diagonal. The kinetic energy matrix is found by using Eq. (3.6) for each dimension. The Hamiltonian will now become a block-structured square matrix with dimension $n = n_x \times n_y$. One can try to choose the optimal grid constants $(\Delta x, \Delta y)$ per dimension, but if all energy levels up to some energy are needed it is profitable to use mass-weighted coordinates ($x' = x\sqrt{m_x}$, $y' = y\sqrt{m_y}$), since then the same grid constant can be used for every dimension. For the maximal representable momentum (p) we have $p\Delta x \approx \pi$. So if we estimate the maximal momentum from $E \approx p^2/(2m)$ we find that we should take Δx proportional to

$$\Delta x \sim \frac{\pi}{\sqrt{2mE}} \quad \text{or} \quad \Delta x\sqrt{m} \sim \frac{\pi}{\sqrt{2E}} \tag{3.14}$$

So in mass-weighted coordinates we can use one grid constant $\Delta' = \Delta x\sqrt{m_x} = \Delta y\sqrt{m_y}$.

3.3 The Lanczos procedure

To find the eigenvalues of a $n \times n$ matrix H (we will restrict ourselves to real symmetric matrices), the user must supply a routine to perform the matrix vector multiplication $H\mathbf{x}$, and a starting vector $\mathbf{q}_1$. Starting

with $\mathbf{q}_1$, an orthonormal basis $Q = \{\mathbf{q}_1, \mathbf{q}_2, \ldots, \mathbf{q}_p\}$ is generated using the following recursion relation ($\beta_1 = 0$):

$$\beta_{i+1}\mathbf{q}_{i+1} = H\mathbf{q}_i - \alpha_i\mathbf{q}_i - \beta_i\mathbf{q}_{i-1} \tag{3.15}$$

$$\alpha_i = (\mathbf{q}_i, H\mathbf{q}_i) \tag{3.16}$$

$$\beta_{i+1} = \|H\mathbf{q}_i - \alpha_i\mathbf{q}_i - \beta_i\mathbf{q}_{i-1}\| \tag{3.17}$$

These equations should not be implemented as given above, but in a slightly different way, which is mathematically equivalent, but numerically favorable [7, 8, 13, 14]. Expressed in the basis Q, H is a symmetric tridiagonal matrix (T_p, after the p^{th} recursion) with diagonal elements α_i and off-diagonal elements β_i. In exact arithmetic this process would halt after n iterations with $\beta_{n+1} = 0$, and all eigenvalues of the tridiagonal matrix T_n would correspond to the eigenvalues of H, but due to round-off errors the vectors $\mathbf{q}_i$ will fail to be orthogonal and β_i usually never even becomes small. But if we follow the spectrum of T_p if p increases we will note some remarkable features. The eigenvalues will start converging from both ends of the spectrum. If for example $n = 10\,000$ (corresponding to a $10\,000 \times 10\,000$ matrix) the first eigenvalue may be converged after 50 iterations (recursion steps). In the next iterations, where other eigenvalues start converging, the process seems to "forget" that it has found the first one and begins to produce a copy of this first eigenvalue. Converged eigenvalues do not disappear if the iterations proceed and so the multiple copies are a reliable indicator to detect converged eigenvalues.

Besides those multiple copies also some "incorrect eigenvalues" are produced. Those eigenvalues, called spurious, can be identified by the following procedure [8]: after the eigenvalues ϵ_α of T (we dropped the index p) are computed, a tridiagonal matrix $T^{(u)}$ is formed by removing the first row and the first column of T. The eigenvalues ϵ_α of T and $\epsilon_\alpha^{(u)}$ of $T^{(u)}$ should form a so-called Sturm sequence [10]: $\epsilon_\alpha < \epsilon_\alpha^{(u)} < \epsilon_{\alpha+1} < \epsilon_{\alpha+1}^{(u)}$. If, however, a value in one list is equal to a value in the other list, it can be labeled as spurious. Some of the remaining values, which neither have multiple copies, nor can be labeled as spurious, will be converged and some not. These remaining values could of course be checked by computing the corresponding eigenvectors ψ_α and verifying whether the residues $\|H\psi_\alpha - \epsilon_\alpha\psi_\alpha\|$ are small, but this can be a very time-consuming job (see Section 3.5). Again there is an easy way around [13]: the residues can be estimated as the product of β_i (of the last iteration) and the last component of an eigenvector of T. This takes little computer time since T is tridiagonal and is usually of much lower dimension than H. Since the eigenvalues of T are known accurately, an eigenvector of T can be found by one step of inverse iteration [15].

3.4 RRGM

Very often not all components of an eigenvector are needed, but just the square of the scalar product with some other vector, e.g., Franck-Condon factors. With the recursive residue generation method [10-12] we can compute the squares of these inner products (called residues, not to be confused with the residues in Section 3.3), without the need to compute the eigenvectors! First we have to start the Lanczos procedure with the vector $\mathbf{q}_1$, for which we want the residues. Then we have to calculate the two lists of eigenvalues ϵ_α and $\epsilon_\alpha^{(u)}$, and remove (from *both* lists) the multiple copies and the spurious values. Now we can use the following formula to calculate the residues (after p iterations):

$$R(\alpha) = |<\mathbf{q}_1|\psi_\alpha>|^2 = \frac{(\epsilon_\alpha - \epsilon_1{}^{(u)})\cdots(\epsilon_\alpha - \epsilon_{p-1}{}^{(u)})}{(\epsilon_\alpha - \epsilon_1)\cdots(\epsilon_\alpha - \epsilon_{\alpha-1})(\epsilon_\alpha - \epsilon_{\alpha+1})\cdots(\epsilon_\alpha - \epsilon_p)} \tag{3.18}$$

Note that we did *not* remove the unconverged eigenvalues from the lists.

3.5 Eigenvectors

Despite the RRGM it is sometimes desirable to compute the eigenvectors, e.g., to check the program, to check the convergence or to make a plot of a two-dimensional wave function to unambiguously assign quantum numbers. The most obvious way to get an eigenvector of H is to take an eigenvector of T and use the basis Q to transform it back [13, 14]. If the basis vectors are too large to be stored (even on a secondary storage device) during the Lanczos process, they can be regenerated to do the back transformation, for each eigenvector. A disadvantage of this approach is that the optimum number of iterations must be determined *before* the regeneration of the basis. This must be done to avoid the regeneration of too many basis vectors, which may cause an accumulation of round-off errors. An alternative approach is inverse iteration directly on $(H - \epsilon_\alpha I)$ [14], solving

$$(H - \epsilon_\alpha I)\psi = \mathbf{q}_1 \tag{3.19}$$

This is done using the SYMMLQ routine [16, 17]. This routine is essentially the Lanczos procedure, followed by an LQ decomposition to solve the resulting tridiagonal indefinite set of equations. The routine is implemented in such a way that it can be applied iteratively: at every step of the Lanczos procedure the LQ decomposition and its solution are updated.

3.6 Examples

3.6.1 The Morse-oscillator; Convergence behavior

In a numerical example we will show that the order of convergence of the method is equal to $2N$ (Eq. 3.6), as it should be. Furthermore, we will show the effect of the choice of the boundaries of the grid. As a model problem we take a $1D$ Hamiltonian with the Morse potential used by Dagher and Kobeissi [18]:

$$V(x) = D(1 - e^{-\alpha(x-x_0)})^2 \tag{3.20}$$

with

$$\begin{aligned} D &= \omega_e^2/4\omega_e x_e && (3.21)\\ \alpha &= (k\omega_e x_e)^2 && (3.22)\\ x_0 &= 2.408\,73 && (3.23)\\ \omega_e &= 48.668\,88 && (3.24)\\ \omega_e x_e &= 0.977\,888 && (3.25)\\ k &= 1 && (3.26) \end{aligned}$$

The theoretical eigenvalues are

$$E_\nu = \omega_e(\nu + \frac{1}{2}) - \omega_e x_e(\nu + \frac{1}{2})^2 \tag{3.27}$$

Note that we use Dagher's units, Å and cm^{-1}, and that now in Eq. (3.1) $m = 0.5$. We will consider the $\nu = 10$ energy level with $E_{10} = 403.211\,088$ cm^{-1}. The classical turning points of this level are 1.81 and 4.12 Å. For the left boundary of the grid we take a "safe" value of $x_{\text{left}} = 0.8$ Å throughout and for the right boundary we first take a rather tight value of $x_{\text{right}} = 4.64$ Å. We check the order of convergence for $N = 1$, $N = 3$, and $N = 5$. For each value of N the grid constant (Δx) is varied between 0.01 and 0.16 Å. The absolute value of the relative error in $\tilde{E}_{10}$ as a function of the grid constant is shown in a double logarithmic plot (Figure 1).

Curves A, B, and C correspond to, respectively, N=1, 3, and 5. The slopes of those curves are (within a few percent) equal to the order $(2N)$ of the method used, as they should, except that the errors become approximately constant below a critical grid constant (curves B and C). In order to show that the choice of the right boundary of the grid causes this limited accuracy, we slightly relaxed the right boundary to $x_{\text{right}} = 4.96$ Å and repeated the calculation for $N = 5$ (curve D). This 0.32 Å increase

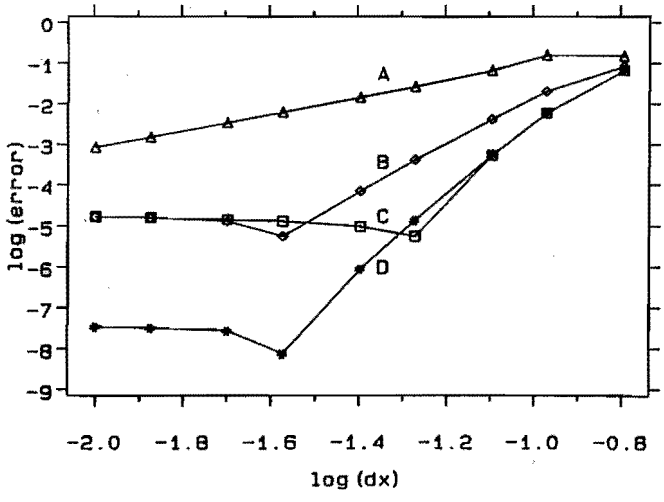

Figure 1. The error in the tenth energy level of the Morse-oscillator (Eq. 3.20), as a function of the grid constant dx. (A) Using the second order approximation for the Laplacian, (B) the sixth order, (C) the tenth order, (D) also the tenth order, but with an extended grid. It is clear that the limited accuracy for small grid constants is caused by the grid size.

of the grid size already gives a 500 times better accuracy. The "dip" in curves B, C, and D is caused by a change of the sign of the error: For large grid constants the calculated energy is too low, while for small grid constants the energy is "pushed up" at the boundaries.

3.6.2 The Hénon-Heiles potential

In this second example we will show the application of our method to calculate the energy levels and Franck-Condon (FC) factors in a two-dimensional system. We use the same potential model as Gray [19] in a study to bound-bound FC factors. The masses are $m_x = m_y = 1$. The lower potential energy surface is given by

$$V_l(x,y) = \frac{1}{2}0.36(x-2)^2 + \frac{1}{2}1.96(y-2)^2 \tag{3.28}$$

and the upper potential energy surface is given by

$$V_u(x,y) = \frac{1}{2}0.49x^2 + \frac{1}{2}1.69y^2 - 0.1x(y^2 + 0.1x^2) \tag{3.29}$$

Gray gives the quantum mechanical eigenvalues and FC factors for eight vibrational levels. The upper surfaces has also been used by Swimm and Delos [20], who report the quantum mechanical eigenvalues (calculated by Don Noid) of all (83) levels up to the escape energy. The escape energy, i.e., the energy of the saddle point of the potential energy surface at $(x, y) = (8.45,\ 4.47)$, is 11.46. We used the analytic expression of the lowest harmonic oscillator function corresponding to the lower surface to generate the starting vector for the Lanczos procedure. Convergence was established in the following way: on a grid with $x_{\min} \cdots x_{\max} = -6.8 \cdots 10.8$ and $y_{\min} \cdots y_{\max} = -7.0 \cdots 7.0$ we did three calculations with a grid constant Δx of, respectively, 0.4, 0.2, and 0.1 (calculations A, B, and C), then we repeated the one with Δx=0.1 on an extended grid with $x_{\min} \cdots x_{\max} = -7.6 \cdots 11.6$ and $y_{\min} \cdots y_{\max} = -7.8 \cdots 7.8$ (calculation D). For those four calculations, respectively, 1500, 2000, 3800, and 3800 Lanczos steps were required. A convergence factor was calculated for each energy level with the following formula:

$$\mathrm{conv}_i = \frac{E_i^{(\mathrm{A})} - E_i^{(\mathrm{B})}}{E_i^{(\mathrm{B})} - E_i^{(\mathrm{C})}} \tag{3.30}$$

(for the highest energy levels it is of course not always possible to match corresponding levels). Theoretically these values should be equal to 1024 in the convergence area. We selected all values with $\mathrm{conv}_i > 200$. Then we estimated the relative error of these energies as

$$D1_i = \frac{E_i^{(\mathrm{B})} - E_i^{(\mathrm{C})}}{E_i^{(\mathrm{C})}} \tag{3.31}$$

and

$$D2_i = \frac{E_i^{(\mathrm{D})} - E_i^{(\mathrm{C})}}{E_i^{(\mathrm{C})}} \tag{3.32}$$

for, respectively, the error due to the noninfinitesimal grid constant and the error due to the finite grid size. In Table II we give all $E_i^{(\mathrm{D})}$ with $\mathrm{conv}_i > 200$, $D1_i < 10^{-5}$, and $D2_i < 10^{-5}$. In a similar analysis of the FC factors we found that these are accurate to at least seven figures. If we add up all the FC factors of the converged levels we find that they cover more then 99.98% of the spectrum. Our results are in virtual perfect agreement with the energy levels reported by Swimm *et al.* [20] and the FC factors of Gray [19].

Finally we calculated the eigenvector corresponding to the 52nd energy level $[(N_x, N_y) = (5, 4), E_{52} = 9.1882]$. A contour map of this function is shown in Figure 2. For this function the residue $\|H\psi\|/\|\psi\|$ is 2.5×10^{-10}

Table II. The quantum numbers, energy levels, and Franck-Condon factors for the Hénon-Heiles system.

n	N_x	N_y	E_n	FC	conv[a]	$\log(D1)$[b]	$\log(D2)$[c]
1	0	0	0.995 52	0.023 556	766	-8.7	-12.8
2	1	0	1.686 99	0.029 224	780	-8.8	-12.9
3	0	1	2.278 13	0.080 722	732	-7.9	-14.0
4	2	0	2.375 04	0.019 003	802	-8.6	-13.0
5	1	1	2.958 35	0.083 551	728	-8.0	-14.0
6	3	0	3.059 55	0.008 347	796	-8.2	-11.9
7	0	2	3.547 95	0.127 752	698	-7.4	-14.0
8	2	1	3.634 66	0.044 951	734	-8.1	-14.0
9	4	0	3.740 44	0.002 643	775	-7.8	-10.9
10	1	2	4.216 18	0.104 693	692	-7.4	-14.0
11	3	1	4.306 91	0.015 994	748	-8.0	-12.5
12	5	0	4.417 58	0.000 605	748	-7.4	-10.0
13	0	3	4.804 26	0.122 768	663	-6.9	-13.1
14	2	2	4.879 94	0.043 927	688	-7.5	-12.9
15	4	1	4.974 93	0.003 886	755	-7.8	-11.6
16	6	0	5.090 86	0.000 094	718	-7.1	-9.1
17	1	3	5.459 66	0.073 642	656	-6.9	-13.5
18	3	2	5.538 99	0.011 715	690	-7.5	-12.1
19	5	1	5.638 52	0.000 612	745	-7.5	-10.6
20	7	0	5.760 14	0.000 008	684	-6.8	-8.4
21	0	4	6.046 27	0.079 246	628	-6.5	-13.0
22	2	3	6.109 89	0.021 888	650	-7.0	-13.2
23	4	2	6.193 07	0.001 890	698	-7.4	-11.0
24	6	1	6.297 46	0.000 051	723	-7.2	-9.8
25	8	0	6.425 27	0.000 000	639	-6.6	-7.6
26	1	4	6.687 82	0.030 559	620	-6.5	-13.6
27	3	3	6.754 62	0.003 776	647	-7.0	-12.1
28	5	2	6.841 87	0.000 145	706	-7.3	-10.1
29	7	1	6.951 49	0.000 001	696	-6.9	-9.0
30	9	0	7.086 07	0.000 000	572	-6.3	-7.0
31	0	5	7.273 05	0.035 905	594	-6.2	-14.0
32	2	4	7.323 37	0.005 343	613	-6.5	-12.5
33	4	3	7.393 45	0.000 266	647	-7.0	-11.0
34	6	2	7.485 01	0.000 001	701	-7.2	-9.2
35	8	1	7.600 29	0.000 000	665	-6.7	-8.3
36	10	0	7.742 35	0.000 000	471	-6.1	-6.4
37	1	5	7.899 55	0.006 922	586	-6.2	-13.3

n	N_x	N_y	E_n	FC	conv[a]	log($D1$)[b]	log($D2$)[c]
38	3	4	7.952 40	0.000 401	608	-6.6	-11.3
39	5	3	8.025 88	0.000 000	650	-7.0	-10.1
40	7	2	8.122 03	0.000 001	679	-7.0	-8.4
41	9	1	8.243 47	0.000 000	624	-6.5	-7.6
42	11	0	8.393 85	0.000 000	343	-5.8	-5.8
43	0	6	8.483 48	0.011 598	563	-5.9	-13.5
44	2	5	8.518 97	0.000 422	578	-6.2	-12.0
45	4	4	8.574 28	0.000 000	605	-6.6	-10.1
46	6	3	8.651 29	0.000 003	653	-6.9	-9.2
47	8	2	8.752 36	0.000 000	632	-6.7	-7.7
48	10	1	8.880 52	0.000 000	565	-6.3	-7.0
49	12	0	9.040 27	0.000 000	220	-5.4	-5.3
50	1	6	9.093 44	0.000 566	554	-5.9	-11.7
51	3	5	9.130 48	0.000 000	572	-6.2	-10.7
52	5	4	9.188 22	0.000 008	602	-6.6	-9.1
53	7	3	9.268 90	0.000 001	644	-6.8	-8.3
54	9	2	9.375 22	0.000 000	546	-6.5	-7.0
55	11	1	9.510 75	0.000 000	478	-6.0	-6.4
56	0	7	9.676 24	0.002 663	534	-5.6	-12.9
57	13	0	...	...	...	...	...
58	2	6	9.694 81	0.000 003	546	-5.9	-9.3
59	4	5	9.733 06	0.000 024	567	-6.2	-11.5
60	6	4	9.793 16	0.000 001	592	-6.5	-8.1
61	8	3	9.877 61	0.000 000	604	-6.6	-7.7
62	10	2	9.989 53	0.000 000	404	-6.2	-6.3
63	12	1	10.133 1	0.000 000	362	-5.8	-5.9
64	1	7	10.267 6	0.000 005	525	-5.7	-10.1
65	3	6	10.286 1	0.000 011	538	-5.9	-9.0
66	14	0	...	...	...	...	...
67	5	5	10.325 3	0.000 001	530	-6.2	-8.0
68	7	4	10.387 6	0.000 000	279	-6.1	-7.3
...	...	...	...	...	...	...	...
72	0	8	10.847 8	0.000 017	477	-5.6	-6.6
73	2	7	10.849 3	0.000 412	511	-5.5	-7.3
74	4	6	10.865 7	0.000 026	296	-5.7	-5.9

[a]The convergence factor (Eq. 3.30).
[b]Estimate of the relative error due to the noninfinitesimal grid constant (Eq. 3.31).
[c]Estimate of the relative error due to the finite grid size (Eq. 3.32).

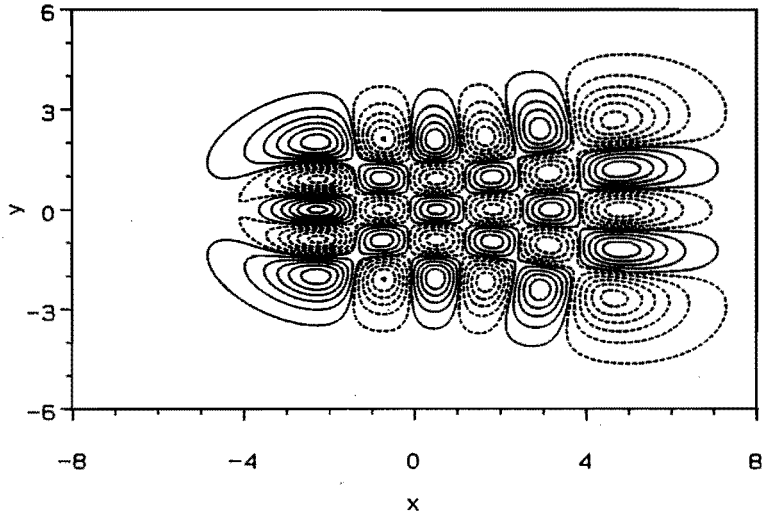

Figure 2. A contour map of the vibrational wave function (5,4) for the Hénon-Heiles system. The contour levels are shown for the following values: $\pm 0.001, \pm 0.005, \pm 0.010, \pm 0.015, \pm 0.020$, and ± 0.025.

and the energy agrees with the Lanczos value to more then 12 significant figures. The FC factor calculated from this eigenfunction agrees with the one calculated with the RRGM to 10^{-12} (seven significant figures).

3.7 Conclusion

We have presented a new method to solve a low-dimensional Schrödinger equation. The method is based on a discrete representation of the problem and so it can handle arbitrary potential energy surfaces without the need to evaluate complicated integrals. In this sense it compares favorably to conventional basis expansion methods. Although our method is not variational we have shown that numerical convergence can easily be obtained.

The implementation of the method on a computer is simple, it can be split in four separate programs: (1) a program to generate the potential energy surface and the starting vector, (2) the Lanczos procedure, to generate the tridiagonal matrices T and $T^{(u)}$ and to find their eigenvalues, (3) a program to analyze the output of (2) and to remove the spurious values, to find the converged ones, and to calculate the residues (the FC factors),

and (4) a program to find eigenvectors if required.

The method is extremely efficient for $1D$ potentials and a microcomputer will be sufficient to handle most $1D$ cases. In fact Turbo Pascal on an IBM AT was used to develop and test the programs. $2D$ problems can better be handled by a main frame: a double precision Fortran 77 version of the program on a VAX 8530 took approximately two hours for the Hénon-Heiles problem calculation D.

Since the most time consuming part of the program is the sparse matrix vector multiplication $H\psi$, which is very well suited for vectorization, it must be possible to tackle fairly complicated $3D$ problems on a (mini) supercomputer.

References

[1] D. Kosloff and R. Kosloff, J. Comput. Phys. **52**, 35 (1983).

[2] R. Kosloff and D. Kosloff, J. Chem. Phys. **79**, 1823 (1983).

[3] E. J. Heller, Acc. Chem. Res. **14**, 368 (1981).

[4] C. J. Lanczos, J. Res. Natl. Bur. Stand. **45**, 255 (1950).

[5] C. C. Paige, Ph.D. thesis, University of London, 1971.

[6] C. C. Paige, J. Inst. Math. Appl. **10**, 373 (1972).

[7] C. C. Paige, J. Inst. Math. Appl. **18**, 341 (1976).

[8] J. Cullum and R. A. Willoughby, J. Comput. Phys. **44**, 329 (1981).

[9] B. N. Parlett and B. Nour-Omid, Comput. Phys. Commun. **53**, 169 (1989).

[10] A. Nauts and R. E. Wyatt, Phys. Rev. Lett. **51**, 2238 (1983).

[11] N. Moiseyev, R. A. Friesner, and R. E. Wyatt, J. Chem. Phys. **85**, 331 (1986).

[12] R. E. Wyatt and D. S. Scott, in *Large Scale Eigenvalue Problems*, edited by J. Cullum and R. A. Willoughby (Elsevier, North-Holland, 1986), p. 67.

[13] B. N. Parlett, *The Symmetric Eigenvalue Problem* (Prentice-Hall, Englewood Cliffs, NJ, 1980), Chap 13.

[14] J. Cullum and R. A. Willoughby, in *Numerical Analysis Proceedings, Dundee 1979*, edited by G. A. Watson (Springer, Berlin, 1980), Lecture Notes in Mathematics No. 773, p. 46.

[15] J. H. Wilkinson and C. Reinsch, *Handbook for Automatic Computation, Vol 2, Linear Algebra* (Springer, Berlin, 1971).

[16] C. C. Paige and M. A. Saunders, *Solution of Sparse Indefinite Systems of Equations and Least Squares Problems*, Tech. Rep. CS 399 (Stanford University, Stanford, CA, 1973).

[17] C. C. Paige and M. A. Saunders, Siam J. Numer. Anal. **12**, 617 (1975).

[18] M. Dagher and H. Kobeissi, J. Comput. Chem. **9**, 647 (1988).

[19] S. K. Gray, M. S. Child, and D. W. Noid, Mol. Phys. **54**, 573 (1985).

[20] R. T. Swimm and J. B. Delos, J. Chem. Phys. **71**, 1706 (1979).

Chapter 4

CEPA-type size consistency corrections for MRSDCI calculations, MRCEPA[1]

Abstract
A new size consistent extension to the multireference CI method is described. The method termed multireference Coupled Electron Pair Approximation (MRCEPA) is akin to a multireference CEPA(0) approach, though nonlinear terms do receive separate attention. We show the performance of the approach in some model systems as well as in an application to calculation of ground and excited $\pi\pi^*$ states of ethylene.

4.1 Introduction

The Coupled Electron Pair Approximation (CEPA) method has the advantage over the SDCI method (CI with all single and double replacements) that it yields size consistent results with only a slight increase in computational effort. Here size consistency means that the energy of two subsystems is additive if the subsystems do not interact. It may be successfully applied to both closed [1] and open [2] shell systems, provided that a single Configuration State Function (CSF), e.g., the restricted Hartree-Fock determinant, is dominant in the correlated wave function. However, if there are low lying excitations (in case of multi-bond dissociation, open shell systems with high symmetry), more than one CSF is needed for a proper zeroth order description of the wave function [3, 4].

Fairly accurate results may be obtained using the MRSDCI method. However, since any restricted CI calculation suffers from size consistency defects, an extension of the CEPA method to Multi Configuration (MC) reference sets is called for. In the following a method is proposed, which includes size consistency corrections in MRSDCI calculations in a manner analogous to the CEPA(0) method, provided that the reference configuration set is complete in the active orbital space. Thus our starting wave

[1] P. J. A. Ruttink, J. H. van Lenthe, R. Zwaans, and G. C. Groenenboom, J. Chem. Phys. (1991), accepted for publication.

function is a second order CI function and the resulting function will accordingly be called the second order CEPA function.

In practice, our method amounts to shifting the diagonal H-matrix elements of the single and double excitations, as in the CI-type implementation of the CEPA method [5]. However, our method differs from the straightforward generalization of the CEPA(0) method to MC reference sets, which should be identical to the linearized version of the MC reference Coupled Cluster development [6-12]. Since the nonlinear terms in our modified MRSDCI equations are potentially important, they should receive proper attention when formulating size consistency corrections for wave functions based on a MC reference configuration set.

The results obtained by this method will be compared to results of the Averaged Coupled Pair Functional (ACPF) theory, as introduced recently by Gdanitz and Ahlrichs [13] and which may also be considered as a generalisation of the CEPA (or CPF) philosophy to MC reference configuration sets.

In Section 4.2 the method used for modifying the MRSDCI equations will be discussed. Applications to some model systems, including comparison with full CI and MRACPF [13] results, are reported in Section 4.3 and the method is applied to the calculation of ground and excited states of ethylene in Section 4.4. Finally conclusions are drawn in Section 4.5.

4.2 Theory

In this section the size consistency corrections for 2$^{\text{nd}}$ order wave functions will be discussed in terms of the spin orbital formalism. Our reasoning is analogous to the derivation of the CPA equations by Hurley [14].

4.2.1 Wave functions

The 2$^{\text{nd}}$ order wave function to be used is designated by

$$|\Psi_C> = \sum_R c_R|R> + \sum_i c_i|A_i> \qquad (4.1)$$

where the reference configuration set $\{|R>\}$ is assumed to be complete within some (small) orbital subset (the active spin orbitals) and the set $\{|A_i>\}$ contains all single and double excitations with respect to any $|R>$.

The size consistency corrections to be applied to the CI secular equations for this function will be calculated in the form of diagonal H-matrix element shifts. These shifts are calculated by assuming that the 2$^{\text{nd}}$ order

CEPA function may be approximated by the corresponding MC reference Coupled Cluster function [6-8] with internal contraction [15]:

$$|\Psi_{CC}>= e^T|0> \tag{4.2}$$

where the reference function $|0>$ is given by:

$$|0>= \frac{\sum_R c_R|R>}{(\sum_R c_R^2)^{\frac{1}{2}}} \tag{4.3}$$

with the same coefficients c_R as in Eq. (4.1). The operator T generates all single and double excitations with respect to any $|R>$,

$$T = \sum_{\mu\rho} t_{\mu\rho}\tau_{\mu\rho} + \sum_{\mu\nu\rho\sigma} t_{\mu\nu,\rho\sigma}\tau_{\mu\nu\rightarrow\rho\sigma} \tag{4.4}$$

where τ is an excitation operator, t is the corresponding connected cluster amplitude, μ and ν are inactive or active spin orbital indices, and ρ and σ are active or external spin orbital indices. According to Eq. (4.3), the reference function $|0>$ is normalized. The excitation operators are defined such that they yield normalised excited functions $\tau|0>$, i.e., we assume

$$<0|\tau^\dagger\tau|0>= 1 \tag{4.5}$$

We do not need the explicit form of T, as given by Eq. (4.4). Instead, we define excitation classes as follows: The excitation class (k,l) contains all excitations with k holes in the inactive orbitals and l particles in the external orbitals. Since the number of electrons in the active orbitals is not fixed, k and l may differ from each other. Equation (4.4) is thus equivalent to

$$T = \sum_{kl} T(k,l)\,;\ 0 \le k,l \le 2,\ \text{except } k = l = 0 \tag{4.6}$$

We also use the corresponding projection operators $P(k,l)$ and the projection operators P_0, P_a, and P_b defined by:

$$\begin{aligned} P_0 &= P(0,0) \\ P_a &= \sum_{kl} P(k,l)\,;\ 0 \le k,l \le 2,\ \text{except } k = l = 0 \\ P_b &= \sum_{kl} P(k,l)\,;\ k > 2 \text{ or } l > 2 \end{aligned} \tag{4.7}$$

Thus P_0 projects to the reference configuration space, P_a projects to the interacting space of the reference configurations spanned by the set $\{|A_i>\}$

and P_b projects to the space spanned by all higher excitations. In practice P_b may be considered to project to the interacting space of the set $\{|A_i>\}$.

In the following we assume that the 2nd order CEPA function may be written as

$$|\Psi_C>=(P_0+P_a)|\Psi_{CC}>=\left[1+P_a e^T\right]|0> \tag{4.8}$$

This function will be used for calculating the size consistency corrections to be applied to the 2nd order SDCI function in order to obtain the 2nd order CEPA function.

4.2.2 The diagonal H-matrix element shift

The Coupled Cluster function is assumed to satisfy the following equations

$$<0|(H-E)e^T|0> = 0 \tag{4.9}$$

$$<0|\tau^\dagger(H-E)e^T|0> = 0\,;\ \text{for each } \tau \tag{4.10}$$

Since the higher excitations in Ψ_{CC} (viz that part of Ψ_{CC} which is given by $P_b\Psi_{CC}$) do not interact with any reference configuration $|R>$, Eq. (4.9) is identical to the first secular equation for the corresponding CI problem:

$$E=<0|H|0>+<0|HT|0>=E_0+E_{corr} \tag{4.11}$$

Using Eqs. (4.2), (4.7) and (4.8), Eq. (4.10) may be rewritten as

$$<0|\tau^\dagger(H-E)|\Psi_C>+<0|\tau^\dagger H P_b e^T|0>=0 \tag{4.12}$$

The second term in Eq. (4.12), which is missing in the secular equations for the SDCI function, will be used to obtain the size consistency corrections wanted. To this end we note that Eq. (4.12) may be rewritten as:

$$<0|\tau^\dagger(H+\Delta H_\tau-E)|\Psi_C>=0 \tag{4.13}$$

provided that the diagonal shift ΔH_τ is given by

$$\Delta H_\tau=\frac{<0|\tau^\dagger H P_b e^T|0>}{<0|\tau^\dagger|\Psi_C>} \tag{4.14}$$

In the following, Eqs. (4.13) and (4.14) will be taken as the set of equations to be satisfied by the 2nd order CEPA function Ψ_C. These equations lead to a pseudo eigenvalue problem, since the shifts ΔH_τ depend on the connected cluster amplitudes in T, or, equivalently, on the configuration coefficients c_i in Ψ_C.

Note that the coefficients c_i in Eq. (4.1) are not identical to the connected cluster amplitudes t in Eq. (4.4) since the c_i will contain contributions from disconnected clusters [16, 17].

In the following, Eq. (4.14) is simplified using two approximations which are analogous to the approximations used in the CEPA(0) method.

4.2.3 The direct term approximation

This approximation was introduced by Kelly and Sessler [18, 19]. In our formalism it takes the following form. In the expansion of $\exp(T)|0>$ in Eq. (4.14) only those terms are retained which contain τ. The selection of terms thus depends on the excitation τ for which the shift is being calculated. In order to determine which terms in $\exp(T)|0>$ contain the excitation $\tau|0>$ and also which terms belong to the interacting space of $\tau|0>$, we divide the excitation operators in T in two groups. The first group, T_τ, contains τ and all excitation operators τ' which only contain spin orbital indices which are also present in τ. The complement of T_τ is denoted by T_τ^c. It contains all other excitation operators. Assuming that all excitation operators mutually commute, we then have:

$$e^T|0>= e^{T_\tau^c} e^{T_\tau}|0> \tag{4.15}$$

The direct term approximation is obtained by projecting the second factor in Eq. (4.15) to $\tau|0>$, after projection by P_b [cf. Eq. (4.14)]. This yields

$$P_b e^T|0> \approx P_b e^{T_\tau^c} \tau|0><0|\tau^\dagger e^{T_\tau}|0> \tag{4.16}$$

Because of the Pauli exclusion principle we have $\tau'\tau|0>= 0$. Therefore, T_τ^c in Eq. (4.15) may be replaced by T. Moreover, since all excitation operators in T_τ^c generate excitations which are orthogonal to $\tau|0>, T_\tau$ in Eq. (4.16) may also be replaced by T. Therefore we have

$$P_b e^T|0> \approx P_b e^T \tau|0><0|\tau^\dagger e^T|0> \tag{4.17}$$

Further we have from Eqs. (4.2), (4.4), and (4.8):

$$<0|\tau^\dagger e^T|0>=<0|\tau^\dagger|\Psi_C> \tag{4.18}$$

By substituting Eqs. (4.17) and (4.18) into Eq. (4.14) we then find:

$$\Delta H_\tau =<0|\tau^\dagger H P_b e^T \tau|0> \tag{4.19}$$

for the diagonal H-matrix element shift. This is equivalent to taking only the first term in Eq. (47) in the evaluation of Eq. (49) of reference [4].

4.2.4 H-matrix element equivalence

In the spin orbital formalism the matrix element between a double and a quadruple excitation is either zero or it is equal to the matrix element between the reference determinant and (another) double excitation [16,

17]. If the quadruple excitation $|Q>$ is doubly excited with respect to the double excitation $|D>=\tau|0>$, we have

$$|Q>=\tau'|D>=\tau'\tau|0> \tag{4.20}$$

and in this case the interaction H-matrix elements are related by:

$$<D|H|Q>=<0|\tau^\dagger H\tau'\tau|0>=<0|H\tau'|0>=<0|H|D'> \tag{4.21}$$

where we have assumed that τ and τ' do not have orbital indices in common. In the CEPA method this relation is used in order to avoid the explicit calculation of matrix elements involving quadruple excitations. In the CEPA (0) variant we use the approximation [9, 10]

$$<D|HT|D>=<0|\tau^\dagger HT\tau|0>\approx<0|HT|0>\text{; for any } \tau \tag{4.22}$$

In the case of a single determinant reference function, the configurations in $P_b\exp(T)\tau|0>$ interacting with $\tau|0>$ consist of the quadruple excitations $T\tau|0>$. Therefore we have

$$<0|\tau^\dagger HP_b e^T\tau|0>=<0|\tau^\dagger HT\tau|0> \tag{4.23}$$

For the diagonal shift we thus have for the single reference CEPA(0) variant:

$$\Delta H_\tau =<0|HT|0> \tag{4.24}$$

For a MC reference set we now consider the analogous relation for the reference configurations $|R>$ and $|S>$:

$$<R|\tau^\dagger HP_b e^T\tau|S>=<R|HT|S> \tag{4.25}$$

Using Eq. (4.25) directly leads again to Eq. (4.24) for the diagonal shift, i.e., we then use Eq. (4.24) with Eq. (4.3). This would be the linearised version of the multireference Coupled Cluster method in its simplest form.

Eq. (4.25) only holds for those terms τ' in T which satisfy the following three conditions:

(i) The corresponding H-matrix element contains only two-electron contributions since in this case the matrix element only depends on the orbital replacements relating the two configurations.

(ii) T and τ have no orbital indices in common.

(iii) $\tau'\tau|0>$ belongs to excitation class (k,l) with $k>2$ or $l>2$.

The first two conditions also apply in the case of a single determinant reference function; the third condition is then automatically satisfied. According to (i), Eq. (4.25) may not be used for the single excitation terms in

T. Because of the Generalized Brillouin theorem [20] the shift contribution $<0|H\tau_{\mu\rho}|0>$ vanishes if the MCSCF values for the reference coefficients c_R are used. These shift contributions may thus be expected to be small. Moreover, the invariance with respect to transformations among the active orbitals can only be preserved by not distinguishing between the single and double excitations. Therefore, no attempts will be made to include corrections to Eq. (4.25) for the single excitation terms. In analogy to the CEPA(0) method the second condition will also be ignored in the present formalism.

Because of these approximations the shifts will only depend on the excitation class of τ. Using condition (iii) and Eqs. (4.7) and (4.25) we then have for any excitation operator $\tau(k,l)$ belonging to the excitation class (k,l) the following shift:

$$\begin{aligned}
\Delta H(k,l) &= <0|\tau^\dagger(k,l)HP_b e^T \tau(k,l)|0> \\
&= <0|\tau^\dagger(k,l)H\sum_{k'l'}\left[e^T\right]_{k'l'}\tau(k,l)|0> \\
&= <0|H\sum_{k'l'}\left[e^T\right]_{k'l'}|0> \qquad (4.26) \\
&= <0|H\sum_{k'l'}P(k',l')|\Psi_C>
\end{aligned}$$

where $k' > 2-k$ or $l' > 2-l$.

The restrictions on k and l follow from the second line of Eq. (4.26) [$k+k' > 2$ or $l+l' > 2$, because of the projection with P_b, cf. Eq. (4.7)]. The result is, that only those excitation classes (k',l') contribute to the shift, that are complementary to (k,l) in the sense that the excitations $\tau(k+k', l+l')$ do not belong to the interacting space of the reference set. This is the essential difference with the single reference determinant result of Eq. (4.24). The reason for excluding the excitations with $k+k' \leq 2$ or $l+l' \leq 2$ is that they are already included in the MRSDCI configuration set, so their interaction matrix element already appears in the CI matrix. This argument only holds exactly if the reference set is complete with respect to the active orbital occupations.

Ignoring condition (ii) implies the introduction of the so-called EPV terms [14]. Further refinements are possible if the EPV terms are considered in more detail. This, however, spoils for example the invariance under transformations within the various orbital subsets. Note that the unsatisfactory behaviour of the CEPA(0) method in cases of near degeneracy will not carry over to the multiconfiguration reference case, provided all configurations which are dominant in the wave function are included in the reference set.

4.2.5 The relation between $\Delta H(k,l)$ and the correlation energy

Equation (4.9) may be used to calculate the energy of Ψ_C. The reference energy is given by

$$E_0 = <0|H|0> \tag{4.27}$$

Using the projection operators of Eq. (4.7), we have

$$E = <0|H|\Psi_C> = E_0 + <0|HP_a|\Psi_C> = \sum_{kl} E(k,l) \tag{4.28}$$

where

$$E(k,l) = <0|HP(k,l)|\Psi_C> \tag{4.29}$$

The shift $\Delta H(k,l)$ may thus be expressed in terms of the correlation energy contributions per excitation class

$$\Delta H(k,l) = \sum_{k'l'} E(k',l')\,;\ k' > 2-k \text{ or } l' > 2-l \tag{4.30}$$

Using Eq. (4.30) in Eq. (4.12) we see that the only difference with the CEPA(0) method is that the shifts depend on the excitation class of the configuration at hand. If our method is applied in the case of a single determinant closed shell reference function with only the double excitations, it is identical to the CEPA(0) method, since then we have only one excitation class, i.e., $k = l = 2$ and thus

$$\Delta H(2,2) = E(2,2) = E - E_0 \tag{4.31}$$

Equation (4.11) then reduces to

$$<0|\tau^\dagger(2,2)(H - E_0)|\Psi_C> = 0 \tag{4.32}$$

and this equation is linear in the coefficients of the double excitations in Ψ_C, as in the CEPA(0) method [11, 12]. However, if we use Eq. (4.26), we have to deal with a nonlinear problem, resulting in a pseudo-eigenvalue problem which has to be solved iteratively. This may be done efficiently by using the Davidson diagonalization method (cf. [21]). The diagonal element shifts then only have the effect of slightly slowing down convergence compared to a normal MRSDCI calculation.

4.2.6 The spin-adapted formalism

The approximations made in the previous section for a wave function based on spin orbitals may equally well be used in a spin adapted formalism, although it is not quite clear whether they will have the same effect. This

is particularly true for the shift contributions of the single excitations if the reference set contains open shell configurations.

The H-matrix element equivalence relation Eq. (4.25) is based on the assumption that the matrix elements do not contain contributions from the one-electron part of H. However, if $|S>$ is singly excited with respect to $|R>$, the Coulomb integral contributions $(\mu\nu/\rho\rho)$ to the left hand side of Eq. (4.25) depend on the orbital indices in τ and therefore Eq. (4.25) does not hold for these terms.

In the spin orbital formalism these terms may be avoided by discarding all single excitation contributions to $E(k,l)$ in Eq. (4.24). For a single configuration reference function this problem is also avoided if SCF orbitals are used, because these orbitals satisfy the Brillouin theorem. In the MC reference case, however, the single excitation contributions may be numerically important because of the relaxation of the reference configuration coefficients in the 2nd order CEPA function with respect to their CASSCF coefficients.

Therefore, treating the single excitations $[(k,l)$ with $k = 1$ or $l = 1]$ in the same way as the other classes introduces an error in the shift, which may be expected to increase with the relaxation of the reference configurations in the MRCEPA calculation. The advantage of this procedure is that the CEPA shifts are easily implemented in a direct MRSDCI program [22], using the spin-adapted formalism. Also the invariance to transformations within the inactive, active, and external orbital sets, respectively, is retained [23].

4.3 Test calculations

MRCEPA is tested for three different test cases. The results are compared with SCF, CASSCF, MRSDCI, Davidson corrected MRSDCI, MRACPF [13] and full CI [24, 25].

The Davidson correction to the MRSDCI [26] uses the following multireference version of this formula [27, 28]:

$$\Delta E = (E_{\mathrm{MRSDCI}} - E_{\mathrm{MCSCF}})(1 - c_0^2)\ ;\ c_0^2 = <\Psi_{\mathrm{MRSDCI}}|\Psi_{\mathrm{MCSCF}}> \quad (4.33)$$

All calculations are done with the GAMESS [29-31] and ATMOL [32, 33] program packages. The Werner and Knowles second order MCSCF program [34] as included in the ATMOL package is used for the CASSCF calculations.

The MRCEPA as derived above assumes that a Complete Active Space, even without space or spin symmetry restrictions, is used as reference configuration set. This requirement does not have to be strictly met. The

Table I. Size consistency tests [energies in hartree, size consistency error ($\Delta = E_{\text{dimer}} - 2E_{\text{monomer}}$) in μhartree].

		monomer	dimer	Δ
He_2	SCF	-2.8616791	-5.7233582	0.0
	MRSDCI	-2.8997195	-5.7988929	546.1
	MRSDCI Dav.	-2.9000040	-5.7999940	14.0
	MRCEPA	-2.9000018	-5.8000035	0.1
O_2	(MC)SCF	-74.8021002	-149.6042003	0.0
	MRSDCI	-74.8570137	-149.7119019	2125.5
	MRSDCI Dav.	-74.8581349	-149.7160232	246.5
	MRCEPA	-74.8581756	-149.7163543	3.1

absence of symmetry restrictions, though, is imperative to obtain size consistency for all possible spin-couplings in, e.g., O_2. In the test calculations on He_2, O_2, H_2O, and BeH_2 consequently no such restrictions were employed. For the H_2O calculations, also results for a C_{2v} restricted CAS reference set are shown to illustrate the rather insensitiveness of MR-CEPA to the actual reference configuration set used. In the calculations on ethylene the reference configurations were all screened on symmetry.

4.3.1 Size consistency of He_2 and O_2

The size consistency of the MRCEPA results is illustrated by calculations on the He dimer using a $<14s,2p/6s,2p>$ basis [35] and on two oxygen atoms using a $<9s,5p/4s,2p>$ double zeta basis [36]. For He the reference wave function was CAS in the Hartree-Fock $1s$ and $2s$ orbitals of each atom. The oxygen atoms were described by single-configuration Hartree-Fock wave functions and the dimers employ the corresponding proper dissociation function. Table I shows the energies of the monomers and of the dimers at large distance and the size consistency errors calculated from these numbers. The singlet and quintet couplings for the oxygen atoms yield identical results.

The results in Table I nicely illustrate that the MRCEPA method yields size consistent results to within the convergence criterion (3×10^{-5}) used. Note that, unlike in CI, the accuracy of the MRCEPA energy is only linear in the accuracy of the CI coefficients.

4.3.2 H_2O

The test calculations involve the cleavage of both OH bonds at a constant angle in the water molecule. Geometry and basis set were chosen according to Gdanitz and Ahlrichs [13]. The 1*s* orbital was frozen on the SCF level, so the MRCEPA results can be compared with full CI results from Bauschlicher and Taylor [25] and MRACPF. Two sets of calculations are reported, featuring different sizes for the active space, that defines the CAS reference space for the MRCEPA and MRACPF calculations. In Table II the CAS space consists of the $3a_1, 4a_1, 1b_1$, and $2b_1$ orbitals. This active space, which is the minimal space required for proper dissociation, yields 12 symmetry allowed CSF's. For the calculations reported in Table III, the active space is extended to the $3a_1, 4a_1, 1b_1, 1b_2, 2b_1$ and $2b_2$ orbitals, yielding a total of 55 symmetry allowed CSF's in the reference space. The equilibrium OH bond length R_{eq} is 1.889 726 bohr, the HOH angle is fixed at 104.5°. The calculations are performed for the three internuclear distances used previously [25]. The calculations employing only the symmetry allowed reference configurations are denoted by a suffix "sym".

The energy difference with full CI is small for all calculations beyond the MCSCF level, though both MRCEPA and MRACPF are an order of magnitude better than straight MRSDCI. The quality of the MRCEPA method seems to follow the quality of the reference wave function, getting better for larger distances and larger reference wave functions. The MRACPF method does not show such regular behaviour.

The symmetry-restricted and complete reference functions yield quite comparable results.

4.3.3 BeH_2

The last comparison with full CI and MRACPF concerns the C_{2v} insertion reaction of H_2 with Be. Geometry and basis set are taken from Bartlett and Laidig [37]. The CAS space in the first set of calculations consists of the $1b_2$ and the $3a_1$ orbitals (cf. [13]) which provides proper dissociation to Be and H_2. Since no allowance is made for the near degeneracy in Be itself, the MRCEPA wave function may be expected to be of rather meagre quality. Therefore, we also performed a calculation correlating the Be-atom better by extending the active space to $\{2a_1, 3a_1, 1b_2, 2b_2\}$. This yields a CAS space of 12 symmetry adapted CSF's. The results for this CAS space are labeled large. The results are given in Table IV.

The comparison shows that in this case the MRCEPA and the normal and the corrected MRSDCI values are less good than the ones of MRACPF [13]. For the large CAS space the MRCEPA is better, but the MRSDCI

Table II. Calculation of H_2O with a 12 CSF reference (see text), expressed as the energy differences with full CI (in mhartree)

geometry	1.0 R_{eq}	1.5 R_{eq}	2.0 R_{eq}
full CI energy (hartree)	-76.256 62	-76.071 41	-75.952 27
MCSCF	161.90	146.62	128.59
MRSDCI	4.81	4.29	3.62
MRSDCI Dav.	-1.61	-1.87	-1.15
MRCEPA	-1.15	-1.10	-0.74
MRACPF	-0.12	-0.22	0.18
$MRSDCI_{sym}$	4.96	4.51	3.75
$MRSDCI\ Dav._{sym}$	-1.43	-1.60	-1.00
$MRCEPA_{sym}$	-0.97	-0.84	-0.59

Table III. Calculation of H_2O with a 55 CSF reference (see text), expressed as the energy differences with full CI (in mhartree)

geometry	1.0 R_{eq}	1.5 R_{eq}	2.0 R_{eq}
full CI energy (hartree)	-76.256 62	-76.071 41	-75.952 27
MCSCF	126.74	118.26	112.39
MRSDCI	2.30	1.72	1.54
MRSDCI Dav.	-1.45	-1.93	-1.75
MRCEPA	-0.85	-0.73	-0.61
MRACPF	-0.40	-0.79	-0.78
$MRSDCI_{sym}$	2.50	2.04	1.79
$MRSDCI\ Dav._{sym}$	-1.21	-1.57	-1.48
$MRCEPA_{sym}$	-0.62	-0.39	-0.34

Table IV. Energy differences with the full CI energy for Be/H_2 (in mhartree). The geometries G1, G2, and G3 are taken from reference [37].

geometry	G1	G2	G3
full CI energy (hartree)	-15.622 88	-15.602 92	-15.624 96
MCSCF	53.31	64.35	66.68
MRSDCI	0.78	1.91	3.05
MRSDCI Dav.	-2.57	-5.02	-4.02
MRCEPA	-1.65	-2.55	-5.88
MRACPF	-0.90	-0.90	-0.53
MR LCCM	-2.62	-2.40	-5.50
MCSCF-large	9.06	15.97	23.66
MRSDCI-large	0.04	0.08	0.18
MRSDCI Dav.-large	-0.11	-0.66	-1.07
MRCEPA-large	-0.06	-0.41	-1.16

itself is even closer to the full CI. This suggests an overcorrection of the unlinked cluster contributions in this case.

4.4 Application to ethylene

4.4.1 Introduction

To investigate the behaviour of the MRCEPA in a practical application, we applied the method to the ground state (N) and the $V^1(\pi,\pi^*)$ state of ethylene in its planar and perpendicular twisted conformation. The resulting potential energy surfaces will be used in a calculation of the UV-absorption spectrum of the system [38]. We performed calculations with different numbers of reference configurations and compared the result with those of the MCSCF and MRSDCI approaches. Ethylene provides an interesting test problem because obtaining a proper description of its $V \leftarrow N$ transition has been a major challenge for many years of theoretical studies.

The first problem encountered is the calculation of the vertical transition energy. Diffuse functions must be included in the basis set to account for the diffuse character of the V state, but at the SCF level this results in a vertical transition energy which is too low, while the state becomes very

diffuse and so the oscillator strength becomes too small [39, 40]. These results can be improved by a SDCI calculation, but several studies have shown that for a good description of the V state a MRSDCI calculation is needed [41-43] . Furthermore, the inclusion of higher-order excitations, e.g. by using the Davidson size consistency correction, does have a significant effect on the calculated vertical transition energy. Recently it was shown by Cave [44] that size inconsistency of CI calculations can also have a significant effect on the calculated molecular properties of the V state of ethylene.

The most important geometry change in ethylene upon excitation to the V state is the relaxation to a 90° twisted conformation, so we included this geometry in our test calculations.

4.4.2 Method

For the calculations on the planar conformation (symmetry D_{2h}) we used the experimental ground state geometry reported by Kuchitsu [45]: R_{CC}= 1.330 Å, R_{CH}=1.076 Å, α_{CCH} = 121.7°. This geometry is also used in other theoretical studies, but it is slightly different from the "standard" geometry of Herzberg [46]: R_{CC}=1.339 Å, R_{CH}=1.086 Å and α_{CCH} = 121.2°. These differences are not relevant in this study, since we will not compare with experimental data. For the twisted conformation these parameters are left unchanged, except for the C-C torsional angle which is put to 89.9°, forcing the symmetry point group to D_2 (a torsional angle of 90° would give a D_{2d} symmetry which is reduced to C_{2v} by our CI program, causing the V state to be of A_1 symmetry).

To define the symmetry labels for the planar conformation we use the following axis assignments: The z axis is taken to be along the C-C bond and the x axis is perpendicular to the plane of the molecule. For the twisted conformation we use the same choice for the z axis. This causes the B_2 and B_3 representation in D_2 to correlate with the twofold degenerate E representation in D_{2d}.

The AO basis set employed is the triple-zeta basis set due to Dunning [47] with a $<5s/3s>$ contraction for hydrogen and a $<10s6p/5s3p>$ contraction for carbon, augmented with polarization functions on the carbon and the hydrogen [48] and a set of diffuse s and p functions (exponent 0.02 bohr^{-2}) on each carbon atom, giving a total number of 72 functions.

For both geometries and both states a series of calculations with different sets of configurations is done. First, we do a CASSCF calculation for four different sets of active orbitals. Those CAS functions constitute the reference space for the subsequent MRSDCI and MRCEPA calcula-

Table V. Summary of the active orbital spaces (CAS), the number of reference configurations (N_{ref}) and the total number of configurations (N_{conf}) for the calculations on the $V\ ^1(\pi,\pi^*)$ state and the ground state (N) of ethylene.

state	method	CAS	N_{ref}	N_{conf} planar	N_{conf} twisted
V	A'	π,π^*	1	22121	38739
	B'	$\pi,\pi^*,2\pi,2\pi^*$	4	78950	129976
	C'	$\pi,\pi^*,\sigma,\sigma^*$	4	83298	146800
	D'	$\pi,\pi^*,2\pi,2\pi^*,\sigma,\sigma^*$	13	294950	507702
N	A	π,π^*	2	19525	34465
	B	$\pi,\pi^*,2\pi,2\pi^*$	6	74142	123468
	C	$\pi,\pi^*,\sigma,\sigma^*$	7	105674	184612
	D	$\pi,\pi^*,2\pi,2\pi^*,\sigma,\sigma^*$	19	310236	533280

tions. So the orbitals entering the MRSDCI and MRCEPA calculations are optimized for each state separately in a CASSCF calculation for the reference configurations. The SCF ground state configuration is, for the planar geometry (D_{2h}),

$$1a_g^2\ 1b_{1u}^2\ 2a_g^2\ 2b_{1u}^2\ 1b_{2u}^2\ 3a_g^2\ 1b_{3g}^2\ 1b_{3u}^2 \tag{4.34}$$

and for the twisted geometry (D_2)

$$2^{-\frac{1}{2}}\ 1a_1^2\ 1b_1^2\ 2a_1^2\ 2b_1^2\ 1b_2^2\ 1b_3^2\ 3a_1^2\ (2b_3^2+2b_2^2) \tag{4.35}$$

The active orbital spaces are summarized in Table V. The smallest set (A) consists of just the $\pi(1b_{3u}/2b_3)$ and $\pi^*(1b_{2g}/2b_2)$ orbitals. Set (B) has an additional pair of orbitals of π and π^* symmetry, while (C) has an additional $\sigma(3a_g/3a_1)$ / $\sigma^*(3b_{1u}/3b_1)$ pair. The largest set (D) has both the additional π/π^* and σ/σ^* orbitals. The number of electrons in the active space is two for (A) and (B) and four for (C) and (D).

In the MRSDCI and MRCEPA calculations all single and double excitations relative to the reference configurations are included, but the two lowest σ orbitals and their complements are kept doubly occupied and unoccupied, respectively. The resulting numbers of configurations are given in Table V.

4.4.3 Results and discussion

The results of all the calculations for the planar and the twisted geometries on the N and the V states with the four different sets of reference configurations are given in Table VI.

First, we will show how the results depend on the choice of the reference set. For this purpose we plot in Figure 1 the energy of the CASSCF, MRSDCI and MRCEPA calculations for method (A), (B), and (C) (see Table V) relative to the energy of the corresponding calculation with the largest number of configurations (D). This is done for both states and both geometries.

The CASSCF and the MRSDCI energies are decreasing as a function of the number of configurations, which is to be expected because of the variational character of these methods. Strictly speaking this argument is not valid for comparing (B) and (C), because (C) does not include all configurations of (B), but it is correct for the series A-B-D and A-C-D.

In contrast, the MRCEPA results are almost independent of the number of configurations, except for the V state of the planar geometry. In this case the MRCEPA calculations based on a reference space which contains only one configuration of the $\pi\pi^\star$ type (A' and C') gives energies which are far lower than any reasonable full CI estimate. These results suggest that increasing the reference space hardly affects the MRCEPA result, as soon as the most important configurations are included in the reference space. So for the description of the V state at the planar geometry, it is essential to include at least two orbitals of $\pi^\star$ symmetry in the reference space. This observation is consistent with the conclusions of several other CI studies [41-43]. The omission of an important reference configuration in a MRCEPA calculation can be identified *a posteriori* by the inspection of the MRCEPA vector: One or more configurations not included in the reference space gain a large coefficient, while the sum of the squares of the coefficients of the reference configurations

$$\tilde{c}_0^2 = \sum_{i \in \mathrm{ref}} c_i^2 \tag{4.36}$$

is much smaller than unity. This was also observed by Bauschlicher *et al.* [49] in MRACPF calculations. It is of course not possible to give rock-solid criteria, but for the aforementioned calculations (A') and (C') we find $\tilde{c}_0^2$ =0.38 and 0.50, respectively, while in all other MRCEPA calculations $\tilde{c}_0^2$ varies between 0.83 and 0.90.

The Davidson corrected values are less dependent on the reference set than the MRSDCI results, if the calculations (A') and (C') for the V state at the planar geometry are discarded, but the results are not as constant

Table VI. (a) The energies for the $V\ ^1(\pi,\pi^*)$ and the ground state (N) of ethylene at the planar geometry (in hartree).

state	method[a]	CASSCF	MRCI	MRCI+Q[b]	MRCEPA
V	A'	-77.788956	-78.048851	-78.072631	-78.105601
	B'	-77.789848	-78.052931	-78.083973	-78.088006
	C'	-77.803410	-78.057360	-78.080918	-78.103483
	D'	-77.819459	-78.061782	-78.089629	-78.090364
N	A	-78.088898	-78.360411	-78.383378	-78.387806
	B	-78.091346	-78.362727	-78.385928	-78.389365
	C	-78.114552	-78.365828	-78.385731	-78.389008
	D	-78.120212	-78.368371	-78.388118	-78.390216

Table VI. (b) *idem* for the twisted geometry.

state	method[a]	CASSCF	MRCI	MRCI+Q[b]	MRCEPA
V	A'	-77.840353	-78.137756	-78.167029	-78.175100
	B'	-77.847814	-78.141044	-78.169999	-78.175682
	C'	-77.861986	-78.144131	-78.171392	-78.175839
	D'	-77.875360	-78.148174	-78.174576	-78.176394
N	A	-77.968708	-78.241862	-78.265962	-78.271938
	B	-77.969383	-78.243034	-78.267464	-78.272423
	C	-77.983954	-78.245970	-78.268852	-78.272646
	D	-77.993097	-78.248223	-78.270489	-78.272600

[a] see Table V
[b] the Davidson corrected MRCI

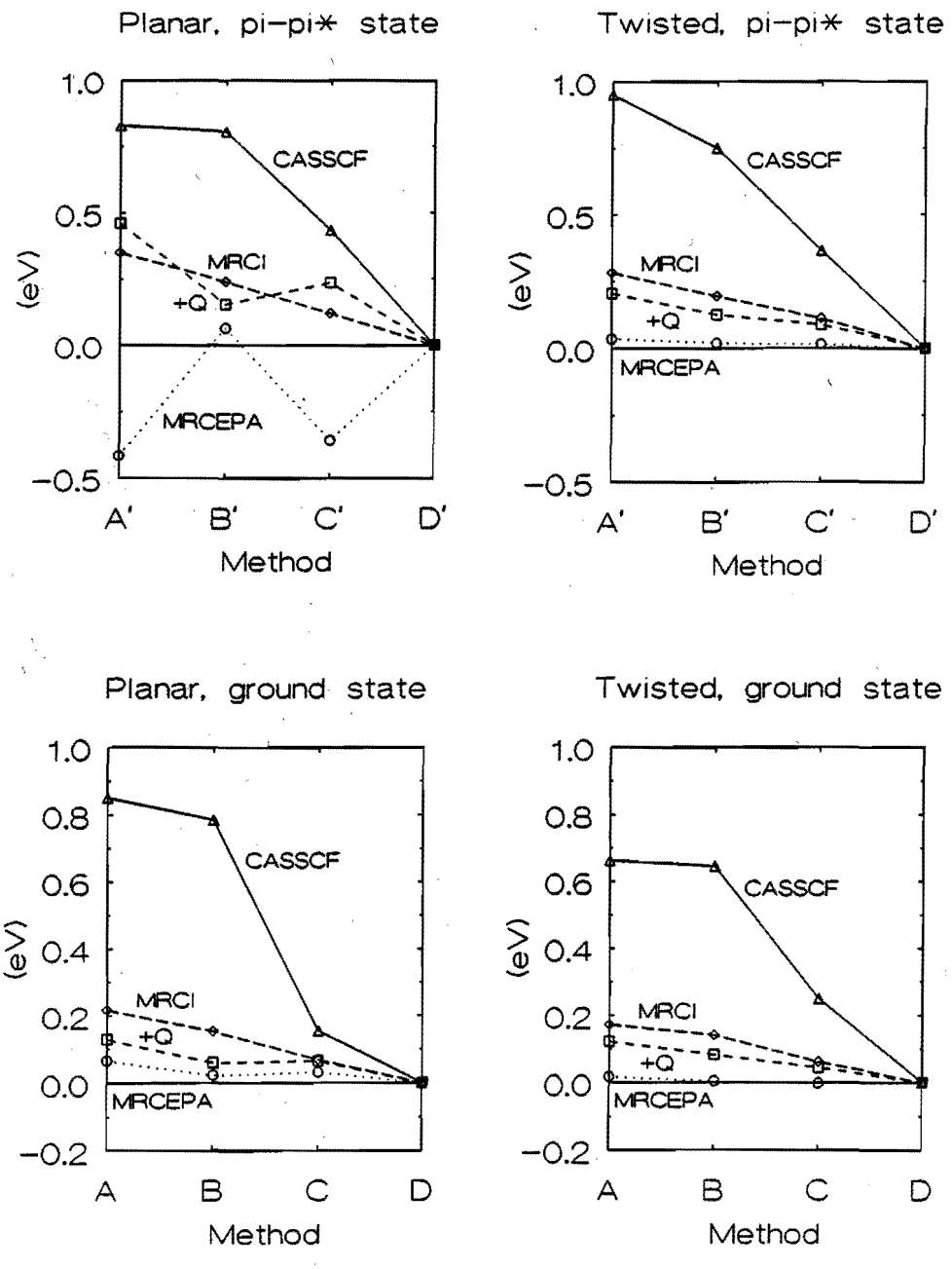

Figure 1. Relative energies calculated for the reference sets of Table V.

as for the MRCEPA. Furthermore, it would have been difficult to discard the results (A') and (C') by inspection of the MRSDCI vector.

Generally one is interested in relative energies, rather than in absolute values, so we extracted from Table VI the vertical transition energies at both geometries (Table VII) and the difference between the energies of the twisted and the planar geometry, i.e., the torsional barriers in both states (Table VIII).

Although we lack full CI data to compare with, we can draw some interesting conclusions from Tables VII and VIII. Considering the vertical transition energy of the planar geometry, we first note that we should discard the MRCEPA results of methods (A') and (C') because of reasons mentioned above. The remaining MRCEPA values (8.20 and 8.16 eV) are respectively 0.23 and 0.18 eV lower than the corresponding MRSDCI values. Comparable size consistency effects on the vertical transition energy of ethylene have been found before. For example, Cave [44] reports the values 8.35 and 8.17 eV for, respectively, a two-reference CI and a quasidegenerate variational perturbation theory (QDVPT) [50, 51] calculation (they use the same geometry but a different basis set). The Davidson corrected results show the same trend but have a larger spread.

For the vertical transition energy at the twisted geometry the favorable behavior of the MRCEPA is evident; it gives almost constant values. For the larger reference spaces the MRSDCI and particularly the Davidson corrected values tend to the same results.

From Table VIII it is clear that the size consistency effects for the torsional barriers are rather small: Both the MRCEPA and the Davidson correction give a lowering of 0-2 kcal/mol, except again for the calculations (A') and (C') for the V state.

4.5 Conclusion

We have given the theory for a multireference CEPA approach. It shows in test calculations to compare well with full CI. The resulting potential curves are seen to converge to the full CI result as the reference configuration set is increased.

We have demonstrated by a series of calculations on the ground and the $V\ ^1(\pi,\pi^*)$ state for the planar and the twisted conformation of ethylene that the MRCEPA energy depends on the set of reference configurations in a very favorable way: If the most important configurations are contained in the CAS-space which constitutes the reference space, a result is obtained which hardly changes upon increasing the reference set. The omission of an important reference configuration can easily be identified by inspection

Table VII. The vertical excitation energies (in eV).

geometry	method	CASSCF	MRCI	MRCI+Q	MRCEPA
planar	A	8.16	8.48	8.46	7.68
	B	8.20	8.43	8.22	8.20
	C	8.47	8.39	8.29	7.77
	D	8.18	8.34	8.12	8.16
twisted	A	3.49	2.83	2.69	2.63
	B	3.31	2.78	2.65	2.63
	C	3.32	2.77	2.65	2.63
	D	3.20	2.72	2.61	2.62

Table VIII. The torsional barriers (in kcal/mol).

state	method	CASSCF	MRCI	MRCI+Q	MRCEPA
V	A'	-32.3	-55.8	-59.2	-43.6
	B'	-36.4	-55.3	-54.0	-55.0
	C'	-36.8	-54.4	-56.8	-45.4
	D'	-35.1	-54.2	-53.3	-54.0
N	A	75.4	74.4	73.7	72.7
	B	76.5	75.1	74.3	73.4
	C	82.0	75.2	73.3	73.0
	D	79.8	75.4	73.8	73.8

of the CEPA vector: The contributions of the reference configurations to the CEPA vector ($\tilde{c}_0^2$) are then far from unity.

The calculation of the torsional barriers and the vertical transition energies in ethylene suggest that the MRCEPA is a promising tool for the calculation of both ground and excited state potential energy surfaces.

Acknowledgments

The Cyber 205 computer time was financed by the Foundation SURF from the National Fund Supercomputers (NFS). We thank the SARA supercomputer advisers for support.

References

[1] W. Meyer, J. Chem. Phys. **58**, 1017 (1975).

[2] V. Staemmler and R. Jaquet, Theoret. Chim. Acta (Berl.) **59**, 487 (1981).

[3] K. Jankowski and J. Paldus, Int. J. Quantum Chem. **18**, 1243 (1980).

[4] W. Kutzelnigg, in *Methods of electronic structure theory, Vol. 3*, edited by H. F. Schaefer III (Plenum Press, New York, 1977).

[5] W. Meyer and P. Rosmus, J. Chem. Phys. **63**, 2356 (1976).

[6] B. Jeziorksi and H. J. Monkhorst, Phys. Rev. A **24**, 1668 (1981).

[7] A. Banerjee and J. Simons, Int. J. Quantum Chem. **19**, 207 (1981).

[8] A. Banerjee and J. Simons, J. Chem. Phys. **76**, 4548 (1982).

[9] K. Tanaka and H. Terashima, Chem. Phys. Lett. **106**, 558 (1984).

[10] H. Baker and M. A. Robb, Mol. Phys. **50**, 1077 (1983).

[11] S. Koch and W. Kutzelnigg, Theoret. Chim. Acta (Berl.) **59**, 387 (1981).

[12] R. Ahlrichs, Comput. Phys. Commun. **17**, 31 (1979).

[13] R. J. Gdanitz and R. Ahlrichs, Chem. Phys. Lett. **143**, 413 (1988).

[14] A. C. Hurley, *Electron Correlation in Small Molecules* (Academic Press, New York, 1976).

[15] H. J. Werner and P. J. Knowles, J. Chem. Phys. **89**, 5803 (1988).

[16] J. Čížek, J. Paldus and L. Sroubková, Int. J. Quantum Chem. **3**, 149 (1969).

[17] J. Paldus, P. E. S. Wormer, F. Visser and A. v. d. Avoird, J. Chem. Phys. **76**, 2458 (1982).

[18] H. P. Kelly and A. M. Sessler, Phys. Rev. **132**, 2091 (1963).

[19] H. P. Kelly, Phys. Rev. **134**, A 1450 (1964).

[20] B. Levy and G. Berthier, Int. J. Quantum Chem. **2**, 307 (1976).

[21] C. Zirz and R. Ahlrichs, in *Proceedings of Daresbury weekend on electron correlation*, edited by M. F. Guest and S. Wilson, Daresbury, 1979.

[22] V. R. Saunders and J. H. v. Lenthe, Mol. Phys. **48**, 923 (1983).

[23] R. Zwaans, *MRCEPA Tests*, Internal Report (Theoretical Chemistry Group, Utrecht, 1988).

[24] G. D. Purvis, R. Shepard, F. B. Brown and R. J. Bartlett, Int. J. Quantum Chem. **23**, 835 (1983).

[25] C. W. Bauschlicher and P. R. Taylor, J. Chem. Phys. **85**, 2779 (1986).

[26] S. R. Langhoff and E. R. Davidson, Int. J. Quantum. Chem. **8**, 61 (1974).

[27] R. Ahlrichs, Private Communication (1985).

[28] J. Verbeek, J. H. v. Lenthe, P. J. J. A. Timmermans, A. Mackor and P. H. M. Budzelaar, J. Organ. Chem. **52**, 2955 (1987).

[29] M. Dupuis, D. Spangler and J. J. Wendoloski, *NRCC Program QG01, GAMESS* (Lawrence Berkeley Laboratory, 1980).

[30] M. F. Guest and J. Kendrick, *GAMESS User Manual* (Daresbury Laboratory, Daresbury, 1986).

[31] M. F. Guest, R. J. Harrison, J. H. v. Lenthe and L. C. H. v. Corler, Theor. Chim. Acta **71**, 117 (1987).

[32] V. R. Saunders and M. F. Guest, *ATMOL3* (1976).

[33] M. F. Guest and V. R. Saunders, Mol. Phys. **28**, 819 (1974).

[34] P. J. Knowles and H. J. Werner, Chem. Phys. Lett. **115**, 259 (1985).

[35] M. Gutowski, J. H. v. Lenthe, J. Verbeek, F. B. v. Duijneveldt and G. Chalasinski, Chem. Phys. Lett. **124**, 370 (1986).

[36] F. B. v. Duijneveldt, *IBM Research Report, RJ 945*, Internal Report (IBM - San Jose, 1971).

[37] W. D. Laidig and R. J. Bartlett, Chem. Phys. Lett. **104**, 424 (1984).

[38] see Chapter 5.

[39] S. Huzinaga, J. Chem. Phys **36**, 453 (1962).

[40] T. H. Dunning Jr., W. J. Hunt, and W. A. Goddard III, Chem. Phys. Lett. **4**, 147 (1969).

[41] L. E. McMurchie and E. R. Davidson, J. Chem. Phys. **66**, 2959 (1977).

[42] B. R. Brooks and H. F. Schaefer III, J. Chem. Phys. **68**, 4839 (1978).

[43] C. Petrongolo, R. J. Buenker, and S. D. Peyerimhoff, J. Chem. Phys. **76**, 3665 (1982).

[44] R. J. Cave, J. Chem. Phys. **92**, 2450 (1990).

[45] K. Kuchitsu, J. Chem. Phys. **44**, 906 (1966).

[46] G. Herzberg, *Electronic Spectra of Polyatomic Molecules* (Van Nostrand, New York, 1966).

[47] T. H. Dunning Jr., J. Chem. Phys. **55**, 716 (1971).

[48] R. Ahlrichs and P. R. Taylor, J. Chim. Phys. **78**, 315 (1981).

[49] C. W. Bauschlicher Jr., S. R. Langhoff, T. J. Lee, and P. R. Taylor, J. Chem. Phys. **90**, 4296 (1989).

[50] R. J. Cave and E. R. Davidson, J. Chem. Phys. **88**, 5770 (1988).

[51] R. J. Cave and E. R. Davidson, J. Chem. Phys. **89**, 6798 (1988).

Chapter 5

Three-dimensional quantum calculations on the ground and excited state vibrations of ethylene

Abstract
Three-dimensional potential energy surfaces of the ground (N), $V\,^1(\pi,\pi^*)$, and $R_y\,^1(\pi,3p_y)$ states of ethylene have been calculated at the MRCEPA level. The modes included are the torsion, the CC stretch, and the symmetric scissors. Full vibrational calculations have been performed using the Lanczos/grid method. The avoided crossing between the V and the R state has been dealt with in a diabatic model. The ground state results agree within 3% up to the highest vibrational level known experimentally. The origin and the maximum of the $V \leftarrow N$ band are calculated at 5.68 and 7.82 eV, respectively, approximately 0.2 eV above the - somewhat ambiguous - experimental values. This work considerably diminishes the existing gap of approximately 0.5 eV between theory [C. Petrongolo, R. J. Buenker, and S. D. Peyerimhoff, J. Chem. Phys. **76**, 3655 (1982)] and experiment.

5.1 Introduction

The vacuum ultraviolet absorption spectrum of ethylene was measured by Stark and Lipp as early as 1913 [1]. Mulliken [2] was the first to attribute the strong and very broad band with a maximum at 7.66 eV to the $V\,^1(\pi,\pi^*) \leftarrow N$ transition. Its vibrational structure consists of a long, somewhat irregular progression of diffuse bands that can not be rotationally resolved [3]. Although the progression was first thought to originate from a large increase of the CC length [3], it is now generally assigned to torsion [4].

The main subject of a series of experimental studies has been the location of the band origin [4-7]. Although the results are far from unambiguous, the isotopic studies suggest a value of approximately 5.4-5.6 eV, a few tenth of an eV below the lowest observed band at 6.0 eV. Of

the numerous *ab initio*/CI studies on ethylene surprisingly few have focussed on the location of the band origin. This is the more surprising since in the most extensive *ab initio*/CI study, of Petrongolo, Buenker, and Peyerimhoff [8] (PBP), it is claimed that the band origin is 6.0 eV, approximately 0.5 eV above what was expected on the basis of the experimental studies. Although part of this difference can be accounted for by the constraints imposed on the geometric parameters in the PBP study, we challenge the accuracy of the calculations that is apparently supposed.

In this study we will employ the recently introduced multireference Coupled Electron Pair Approximation (MRCEPA, see Chapter 4) instead of the "full CI estimate" used by PBP. Three electronic states are involved in the calculations: the ground state (N), the $V\,^1(\pi,\pi^*)$ state, and the $R_y\,^1(\pi,3p_y)$ Rydberg state. For each state a three-dimensional potential energy surface ($3D$ PES) is constructed, based on a series of single point MRCEPA calculations. The three vibrational modes are the torsion (ν_4), the C=C stretch (ν_2) and the symmetric scissors (ν_3). The $3D$ PES's are constructed in the following way: First, a torsional potential curve is calculated with all other coordinates being fixed. Subsequently $2D$ PES's involving the stretching and the scissors mode are calculated for the planar and the perpendicular conformation. Finally the $3D$ PES is formed by interpolation. For these three states and three modes we perform fully quantum mechanical vibrational calculations with our recently introduced Lanczos/grid method [9].

The choice of the coordinates is based on data from the resonance Raman spectrum of ethylene [10]. A resonance Raman spectrum shows ground state vibrational frequencies, just like an off-resonance Raman spectrum, but if the exciting radiation is in resonance with an allowed electronic transition the intensities of those modes are enhanced whose excited state potential curves are significantly different from the corresponding ground state curves. For example, the Raman spectrum in resonance with the $V \leftarrow N$ transition exhibits a very long (ground state) torsional progression, because the V state has a perpendicular conformation while the ground state is planar. Since only two quanta are observed in the scissors progression and six in the stretching progression we choose the PES's to depend harmonically on the scissors-coordinate, while a Morse potential is used for the stretching coordinate. Other transitions that can be observed in the resonance Raman spectrum mainly involve single quanta of wagging modes (ν_7 and ν_{12}) in combination with the torsion mode (ν_4).

In the next section we will give the details of the dynamical methods used. We start with the description of the methods applicable to the ground state. For the electronically excited states a slight extension of the

formalism is necessary because of a nonadiabatic interaction between the V and the R state. An exact description of the Franck-Condon spectrum would require the nonadiabatic coupling functions (see, e.g., [8]). However, at this moment we can not calculate these couplings at the MRCEPA level. Fortunately, in this case a rather well-defined avoided crossing exists between the states and we were able to create a simple diabatic model in which all information needed is extracted directly from the shape of the adiabatic surfaces. This diabatic model is given in Section 5.2.7

Most of the details of the electronic structure calculations are given in the previous chapter. In that study the dependence of the MRCEPA results on the choice of the reference set was investigated for the planar and the perpendicular conformation, and it was found that rather accurate results can be obtained with relative small reference sets: four or six configurations for the V and the ground state, respectively. A complication in this study is the relatively sharply avoided crossing between the V and the R state. It appears that in the avoided crossing region a larger number of reference configurations is needed to get convergence. In the previous study (Chapter 4) full orbital optimization for the MCSCF function consisting of the reference configuration was simple because the states involved were the lowest in energy of a certain symmetry. However, the V and the R state are of the same symmetry for all torsion angles except the planar and perpendicular conformation and the orbital optimization for the upper state causes problems, in particular in the avoided crossing region. This problem had to be solved by using an averaged state calculation with suitable weight coefficients. More details of the electronic structure calculations are given in Section 5.3.

In this study we will arrive at a calculated band origin of 5.68 eV. The calculated torsional levels of the V state compare quite well with experiment and the ground state results are excellent up to the highest measured levels, especially if one takes into account that no scaling whatsoever was employed. These results are discussed in Section 5.4.

5.2 Dynamical methods

5.2.1 Coordinates

The three internal coordinates used in the vibrational calculations are the symmetric scissors angle (α), the C=C stretch (R), and the torsion angle (θ). The C-H distance (R_{CH}) is kept fixed at 1.076 Å. In fact α is the deviation from the experimental ground state equilibrium value $\alpha_1 = 58.3°$ [11] (Figure 1). Since the overall rotation of the molecule

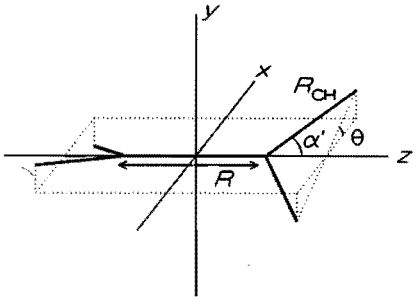

Figure 1. The internal coordinate system.

is not considered we can simply express the cartesian coordinates of the atoms in the internal coordinates:

$$\begin{aligned} x_C &= 0;\ y_C = 0;\ z_C = \frac{1}{2}R \\ x_H &= R_{CH} \sin\alpha' \sin\theta \\ y_H &= R_{CH} \sin\alpha' \cos\theta \\ z_H &= \frac{1}{2}R + R_{CH} \cos\alpha' \end{aligned} \tag{5.1}$$

where

$$\alpha' = \alpha + \alpha_1 \tag{5.2}$$

The cartesian coordinates of all other coordinates are related via the symmetry operations of the D_2 point group. Note that in this coordinate system the periodicity of the torsional potential will be $\pi/2$ so that the perpendicular conformation corresponds to $\theta = \pi/4$.

5.2.2 Potential energy surface

The ground state PES is constructed as follows: For the ground state equilibrium values of $\alpha = 0$ and $R = R_1 = 1.330$ Å a torsional potential is calculated at seven equidistant points and interpolated by a Fourier expansion:

$$V_0(\theta) = \sum_{i=1}^{n_t} c_i \cos 4(i-1)\theta;\ n_t = 7 \tag{5.3}$$

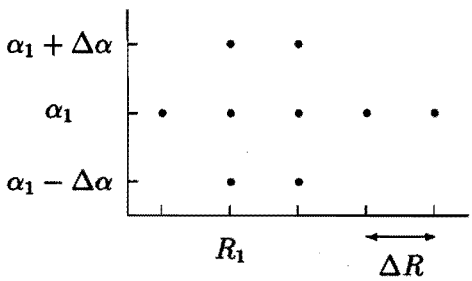

Figure 2. The grid points used to construct the $2D$ PES's.

For the planar and for the perpendicular twisted conformation the R-dependence of the PES is described as a Morse-oscillator:

$$V_i(R) = A_i + D_i(1 - e^{-\beta_i(R-R_i^0)})^2;\ i = p(\text{lanar}),\ t(\text{wisted}) \tag{5.4}$$

The four parameters A_i, D_i, β_i, and R_i^0 are found by a nonlinear least squares fit [12] to five points at $\alpha = 0$ (Figure 2), followed by a shift of the constants A_i such that $V_i(R_1) = 0$. The coupling between θ and R is chosen to be linear in $\cos^2 2\theta$ (or $\cos 4\theta$, cf. Eq. 5.3):

$$V_1(\theta, R) = V_0(\theta) + V_p(R)\cos^2 2\theta + V_t(R)\sin^2 2\theta \tag{5.5}$$

The α-dependence of the $3D$ PES is described as a displaced harmonic oscillator in which the force constant (k) and the displacement ($-f/k$) depend on θ and R:

$$V(\alpha, \theta, R) = V_1(\theta, R) + \frac{1}{2}k(\theta, R)\alpha^2 + f(\theta, R)\alpha \tag{5.6}$$

k and f are again chosen to be linear in $\cos^2 2\theta$:

$$k(\theta, R) = k_p(R)\cos^2 2\theta + k_t(R)\sin^2 2\theta \tag{5.7}$$
$$f(\theta, R) = f_p(R)\cos^2 2\theta + f_t(R)\sin^2 2\theta \tag{5.8}$$

Since we choose the functions $k_i(R)$ and $f_i(R)$ to be linear in R, another eight single point calculations are needed (Figure 2) to finally determine the $3D$ PES.

5.2.3 Representation of ψ

For the Lanczos procedure it is important that the operation of the Hamiltonian on the wave function ($\hat{H}\psi$) is programmed most efficiently. Therefore, we choose a mixed representation of the wave function: The stretching and torsion coordinate are represented on a grid, while a basis set expansion is used for the scissors mode. We will write the vibrational wave function as:

$$\psi(\alpha,\theta,R) = \sum_{i=0}^{n_\alpha} H_i(\alpha)\Psi_i(\theta,R) \tag{5.9}$$

Here $H_i(\alpha)$ are the harmonic oscillator basis functions used to expand the scissors mode:

$$H_i(\alpha) = N_i^{-\frac{1}{2}}\widetilde{H}_i(b\alpha)e^{-\frac{1}{2}(b\alpha)^2} \tag{5.10}$$

In which N_i is the normalisation:

$$N_i = b\pi^{\frac{1}{2}}2^i i! \tag{5.11}$$

and $\widetilde{H}_i$ are the Hermite polynomials [13]. The function $\Psi_i(\theta,R)$ is expanded on a grid (θ_j,R_k) with:

$$\theta_j = j\frac{\pi}{4n_\theta} \quad ; \quad j = 0,\ldots,n_\theta \tag{5.12}$$

$$R_k = R_A + k\frac{R_B - R_A}{n_R} \quad ; \quad k = 0,\ldots,n_R \tag{5.13}$$

The symmetry properties of the electronic states of ethylene at fixed nuclear geometries can be described using the D_{2h}, D_2, and D_{2d} point groups for, respectively, the planar, the twisted, and the perpendicular conformation. However, the internal rotation functions and the total wave function must be described with a permutation-inversion group. This was done by Merer and Watson [14] (MW) using the $G_{16}^{(2)}$ double group. They show that there are four possible single valued representations for the torsional functions (Table I). As explained by MW there is no need to use the double-valued representations and we will not do so. For the ground state the A_{1g}^+ and the B_{1g}^+ levels are nearly degenerate because of the height of the torsional barrier, just like the A_{1u}^- and B_{1u}^- levels. In the resonance Raman spectrum [10] no tunnel splitting is observed in any vibrational level. Furthermore, in the resonance Raman spectrum only transitions involving even quanta of the torsion are allowed, e.g. from the lowest A_{1g}^+ level to the $2n^{\text{th}}A_{1g}^+$ level. The ungerade levels are observed only in combination with the wagging modes not considered in this study.

Table I. The symmetry species of the torsional functions.

$G_{16}^{(2)}$	Torsional basis
A_{1g}^{+}	$\cos(4n)\theta$
A_{1u}^{-}	$\sin(4n+2)\theta$
B_{1g}^{+}	$\cos(4n+2)\theta$
B_{1u}^{-}	$\sin(4n)\theta$

We note that care is needed with the normalisation of these torsional functions. If we take the normalisation on the full 2π range to be unity:

$$\sum_{j=0}^{8n_\theta} |\phi_j|^2 = 1 \tag{5.14}$$

we find that, when exploiting the symmetry, we should use the following normalisation:

$$4|\phi_0|^2 + 8\sum_{j=1}^{n_\theta-1} |\phi_j|^2 + 4|\phi_{n_\theta}|^2 = 1 \tag{5.15}$$

5.2.4 $\hat{H}\psi$

Now that we have given the representation of ψ, we will show how to operate the vibrational Hamiltonian on it. Let

$$\psi' = \hat{H}\psi \tag{5.16}$$

where ψ is given as a set of grid functions $\Psi_j(\theta, R)$ (cf. Eq. 5.9)

$$\psi = \sum_j H_j(\alpha)\Psi_j(\theta, R) \tag{5.17}$$

The problem is to find the set of grid functions $\Psi'_j(\theta, R)$ defining ψ', written in the same form:

$$\psi' = \sum_j H_j(\alpha)\Psi'_j(\theta, R) \tag{5.18}$$

The basic solution is found by taking the scalar product of $H_i(\alpha)$ with the left and the right hand side of Eq. (5.16) and using the orthogonality of

the harmonic oscillator basis functions:

$$\Psi'_i(\theta,R) = \sum_j <H_i(\alpha)|\hat{H}|H_j(\alpha)>_\alpha \Psi_j(\theta,R) \tag{5.19}$$

These expressions are only exact if a complete set of functions $H_i(\alpha)$ is used. We will work with a truncated set and the number of functions actually used will be given in Section 5.4.

The Hamiltonian can be written in the following form:

$$\hat{H} = \sum_t \hat{H}_t = \sum_t \hat{H}_t(\alpha)\hat{H}_t(\theta,R) \tag{5.20}$$

If we substitute this into Eq. (5.19) and we define

$$h^t_{i,j} = <H_i(\alpha)|\hat{H}_t(\alpha)|H_j(\alpha)>_\alpha \tag{5.21}$$

$$\Psi^t_i(\theta,R) = \sum_j h^t_{i,j}\hat{H}_t(\theta,R)\Psi_j(\theta,R) \tag{5.22}$$

we get

$$\Psi'_i(\theta,R) = \sum_t \Psi^t_i(\theta,R) \tag{5.23}$$

So for all the terms of the Hamiltonian we need the matrix elements $h^t_{i,j}$ for the α-dependent part and a procedure to evaluate $\hat{H}_t(\theta,R)\Psi_j(\theta,R)$ for the θ,R-dependent part. First we will deal with the kinetic energy operator $\hat{T}$.

5.2.5 The kinetic energy operator $\hat{T}$

Basically there are two ways to obtain a correct quantum mechanical kinetic energy operator in internal coordinates [15-17]. A straightforward method is to write down the operator in cartesian coordinates and use the chain rule to perform the coordinate transformation [17]. Alternatively one can start with the classical kinetic energy expression and use the Podolsky transformation [16]. These methods are equivalent if no constraints are imposed on the motion. However, since we want to fix the R_{CH} distance we have a constrained motion problem and so we will use the Podolsky transformation method.

Using the coordinates defined in Section 5.2.1 we introduce the vector notation:

$$\begin{aligned} \mathbf{x} &= \{x_1,\ldots,x_4\} = \{z_C, x_H, y_H, z_H\} \\ \mathbf{q} &= \{q_1,\ldots,q_3\} = \{\alpha,\theta,R\} \\ \mathbf{m} &= \{m_1,\ldots,m_4\} = \{2m_C, 4m_H, 4m_H, 4m_H\} \end{aligned} \tag{5.24}$$

The elements of the classical G-matrix (dimension 3×3) are given by:

$$G_{i,j} = \sum_{k=1}^{4} m_k \frac{\partial x_k}{\partial q_i} \frac{\partial x_k}{\partial q_j} \tag{5.25}$$

Note that the G-matrix elements are functions of the internal coordinates α, θ, and R. The kinetic energy operator expressed in internal coordinates given by the Podolsky transformation is (in atomic units, so $\hbar = 1$):

$$\hat{T}' = -\frac{1}{2} \sum_{i,j} g^{-\frac{1}{2}} \frac{\partial}{\partial q_i} g^{\frac{1}{2}} G^{i,j} \frac{\partial}{\partial q_j} \tag{5.26}$$

where g is the determinant of G and $G^{i,j}$ are the matrix elements of the inverse G-matrix. The volume element of the integration is:

$$dx_1 \ldots dx_4 = g^{\frac{1}{2}} \, d\alpha \, d\theta \, dR \tag{5.27}$$

To avoid the $g^{\frac{1}{2}}$ factor in the integration we absorb a factor $g^{\frac{1}{4}}$ into the wave function:

$$\psi''(\alpha, \theta, R) = g^{\frac{1}{4}} \psi'(\alpha, \theta, R) \tag{5.28}$$

So that the normalisation becomes:

$$\iiint |\psi''(\alpha, \theta, R)|^2 \, d\alpha \, d\theta \, dR = 1 \tag{5.29}$$

The kinetic energy operator associated with this normalisation is:

$$\hat{T} = g^{\frac{1}{4}} \hat{T}' g^{-\frac{1}{4}} = -\frac{1}{2} \sum_{i,j} g^{-\frac{1}{4}} \frac{\partial}{\partial q_i} g^{\frac{1}{2}} G^{i,j} \frac{\partial}{\partial q_j} g^{-\frac{1}{4}} \tag{5.30}$$

Working out this expression is a very tedious job, but fortunately it can be done by computer algebra. The REDUCE program [18] listed in Appendix A gives the following result:

$$\begin{aligned} \hat{T} \;=\; & t_{1,1}(\alpha) \frac{\partial^2}{\partial \alpha^2} + t_{2,2}(\alpha) \frac{\partial^2}{\partial \theta^2} + t_{3,3}(\alpha) \frac{\partial^2}{\partial R^2} + \\ & t_{1,3}(\alpha) \frac{\partial^2}{\partial \alpha \partial R} + t_1(\alpha) \frac{\partial}{\partial \alpha} + t_3(\alpha) \frac{\partial}{\partial R} + t_0 \end{aligned} \tag{5.31}$$

where

$$\begin{aligned} t_{1,1}(\alpha) &= -\frac{M}{2 m_\alpha m_{\mathrm{H}} R_{\mathrm{CH}}^2} \\ t_{2,2}(\alpha) &= -\frac{1}{2 m_{\mathrm{H}} R_{\mathrm{CH}}^2 \sin^2 \alpha} \end{aligned}$$

$$
\begin{aligned}
t_{3,3}(\alpha) &= -\frac{2}{m_\alpha} \\
t_{1,3}(\alpha) &= -\frac{2\sin\alpha}{m_\alpha R_{CH}} \\
t_1(\alpha) &= -\frac{M\sin\alpha\cos\alpha}{m_\alpha^2 R_{CH}^2} \\
t_3(\alpha) &= -\frac{(M+m_H\sin^2\alpha)\cos\alpha}{m_\alpha^2 R_{CH}} \\
t_0(\alpha) &= \frac{M[4m_H(m_C-m_H\cos^2\alpha)\sin^4\alpha+(m_H^2-m_C^2)\sin^2\alpha-M^2]}{8m_\alpha^3 m_H R_{CH}^2\sin^2\alpha}
\end{aligned}
\tag{5.32}
$$

and

$$
\begin{aligned}
M &= m_C + m_H \\
m_\alpha &= m_C + m_H\cos^2\alpha
\end{aligned}
\tag{5.33}
$$

The coupling between θ and the other modes occurs only through the factor $t_{2,2}(\alpha)$ in the second term of Eq. (5.31). Terms with only a first derivative of θ do not occur. This can be traced back to the block structure of the G-matrix (Eq. 5.25), which can be understood from simple symmetry considerations.

For the α-dependent parts of this kinetic energy operator we will need the matrix elements (Eq. 5.21). However, the expressions are quite complicated and it will not be possible to evaluate them analytically. What is even worse is that using all of these matrix elements would ruin the sparsity of the Hamiltonian. Therefore, we will use Taylor expansions for the factors $t_{i,j}(\alpha)$ and $t_i(\alpha)$ and truncate them. This should not cause a severe error since the very reason we introduced the harmonic approximation for the scissors-mode is that we do not expect it to be a large amplitude mode.

Utmost care is needed when truncating the Taylor expansions because it might cause the operator to become nonsymmetric (non Hermitian), and even the slightest deviation in the symmetry of the operator is fatal for the Lanczos procedure. The reason for this possibly surprising effect of truncating the Taylor expansions is that although the sum of the terms is symmetric, some of the separate terms are not.

From inspection of Eq. (5.31) we can find combinations of terms that can easily be shown to be symmetric. First note that

$$
\frac{\partial t_{1,1}(\alpha)}{\partial\alpha} = t_1(\alpha) \tag{5.34}
$$

so the first and the fifth term of Eq. (5.31) can be written as:

$$t_{1,1}(\alpha)\frac{\partial^2}{\partial\alpha^2} + t_1(\alpha)\frac{\partial}{\partial\alpha} = \frac{\partial}{\partial\alpha}\left(t_{1,1}(\alpha)\frac{\partial}{\partial\alpha}\right) \tag{5.35}$$

which is evidently symmetric. Furthermore we can verify that

$$\frac{1}{2}\frac{\partial t_{1,3}(\alpha)}{\partial\alpha} = t_3(\alpha) \tag{5.36}$$

so a second symmetric combination is:

$$t_{1,3}(\alpha)\frac{\partial^2}{\partial\alpha\partial R} + \frac{1}{2}\frac{\partial t_{1,3}(\alpha)}{\partial\alpha}\frac{\partial}{\partial R} = \frac{1}{2}\left\{\frac{\partial}{\partial\alpha}\left(t_{1,3}(\alpha)\frac{\partial}{\partial R}\right) + \frac{\partial}{\partial R}\left(t_{1,3}(\alpha)\frac{\partial}{\partial\alpha}\right)\right\} \tag{5.37}$$

If we now introduce the Taylor expansion at $\alpha = 0$:

$$\begin{aligned} t_{i,j}(\alpha) &= t_{i,j}^{(0)} + \alpha t_{i,j}^{(1)} + \ldots \\ t_i(\alpha) &= t_i^{(0)} + \alpha t_i^{(1)} + \ldots \end{aligned} \tag{5.38}$$

and we substitute this into Eq. (5.31) using Eqs. (5.34) and (5.36) we can find the following truncated symmetric kinetic energy operator:

$$\begin{aligned} \hat{T} = \; & \{t_{1,1}^{(0)}\frac{\partial^2}{\partial\alpha^2} + t_{1,1}^{(1)}(\alpha\frac{\partial^2}{\partial\alpha^2} + \frac{\partial}{\partial\alpha}) + t_0^{(0)} + \alpha t_0^{(1)}\} + \\ & \{t_{1,3}^{(0)}\frac{\partial}{\partial\alpha} + t_{1,3}^{(1)}(\alpha\frac{\partial}{\partial\alpha} + \frac{1}{2})\}\frac{\partial}{\partial R} + \\ & \{t_{3,3}^{(0)} + t_{3,3}^{(1)}\alpha\}\frac{\partial^2}{\partial R^2} + \\ & \{t_{2,2}^{(0)} + t_{2,2}^{(1)}\alpha\}\frac{\partial^2}{\partial\theta^2} \end{aligned} \tag{5.39}$$

We could of course use different numbers of terms, but we should always use one more term in the expansion of $t_{1,1}(\alpha)$ and $t_{1,3}(\alpha)$ than for $t_1(\alpha)$ and $t_3(\alpha)$.

5.2.6 Implementation of the Hamiltonian

First we have to add the potential energy and the kinetic energy together. The PES, $V(\alpha, \theta, R)$, consists of three terms that can each be split into an α-and a θ, R-dependent part (Eq. 5.6). The α-matrix elements are given in Appendix B. The operation of $\hat{V}_1(\theta, R)$, $\hat{k}(\theta, R)$, and $\hat{f}(\theta, R)$ on a grid function is simply a pointwise multiplication. For the operation of the $\frac{\partial^2}{\partial R^2}$ operator on the grid functions we use a 10^{th} order finite difference formula

Table II. Possible combinations of the $G_{16}^{(2)}$ symmetry species of the vibrational functions.

ψ_0	ψ_1'	ψ_2'
B_{1g}^+	B_{1u}^-	A_{1g}^+
A_{1g}^+	A_{1u}^-	B_{1g}^+

[9]. For the $\frac{\partial}{\partial R}$ operator we derive a similar symmetric finite difference formula (in the notation of Chapter 3):

$$\frac{\partial}{\partial R}\psi(x)|_{x=x_i} = \sum_{j=1}^{N} c_j(\psi_{i+j} - \psi_{i-j}) + O(\Delta x)^{2N} \tag{5.40}$$

for $N = 5$ we have:

$$\{c_1, \ldots, c_5\} = \left\{\frac{5}{6}, -\frac{5}{21}, \frac{5}{84}, -\frac{5}{504}, \frac{1}{1260}\right\} \tag{5.41}$$

In Appendix C we list a small REDUCE program to generate the coefficients of n-points finite difference formulas for k^{th} order derivatives. For the $\frac{\partial^2}{\partial\theta^2}$ operator we use the Fourier transform trick of Kosloff *et al.* [19] because this is the most efficient procedure for a cyclic coordinate. The symmetry of the torsional functions (Table I) is exploited by using the "quarter wave" Fourier transform C06 NAGLIB procedures [20].

5.2.7 The diabatic model

For the twisted geometry the V and the R state have the same B_1 symmetry of the D_2 point group. As a result an interaction between these diabatic states gives rise to two adiabatic states showing an avoided crossing. However, the permutation-inversion symmetries of the complete electronic V and R states are different (B_{2u}^+ and A_{2g}^-, respectively) and therefore only certain combinations of permutation-inversion symmetries of the vibrational wave functions will interact. Since both nearly degenerate ground state vibrational levels contribute to the spectrum, two sets of symmetries are possible (see Table II).

To describe the interacting V and R states we will have to extend the formalism. We will assume the existence of two diabatic states for which we may neglect the kinetic nonadiabatic coupling terms, although this will

not be possible exactly in general [21, 22]. Such states may be thought of as arising from a unitary transformation of adiabatic states in such a way that the resulting functions are smoothly varying with the nuclear geometry. This unitary transformation, which reduces the kinetic coupling between the states, at the same time introduces a potential coupling since the electronic Hamiltonian was diagonal for the adiabatic states. Our model will be based on estimating this potential coupling function.

First let us consider the torsional mode ($\alpha = 0; R = R_1$). The electronic Hamiltonian is diagonal in the adiabatic basis:

$$<i|\hat{H}^{el}|j>= E_i(\theta)\delta_{i,j} \tag{5.42}$$

Let the matrix elements in the diabatic basis be given by:

$$<i'|\hat{H}^{el}|j'>= V_{i,j}(\theta) \tag{5.43}$$

$|1'>$ and $|2'>$ correspond to, respectively, the R and the V state. Assuming that the diabatic basis is a unitary transform of the adiabatic basis we have for every θ:

$$E_i = \frac{1}{2}(V_{1,1} + V_{2,2}) \pm \frac{1}{2}[(V_{1,1} - V_{2,2})^2 + 4V_{1,2}^2]^{\frac{1}{2}} \; ; \; i = 1, 2 \tag{5.44}$$

From the symmetry species of the diabatic states we can derive the symmetry of the diabatic potential coupling function $V_{1,2}$:

$$\Gamma(V_{1,2}) = \Gamma(|1'>) \times \Gamma(\hat{H}^{el}) \times \Gamma(|2'>) = A_{2g}^- \times A_{1g}^+ \times B_{2u}^+ = B_{1u}^- \tag{5.45}$$

So the simplest expression we can use for this function is (Table I):

$$V_{1,2}(\theta) = h \sin 4\theta \tag{5.46}$$

We can now find h, $V_{1,1}(\theta)$, and $V_{2,2}(\theta)$ by a nonlinear least squares fit [12] to the adiabatic curves $E_1(\theta)$ and $E_2(\theta)$. In the first step we define our adiabatic curves by a cubic spline interpolation [12] to seven calculated MRCEPA points on the interval $0 \ldots \pi/4$, the boundary conditions being that the first derivatives equal zero in the end points (see Figure 5). A cubic spline function is very suitable since the adiabatic curves show a sharp bend in the avoided crossing region. We expect the diabatic curves to be much smoother but we still want to be able to reproduce the adiabatic curves rather close and therefore we introduce an 18-term Fourier expansions for $V_{i,i}(\theta)$. We now have to fit Eq. (5.44) in more than 18 points because we have one additional variable (h). An 18-term Fourier expansion would fit exactly in 18 points and so to avoid oscillatory behavior we

fit Eq. (5.44) in 36 equidistant points. With the diabatic curves we construct the $3D$ diabatic surfaces $V_i(\alpha, \theta, R)$ following the same procedure as for the ground state.

To solve the vibrational problem we use two-component vibrational wave functions [23]. The vibrational Schrödinger equation then becomes:

$$\begin{bmatrix} \hat{T} + \hat{V}_1(\alpha,\theta,R) - E & \hat{V}_{1,2}(\theta) \\ \hat{V}_{1,2}(\theta) & \hat{T} + \hat{V}_2(\alpha,\theta,R) - E \end{bmatrix} \begin{bmatrix} \psi_1'(\alpha,\theta,R) \\ \psi_2'(\alpha,\theta,R) \end{bmatrix} = \begin{bmatrix} 0 \\ 0 \end{bmatrix} \tag{5.47}$$

To solve these equations we only need a slight extension of our ground state Lanczos/grid program. For the diagonal blocks we can use the same procedures and the potential coupling operator $\hat{V}_{1,2}(\theta)$ can be dealt with by a few lines of FORTRAN.

To find the vibrational intensities with the recursive residue generation method [9, 24] the Lanczos procedure has to be started with a ground state vibrational function times the electronic transition dipole function. For the two-component wave function we have:

$$\begin{bmatrix} \psi_1' \\ \psi_2' \end{bmatrix} = \begin{bmatrix} \mu_{0,1}'\psi_0 \\ \mu_{0,2}'\psi_0 \end{bmatrix} \tag{5.48}$$

The ground state vibrational function ψ_0 is found by inverse iteration using the SYMMLQ algorithm [9, 25]. The transition dipole functions for the *adiabatic* states are rather complicated functions of θ. For the *diabatic* states we assume them to be of the simplest form of the given symmetry (neglecting the α- and R-dependence):

$$\begin{aligned} \mu_{0,1}'(\theta) &= 0.4 \sin 4\theta \qquad [A_{1u}^-] \\ \mu_{0,2}'(\theta) &= 1.3 \cos 2\theta \qquad [B_{1g}^+] \end{aligned} \tag{5.49}$$

The coefficients 0.4 and 1.3 are taken from Figure 4 in [8].

5.3 Electronic structure calculations

The electronic structure calculations are done with the GAMESS and ATMOL program packages [26, 27]. The AO basis set employed is of triple-zeta quality with polarization functions on the carbon and the hydrogen and a set of diffuse s and p functions on each carbon atom. Further details on the basis set are given in Chapter 4.

5.3.1 MRCEPA strategy

One way to construct a multi configurational wave function which is suitable for the description of a global PES is to select all configurations that are necessary to get a qualitatively correct wave function at any part of the PES. In such an approach *all* the selected configurations are used, even at geometries where they are less important, in order to get a smooth surface. By contrast our MRCEPA based strategy (see Chapter 4) will be to try and obtain (almost) converged results for each calculated point on the PES separately. The basic idea to achieve this is to choose a set of orbitals, the active space, to optimize these orbitals in a CASSCF calculation for the state required, and to use all the configurations of this CAS function as reference functions in a subsequent MRCEPA calculation. This procedure is to be repeated for a series of increasing active spaces until convergence is reached. If we could only check the convergence by monitoring the energy as a function of the size of the active space this procedure would be fairly cumbersome. However, the *assumption* is that $\tilde{c}_0^2$ [the contribution of the reference configurations to the MRCEPA function, see Chapter 4, Eq. (4.36)] is an indicator of the convergence process. So if we have found a good reference set for some point of the PES, we can use this set for that part of the surface where $\tilde{c}_0^2$ is larger than about 0.8. In some cases certain configurations have a very small contribution to the CASSCF-function and a MCSCF reference function can be used instead, without affecting the MRCEPA result too seriously. Huge savings in computer time can be obtained in this way, at the cost of an additional selection to be made by the user.

Problems can arise when two states of the same symmetry are close in energy, for example in an avoided crossing region. In such a case it can be difficult to fully optimize the orbitals of the upper state in a two state MCSCF calculation and the MRCEPA convergence may slow down. We will show that these problems can be dealt with by an averaged state calculation with suitable weight coefficients.

In order to give a better insight in the application of our computational strategy to ethylene we will shortly describe the nature of the states in the next section.

5.3.2 The N, R, and V state

The four types of orbitals relevant to this study are π, π^*, in plane (i.p.)π, and i.p.π^*. These orbitals are drawn for the planar structure in Figure 3. Only for the planar structure these orbitals correspond to four different irreducible representations (Table III). However, we will find it

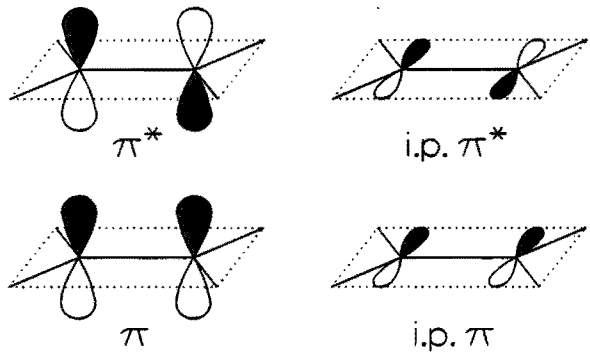

Figure 3. The relevant orbitals.

convenient to use this nomenclature for the other geometries as well, as will be shown below. Starting with the planar structure the three states can be characterizes as π^2 (the ground state, N), $\pi\pi^*(V)$, and $\pi, 2\text{i.p.}\pi(R)$ (Table IV). On the basis of their diffuseness the orbitals can be divided into valence-like (π) and Rydberg-like ($2\text{i.p.}\pi$), while the π^* orbital is somewhere in between. In fact, the exact diffuseness of the V state has been extensively discussed in the literature and the results appear to be very sensitive to the details of the CI treatment [28-30]. At the Hartree-Fock level the diffuseness, calculated as $< x^2 >$, is over 40 a.u. Brooks and Schaefer [29] show that a SDCI calculation hardly changes this value, but that natural orbital iteration results in a much compacter state of about 25 a.u. They also show that a MRSDCI calculation with two or three $\pi\pi^*$ type reference configurations gives a $< x^2 >$ value of about 28 a.u., which decreases by less than 1 a.u. upon natural orbital iteration. Recently Cave [30] has shown that this value is still too high due to the size inconsistency of the 2RSDCI calculation: The quasidegenerate variational perturbation theory (QDVPT) method, which is nearly size consistent, gives a value of 23.3 a.u. for $< x^2 >$. Furthermore, if the number of reference configurations is increased (to 12 and 52) both the MRSDCI and the QDVPT converge to a value of approximately 22 a.u.

We have not calculated $< x^2 >$ values, but if we assume a relation between the correlation energy and the compactness of the wave function we can illustrate the effects by comparing the vertical ($V \leftarrow N$) transition energy, calculated at the MCSCF, MRCI, and MRCEPA level. The ground state, with two electrons in the π orbital, is expected to have the largest correlation energy, and indeed going from MCSCF to MRCI the

Table III. The symmetry species and correlation of the π type orbitals for the planar (D_{2h}), twisted (D_2), and perpendicular (D_{2d}) conformation. The C_{2v} symmetry is used instead of the D_{2d} by the GAMESS and ATMOL program packages.

	D_{2h}	D_2	D_{2d}	C_{2v}
$2\pi^*$	$2b_{2g}$			
2π	$2b_{3u}$	$3b_3$	E	$3b_1/3b_2$
π^*	$1b_{2g}$	$2b_2$		
2i.p.π	$2b_{2u}$	$3b_2$	E	$2b_1/2b_2$
π	$1b_{3u}$	$2b_3$		
i.p.π^*	$2b_{3g}$	$3b_3$	E	$1b_1/1b_2$
i.p.π	$1b_{2u}$	$2b_2$		

Table IV. The electronic state correlation.

	$G_{16}^{(2)}$	D_{2h}	D_2	D_{2d}	C_{2v}	C_{2v}
$R(\pi, \text{i.p.}\pi)$	A_{2g}^-	B_{1g}	$2B_1$	A_2	$2A_2$	$b_1b_2' + b_2b_1'$
$V(\pi, \pi^*)$	B_{2u}^+	B_{1u}	B_1	B_2	$2A_1$	$b_1^2 - b_2^2$
$(\pi^*)^2$	A_{1g}^+	$2A_g$	$2A$	A_1	A_1	$b_1^2 + b_2^2$
$N(\pi)^2$	B_{1g}^+	A_g	A	B_1	A_2	$b_1b_2 + b_2b_1$

($V \leftarrow N$) excitation energy increases by about 0.2 eV and the ($R \leftarrow N$) excitation energy by about 0.4 eV. However, when taking into account the size consistency effects (with the MRCEPA) the correlation energy of the V state increases (the V state becomes more compact), so that the ($V \leftarrow N$) excitation energy decreases by about 0.2eV, while the ($R \leftarrow N$ excitation energy is hardly affected. (This example is taken from Chapter 4, Table VII, method B).

For the twisted geometry the π^* and the i.p.π orbitals are of the same symmetry and so are the V and the R state. However, it is still possible to distinguish between π type MO's consisting of valence p AO's perpendicular on the CH_2 fragments and i.p.π^* type MO's, consisting of Rydberg p AO's in the planes of the CH_2 fragments.

At the perpendicular geometry (of D_{2d} symmetry) the π and the π^* and also the i.p.π and i.p.π^* orbitals become degenerate. In C_{2v} symmetry (as used by the GAMESS and ATMOL program packages instead of D_{2d})

Table V. Convergence checks for the planar geometry. The reference sets actually used are indicated with an arrow. More convergence checks for the N and the V state can be found in Chapter 4. (Energies in hartree).

State	# refs.		CAS orbitals	energy	$\tilde{c}_0^2$
R	1	$\rightarrow$	π, 2i.p.π	-78.0990	0.88
	10		i.p.π^*, π, 2i.p.π, π^*, $2\pi^*$	-78.0985	0.89
V	4	$\rightarrow$	π, π^*, 2π, $2\pi^*$	-78.0880	0.83
	10		i.p.π^*, π, 2i.p.π, π^*, $2\pi^*$	-78.0889	0.85
N	6	$\rightarrow$	π, π^*, 2π, $2\pi^*$	-78.3894	0.90

these degenerate orbitals have one component (b_1) mainly on the first CH_2 fragment and one component (b_2) mainly on the second. The ground state can now be characterized as a diradical A_2 state ($b_1b_2 + b_2b_1$) and the V state as an ionic A_1 state ($b_1^2 - b_2^2$). At this geometry another ionic A_1 state ($b_1^2 + b_2^2$), which correlates with the $(\pi^*)^2$ state, lies just below the V state and is therefore included in Table IV. The Rydberg state has A_2 symmetry, just like the ground state and can be characterized as $b_1b_2' + b_2b_1'$, where the $'$ indicates in plane Rydberg character.

After this introduction about the nature of the states we will be able to describe the reference sets used in the MRCEPA calculations. In the next sections we will give the results of the checks we made to establish convergence.

5.3.3 The planar geometry (D_{2h})

The reference sets used for the N and the V state are CAS sets on the $\pi, \pi^*, 2\pi$, and $2\pi^*$ orbital space with, respectively, six and four configurations (see also Chapter 4, Section 4.4.2, table V, methods B and B'). For the Rydberg state we use the single π, 2i.p.π reference function. At small twisting angles the i.p.π^* and 2i.p.π orbitals appear to play an important role in the description of the V and the R state and so we performed some tests in which these orbitals are included in the active space. Table V shows that the energy differences are less than approximately 0.001 hartree (0.027 eV), which we will consider to be small. Such small deviations are just what we expect because the $\tilde{c}_0^2$ values are greater than about 0.8.

5.3.4 The twisted geometry (D_2)

For the ground state the same CAS reference set is used. For the V and the R state a few complications arise because for this geometry they are of the same symmetry. First of all it appears very troublesome to fully optimize the orbitals of the upper state at the MCSCF level. The reason is that the states are close in energy and optimizing the "upper" state causes it to drop below the "lower" state. This prohibits convergence of the MCSCF calculation. This problem can be avoided by using an averaged state calculation. In most cases it works fine if the upper state gets a weight coefficient of 0.9 or 0.95. However, for $2\theta = 15°$ (note that $2\theta = 90°$ corresponds to the perpendicular conformation) we found that if the upper state is optimized with a weight coefficient of 0.95 (in a 8R calculation, Figure 4), the subsequent MRCEPA calculation does not converge. This problem does not occur if a weight coefficient of 0.5 is employed.

In Table VI we summarize the test calculations for the twisted geometries. First we note that at the MCSCF level the V and R states cross between $2\theta = 30°$ and $2\theta = 45°$, while at the (8R)CEPA level the crossing occurs between $2\theta = 10°$ and $2\theta = 15°$. For small torsion angles ($0° < 2\theta < 30°$) the 4R set is clearly insufficient for the description of the V state: $\tilde{c}_0^2 \approx 0.5$. Inspection of the corresponding MRCEPA vector reveals that the i.p.$\pi^\star$ and one or more (virtual) π^*/i.p.π orbitals must be added to the active space, while the 2π orbital does not seem to be very important. However, adding only a few orbitals to the active space very rapidly increases the size of the CAS based MR-function, while a number of reference configuration obviously get a very small coefficient in both the MCSCF and the MRCEPA function. Therefore, we used the reference sets shown in Figure 4, instead of the CAS references. For $2\theta = 30°$ we tested the effect of adding "unimportant" reference configurations to the set and found that this hardly effects the results indeed (compare the 6R and 12R calculations in Table VI).

The 4R calculations on the R state at $2\theta = 15°$ and $2\theta = 30°$ show that the choice of the weight coefficients has a very small effect for this state. Finally we note that for $\theta > 45°$ the V and R states are well separated, both at the MCSCF and the MRCEPA level and the 4R reference set can be used again.

5.3.5 The perpendicular geometry (D_{2d})

At this geometry no extended reference sets are needed. We already showed in Table IV that in the C_{2v} symmetry the N and R state are both

4R:	$2\pi^*$	−	+	−	+							
	2π	−	−	+	+							
	π^*	+	−	+	−							
	π	+	+	−	−							
6R:	2 i.p.π	−	−	+	−	−	+					
	$2\pi^*$	−	+	−	−	+	−					
	π^*	+	−	−	+	−	−					
	π	+	+	+	ǂ	ǂ	ǂ					
	i.p.π^*	ǂ	ǂ	ǂ	+	+	+					
8R:	2 i.p.π	−	−	−	+	−	−	−	+			
	$3\pi^*$	−	−	+	−	−	−	+	−			
	$2\pi^*$	−	+	−	−	−	+	−	−			
	π^*	+	−	−	−	+	−	−	−			
	π	+	+	+	+	ǂ	ǂ	ǂ	ǂ			
	i.p.π^*	ǂ	ǂ	ǂ	ǂ	+	+	+	+			
12R:	2 i.p.π	−	−	+	−	−	+	−	ǂ	−	ǂ	+	+
	$2\pi^*$	−	+	−	−	+	−	ǂ	−	+	+	−	ǂ
	π^*	+	−	−	+	−	−	+	+	ǂ	−	ǂ	−
	π	+	+	+	ǂ	ǂ	ǂ	−	−	−	−	−	−
	i.p.π^*	ǂ	ǂ	ǂ	+	+	+	+	+	+	+	+	+

Figure 4. The orbital occupancies of the reference sets used in the convergence checks for the twisted geometry (Table VI). Note that the 4R set is the only CAS set. The division between i.p.π and π^* is somewhat arbitrary since these orbitals are of the same symmetry in D_2 (Table III).

Table VI. Convergence checks for the twisted geometries. The column indicated with *weight* gives the weight coefficient and the character of the *upper* state at the MCSCF level. The values actually used are underlined (energies in hartree).

				V		R	
$2\theta(°)$	# refs.[a]	weight		energy	$\tilde{c}_0^2$	energy	$\tilde{c}_0^2$
10	4	0.5	V	-78.1032	0.65	-78.1006	0.88
	6	0.5	V	-78.1152	0.53	<u>-78.1000</u>	0.82
	8	0.5	V	<u>-78.0962</u>	0.83		
15	4	0.0	V			-78.1006	0.90
	4	0.5	V	-78.1186	0.49	-78.1010	0.85
	6	0.5	V	-78.1157	0.64	-78.0998	0.87
	8	0.5	V	<u>-78.1042</u>	0.81	<u>-78.0993</u>	0.87
20	4	0.5	V	-78.1277	0.47	-78.1017	0.88
	6	0.5	V	-78.1184	0.71	<u>-78.0999</u>	0.88
	8	0.5	V	<u>-78.1133</u>	0.78		
30	4	0.0	V			-78.1017	0.89
	4	0.95	V	-78.1402	0.57	-78.1011	0.88
	6	0.95	V	<u>-78.1273</u>	0.81	<u>-78.0991</u>	0.89
	12	0.95	V	-78.1273	0.82	-78.1000	0.88
45	4	0.0	R	<u>-78.1475</u>	0.88		
	4	0.5	R			<u>-78.0969</u>	0.89
60	4	0.0	R	<u>-78.1625</u>	0.88		
	4	0.9	R			<u>-78.0876</u>	0.89
75	4	0.0	R	<u>-78.1723</u>	0.88		
	4	0.9	R			<u>-78.0700</u>	0.89

[a]The reference sets, labeled by the number of reference configurations, are shown in Figure 4.

Table VII. Orbital optimization tests for the perpendicular geometry. All reference sets are $\pi, \pi^\star, 2\pi, 2\pi^\star$ CAS sets. In the C_{2v} calculations all states have a weight coefficient of 0.5 and in the D_2 calculations the states are fully optimized. The C_{2v} calculations are used for the $2D$ PES's at the perpendicular geometry, while the D_2 calculations are used for the torsional potential curves. (Energies in hartree).

State	symmetry	# refs.	energy	$\tilde{c}_0^2$
R	C_{2v}	4	-78.0490	0.74
	D_2	4	-78.0476	0.86
V	C_{2v}	6	-78.1782	0.88
	D_2	4	-78.1757	0.88
N	C_{2v}	4	-78.2740	0.88
	D_2	4	-78.2724	0.88

of A_2 symmetry, while the V state is the second A_1 state. Therefore, we used averaged state calculations with weight coefficients of 0.5. As a check we also performed some calculations in which the orbitals are optimized for the states separately. Since this caused some trouble at the MCSCF level in C_{2v} symmetry, these calculations are done in D_2 symmetry with $2\theta = 89°$. The results are shown in Table VII.

A preliminary conclusion concerning the meaning of the $\tilde{c}_0^2$ values might be that it is a valuable indicator to warn against a missing nearly degenerate configuration in the reference set, but that it can not be used to show whether the orbitals of well separated states have to be optimized.

5.4 Results and discussion

5.4.1 Ground state

Equilibrium properties

In the calculations the C-H distance is kept fixed at the experimental equilibrium value of 1.076 Å [11]. The other geometric parameters, found for the minimum of the PES, correspond quite well with experiment: R_{CC}=1.342 Å (exp.: 1.330 Å) and α_{CCH} = 121.4° (exp.: 121.7°). The lowest vibrational frequencies are calculated both in the harmonic approximation (for the minimum of the PES, with the Wilson GF method [16]) and fully quantum mechanically. The results, together with the ex-

Table VIII. Ground state vibrational frequencies of ethylene (in cm^{-1}) and the deviations from experiment (in %).

	ν_3 (scissors)		ν_2 (stretch)		ν_4 (torsion)	
Harmonic	1393	(+3.6)	1720	(+5.8)	1037	(+1.1)
Full quantum.	1367	(+1.7)	1672	(+2.9)	1002	(-2.3)
Experiment	1344		1625		1026	

perimental data are given in Table VIII.

Torsional barrier

The generally accepted thermal value for the ground state torsional barrier is 65 kcal/mol [31]. For a rigid rotation (R_{CC}=1.330 Å, α_{CCH} = 121.7°) we calculate a barrier of 72.4 kcal/mol. However, if we optimize the structures, the transition state relaxes to R_{CC}=1.463 Å and α_{CCH} = 121.3° and we find a barrier of 64.0 kcal/mol (22 385 cm^{-1}).

Full vibrational calculation

We have calculated all vibrational levels involving the scissors, stretching, and torsional mode that were measured and assigned by Sension *et al.* [10]. Their highest reported level is $(\nu_\alpha, \nu_\theta, \nu_R) = (3, 12, 0)$ at 14 556 cm^{-1}. We choose the grid size, grid constants, and number of basis functions accordingly:

For the stretch coordinate we have: $R_A \ldots R_B$ = 2.0 ... 4.0 bohr and $n_R = 41$ (Eq. 5.13). The range is such that the Morse potential is at least about 20 000 cm^{-1} at the boundaries. The maximal representable kinetic energy on this grid is approximately 34 000 cm^{-1} (the masses are: m_C=12 a.m.u and m_H=1.007 825 a.m.u., 1 a.m.u=1822.887 31 a.u.).

For the scissors mode we take n_α = 15 (Eq. 5.9) and the exponent in the basis functions b=14 $bohr^{-1}$ (Eq. 5.10). Although only two quanta are observed in the scissors progression this number of basis functions is needed because of the strong mixing of the scissors and the stretching mode.

For the torsion mode we take n_θ = 25 (Eq. 5.12) so that the highest representable kinetic energy for the corresponding grid is approximately 50 000 cm^{-1}.

The results are listed in Table IX. The vibrational assignment of the

calculated levels was aided by an artificial isotope effect, for which purpose all levels were recalculated with a 0.2% increased proton mass. The first 184 levels had to be assigned before all levels reported by Sension *et al.* were found. To check the convergence, additional calculations were done: First n_α and n_R were increased to 25 and 61, respectively, and it was found that none of the levels listed in Table IX shifted by more than 1 cm^{-1}. In a second test n_θ was increased from 25 to 40 and all the values reported remained unchanged to less than 0.1 cm^{-1}.

The results of the vibrational calculations can be summarized as follows: Levels involving mainly the stretching and the scissors mode are approximately 2-3% too high compared with experiment, while the torsional levels are 1-2% too low. The errors of all the other levels are somewhere in between.

5.4.2 Excited states

The grids and basis functions used to calculate the vibrational levels of the electronically excited states are identical to those used for the ground state (see above). The most important geometric parameters of the V and the R state are given in Table X. From this table it is clear that vertically the V state is 0.3 eV above the R state, but that upon relaxing the C=C distance, even while keeping the molecule planar, the V state drops below the R state. This causes the conical intersection between these two states. The torsion potential curves are shown in Figure 5. This figure shows the diabatic as well as the adiabatic state. The minimal separation between the adiabatic states is about 0.044 eV (0.0016 hartree) at $2\theta = 12°$.

Franck-Condon spectrum

Approximately 1400 transitions with frequencies from about 45 000 up to about 65 000 cm^{-1} are calculated. The corresponding intensities are found by starting the Lanczos procedure with the lowest ground state vibrational wave function times the transition dipole functions as described in Section 5.2.7 (Eq. 5.48). In Figure 6 the bands are dressed with a Gaussian band width of 50 cm^{-1} and 250^{-1} for the lower and the upper curve, respectively. Experimentally a band width of approximately 250 cm^{-1} is found [32]. The main progression consists of the torsional bands, the other bands being less intense by almost an order of magnitude. The Gaussian line shape is somewhat arbitrary, although it should be mentioned that for a Lorentzian line shape of comparable width the first six or seven bands disappear in the tails of the other bands, while experimentally one expects only a few lines to be undetectable (see below). A Lorentzian line shape

Table IX. The ground state vibrational levels in cm^{-1}.

i	$(\nu_R, \nu_\alpha, \nu_\theta)$	calculated	experiment [10]	deviation (%)
2	(0,1,0)	1 367	1 344	2
3	(1,0,0)	1 672	1 625	3
4	(0,0,1)	2 005	2 046	-2
5	(0,2,0)	2 730	2 658	3
6	(1,1,0)	3 030	2 962	2
7	(2,0,0)	3 334	3 237	3
8	(0,1,1)	3 342	3 373	-1
9	(1,0,1)	3 654	3 660	-0
14	(2,1,0)	4 682	4 565	3
15	(1,1,1)	4 980	4 990	-0
16	(3,0,0)	4 988	4 870	2
17	(2,0,1)	5 294	5 241	1
18	(0,1,2)	5 307	5 395	-2
20	(1,0,2)	5 627	5 676	-1
22	(0,0,3)	5 977	6 087	-2
24	(2,2,0)	6 025	5 905	2
28	(0,2,2)	6 611	6 724	-2
29	(4,0,0)	6 633	6 483	2
31	(1,1,2)	6 925	6 992	-1
34	(2,0,2)	7 249	7 248	0
35	(0,1,3)	7 263	7 405	-2
38	(1,0,3)	7 589	7 678	-1
42	(2,2,1)	7 918	7 890	0
43	(0,0,4)	7 945	8 080	-2
48	(5,0,0)	8 270	8 080	2
51	(0,2,3)	8 543	8 712	-2
61	(0,1,4)	9 211	9 388	-2
73	(0,0,5)	9 899	10 062	-2
74	(6,0,0)	9 900	9 680	2
83	(0,2,4)	10 469	10 676	-2
99	(0,1,5)	11 145	11 353	-2
116	(0,0,6)	11 834	11 997	-1
118	(1,2,4)	12 043	12 313	-2
148	(0,1,6)	13 063	13 277	-2
168	(0,0,7)	13 748	13 937	-1
184	(0,2,6)	14 285	14 556	-2

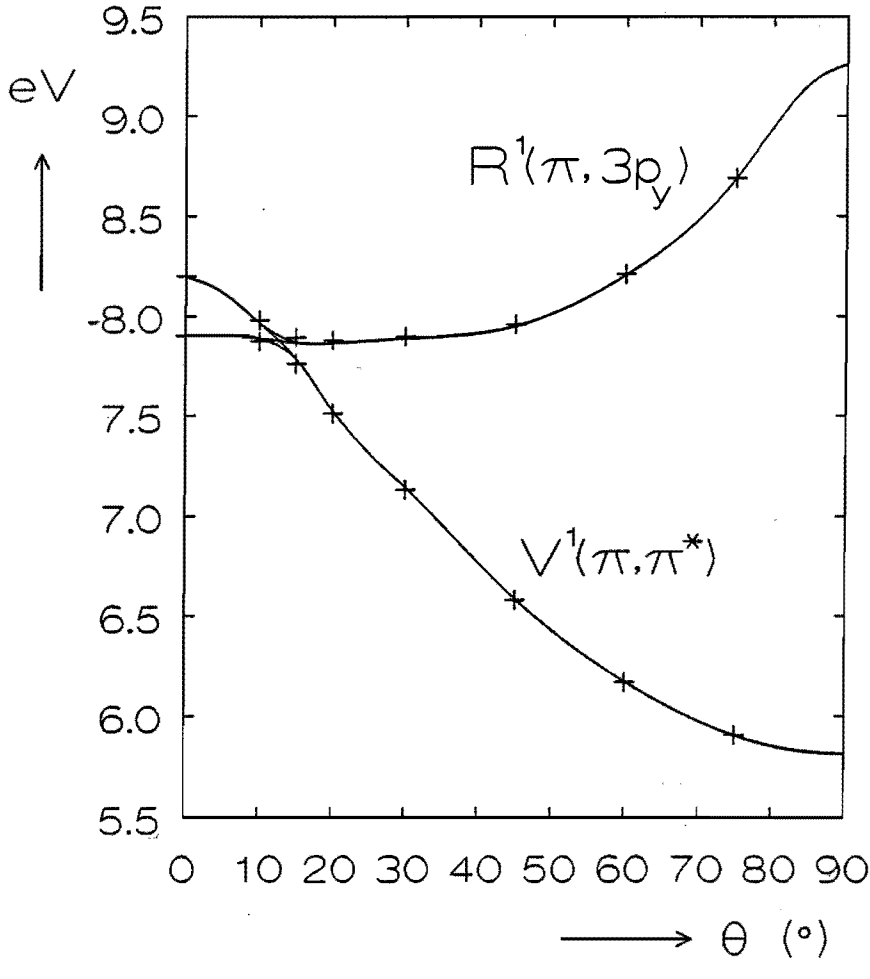

Figure 5. The torsional potential curves for the V and the R state.

Table X. Geometric parameters of the V and the R state. The energy differences with the ground state equilibrium value are given in eV.

	V			R		
	R_{CC} (Å)	α_{CCH}(°)	ΔE	R_{CC} (Å)	α_{CCH}(°)	ΔE
Planar						
vertical	1.330	121.7	8.20	1.330	121.7	7.90
relaxed	1.503	120.0	7.65	1.410	119.8	7.73
Perpendicular						
rigid rotor	1.330	121.7	5.75	1.330	121.7	9.26
relaxed	1.382	123.8	5.64	1.402	120.9	9.15

would have been expected if the line broadening is mainly due to a limited life time of the excited state, so perhaps other vibrational modes or rotational levels must be included to account for the line shape.

The absorption maximum occurs at level 22 (7.82 eV, 63 050 cm^{-1}), 0.16 eV above the experimental value of 7.66 eV [3]. To check the convergence the spectrum was recalculated on the extended grids, as for the ground state, and no deviations were found.

In Table XI we list our calculated torsional levels together with other theoretical [Petrongolo, Buenker, and Peyerimhoff [8] (PBP)] and experimental results [Wilkinson and Mulliken [3] (WM), McDiarmid and Charney [4] (MC), and Foo and Innes [6] (FI)]. The assignments vary considerably between the different studies. Initially WM (1955) incorrectly attributed the progression to the stretching mode (ν_2), so we do not give their original assignment. MC (in 1967) were the first to assign the progression to torsion. On the basis of the isotopic shifts of fully deuterated ethylene they concluded that the band origin should be at 5.79 eV, assuming two undetected bands below the lowest observed band at 5.99 eV (48 331 cm^{-1}). Later (1974) FI also measured the spectra of all partially deuterated isotopomers of ethylene and placed the band origin at 5.43 eV, leaving five bands undetected. In an attempt to experimentally observe the band origin MC measured the spectrum of liquid ethylene in 1977 [7]. Although they found absorptions below 5.79 eV which supported the FI assignment they could not definitely prove it. In 1982 PBP, however, calculated the band origin at 6.00 eV and assumed the previous assignments to be all wrong. The current study places the band origin at 5.68 eV, 0.25 eV above the FI result and 0.32 eV below PBP.

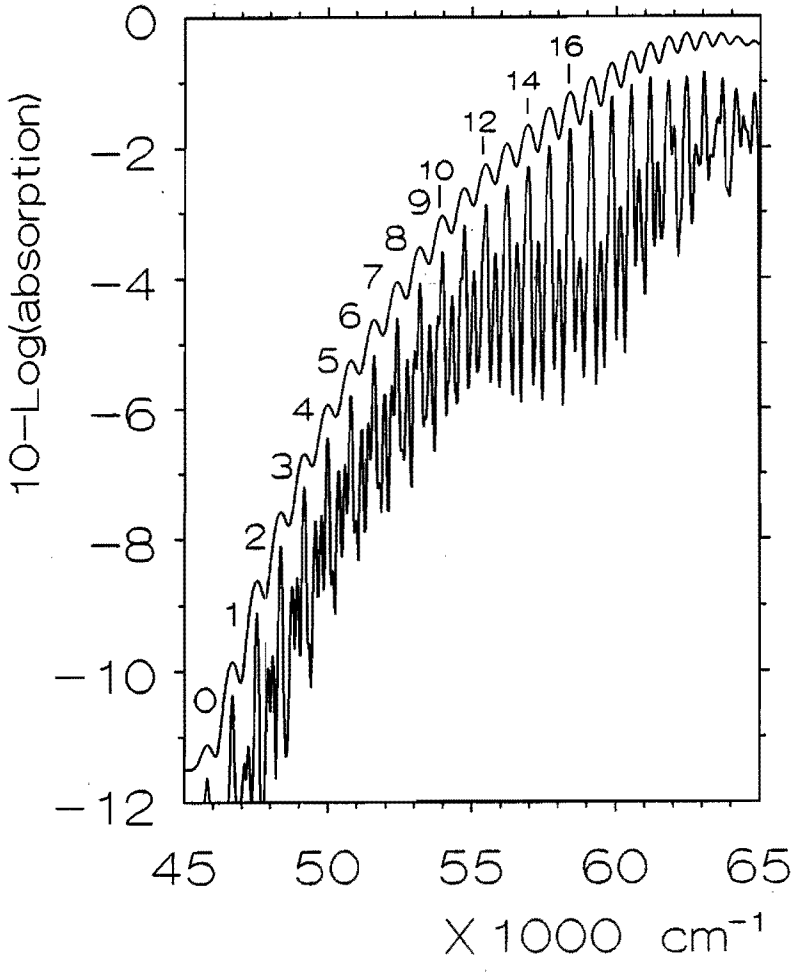

Figure 6. The calculated $V \leftarrow N$ spectrum of ethylene. The lower and upper curve have an artificial Gaussian band width of respectively 50 and 250 cm^{-1}.

Table XI. The torsional levels of the V state of ethylene (in cm^{-1}). PBP is a theoretical study, MC, WM, and FI are experimental studies. The WM assignment is not given since they attributed the progression to the wrong mode.

present work		PBP [8]		MC [4]		WM [3]	FI [6]	
origin	45802	48414		46697			43769	
(eV):	5.68	6.00		5.79			5.43	
0	45802							
1	46665							
2	47520							
3	48354	0	48414	2	48331	48333	(5)	
4	49172	1	49139	3	49148	49140	(6)	
5	49981	2	50021	4	49931	49976	7	49976
6	50789	3	50933	5	50718	50744	8	50758
7	51593	4	51820	6	51579	51602	9	51604
8	52394	5	52675	7	52427	52491	10	52466
9	53186			8	53123	53158	11	53185
10	53966			9	53941	53974	12	53968
11	54731			10	54755	54779	13	54766
12	55482			11	55514	55542	14	55498
13	56226			12	56303	56297		
14	56962							

In order to assess the accuracy of the calculated as well as the experimental data we plot the levels in Figure 7. To show more clearly the differences we subtracted from all the levels the torsional quantum number times the average level spacing and shifted the result by -45941 cm^{-1} (the lowest calculated level). This figure shows that our results compare quite well with experiment, but it also clearly shows the considerable scatter in the experimental data. The model used by FI to derive the band origin from their spectra is the linear anharmonic oscillator (e.g., a Morse-oscillator). For this model to be valid the level spacings should decrease monotonically (giving a parabola in our plot). In an attempt to overcome the limits of a model based on a very simple potential function Siebrand, Zerbetto, and Zgierski [33] (SZZ) very recently worked out a model based on a scaled SCF *ab initio* force field, which also includes the CC stretch and the scissors mode. They were able to fit rather accurately a part of the FI spectrum of deuterated ethylene (the region between 53000 and

56 000 cm^{-1} and they put the band origin at 44 300 cm^{-1} (5.49 eV), which basically agrees with the FI assignment (FI give a band origin of 44 056 cm^{-1} for ethylene-d_4). However the level spacings in the spectrum of ethylene-d_4 are rather irregular too and SZZ conclude that a shift by one or two units in the torsional quantum number is conceivable.

A possible source of error in our calculation is the neglect of nine of the twelve vibrational modes of ethylene; a difference in ground and excited state zero point vibrational frequencies in these modes would affect the band origin. In particular the pyramidalization (the wagging) modes might shift down the band origin [8, 34]. Although the accuracy of the MRCEPA results is the most difficult to assess, we expect on the basis of the convergence test an uncertainty of approximately 0.1 eV. So if we take into account the estimated error ranges for the experimental and current studies we expect the band origin of the $V \leftarrow N$ transition of ethylene to be 5.58±0.1 eV, somewhat below the currently calculated value of 5.68 eV.

Interaction between the V and the R state

In their study on the $V \leftarrow N$ band in an adiabatic basis PBP [8] conclude that the nonadiabatic coupling between the adiabatic state is very important and leads to "a considerable broadening of the overall intensity pattern" near the intensity maximum of the $V \leftarrow N$ band. This suggests that it might be better to use a diabatic basis, which was tried by PBP in a later study [21], but they found that the adiabatic basis gives couplings which are two to four times smaller than in the diabatic basis. To check the importance of the coupling in our diabatic basis we recalculated the Franck-Condon spectrum with the coupling $V_{1,2}(\theta)$ (Eq. 5.47) put to zero. The result was very similar to Figure 6: The upper curve remained almost unchanged (the maximum shifted up by 44 cm^{-1}). Also the main progression of the lower curve (with a band width of 50 cm^{-1}) remained almost unaffected: Only the substructure between the torsional level 21 and 24 slightly weakened. Experimentally their is no evidence for a strong interaction between the V and the R state [10].

5.5 Conclusion

In this study we have tried to diminish the existing gap between theory and experiment for several features of the $V \leftarrow N$ band of ethylene, such as the band origin and the band maximum. For this purpose we used "state of the art" electronic structure and dynamical methods. We

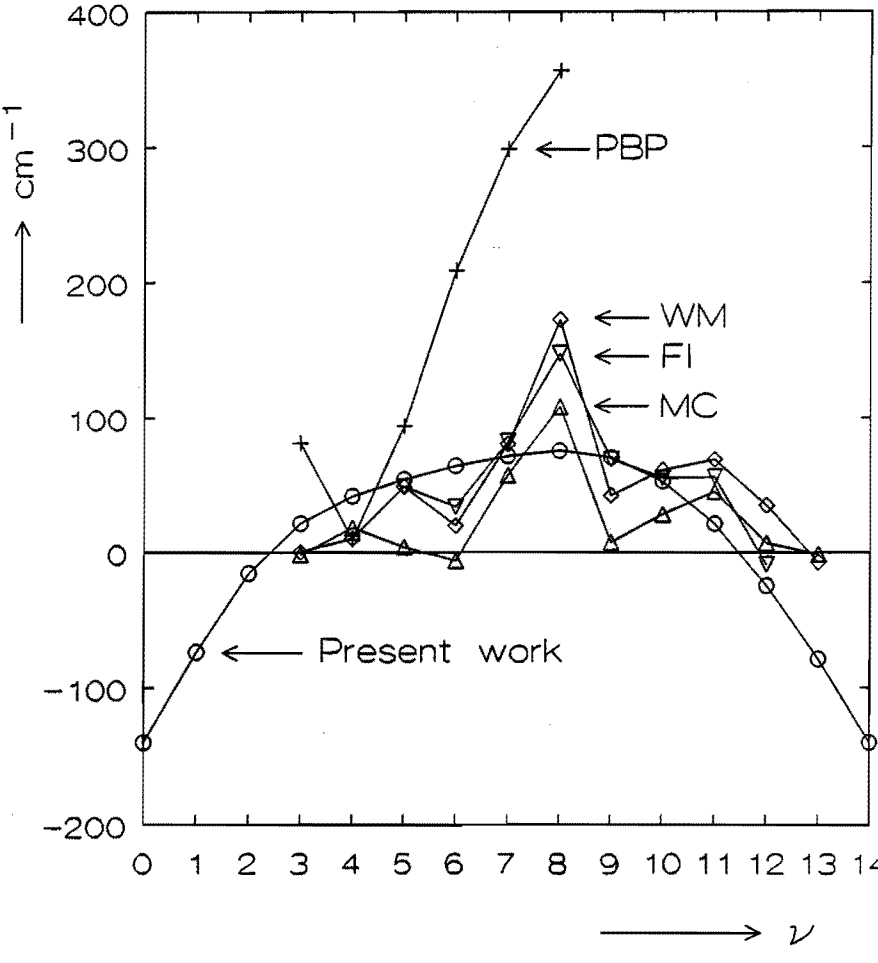

Figure 7. Vibrational levels compared with experiment. The data from Table XI are shifted by $797\nu - 45\,941$.

exploited the feature of the resonance Raman spectrum that it gives a large number of ground state vibrational frequencies for those modes that can be expected to be important for the electronic state in resonance. Mainly as a check of our dynamical method we calculated those ground state vibrational frequencies and found that the errors are only 2-3% and very consistent over the entire available range of experimental data. This suggests that with proper scaling of the PES it must be possible to fit the experimental values very closely, which can be used to identify more bands in the resonance Raman spectrum.

The UV-absorption spectrum is dominated by the torsional progression. We found that transitions involving the scissors and the stretching modes are less intense by an order of magnitude. However, in particular the stretching mode is strongly coupled to the torsion and should be included for a proper description of the V state. We found, in contrast with PBP [21], that the interaction between the V and the R state has only a minor effect on the calculated spectrum.

Comparing our results on the V state with those of PBP [8] shows that we were able to shift the theoretical band origin 0.32 eV in the direction of the experimental result. Approximately 0.11 eV of this difference is accounted for by our geometry optimization of the V state. The remaining part must result from the different treatment of the electron correlation and the basis set (72 functions compared with the 49 in the PBP study).

Although in this chapter we have described probably the most extensive calculations on the $V \leftarrow N$ system of ethylene to date, there are several leads for future work. First of all it might be interesting to calculate the spectra of deuterated ethylene. For ethylene-d_4 the same PES's and implementation of the vibrational Hamiltonian can be used. The partially deuterated ethylenes however give rise to an interesting problem for the dynamical treatment.

Earlier theoretical studies [34] as well as the resonance Raman data [10] suggest that the wagging modes might be relative important in the V state, probably shifting down the band origin. So it might be worthwhile to include this mode, even if it is fully decoupled.

A point which has received little attention in this study is the intensity distribution of the $V \leftarrow N$ band. Here, as well as in other theoretical studies, the intensity ratio between the lowest torsional bands is a few times higher than the experimental value [8, 33]. Furthermore, to our knowledge, the diffuseness of the torsional bands has never been reproduced in a first-principles calculation. Our calculated band maximum is 0.16 eV above the experimental value. Actually the band maximum is hidden under the $R^1(\pi, 3s) \leftarrow N$ transition [35] and the experimental value

is based on the estimated contribution of this transition. So an accurate calculation of this Rydberg state, which should not be too difficult, might be helpful to get a more reliable "experimental" value.

The amount of information on the V state contained in the UV-absorption spectrum is limited because the bands could not be rotationally resolved. However, the resonance Raman spectrum [10] provides a wealth of information on this state. It must be possible to extract detailed geometric information from this spectrum if it is used in combination with accurate (first principles) calculations. Our Lanczos/grid method can be adopted to calculate (resonance) Raman spectra [36]. An effective implementation should exploit the special tricks presented by Moiseyev *et al.* [37].

Finally we note that we took the electronic transition dipole moments from the literature since at present we can not calculate inter state one-electron properties at the MRCEPA level.

Acknowledgment

The Cyber 205 computer time was financed by the Foundation SURF from the National Fund Supercomputers (NFS).

Appendix A: REDUCE program for $\hat{T}$

The listing of the REDUCE [18] program to evaluate the kinetic energy operator (Eq. 5.30) is shown in Figure 8. First, at (1), we tell REDUCE to try hard to divide out the greatest common divisors (on gcd,ezgcd) and we explain REDUCE some basics about goniometric functions. p and n are, respectively, the number of internal and cartesian coordinates. At (2) we introduce the vector notation for the coordinates and the mass (cf. Eq. 5.24). Gi is the inverse of the G-matrix. The definitions at (4) are according to Eq. (5.1). At (5) and (6) the G-matrix is evaluated (Eq. 5.25) and (7) gives the desired kinetic energy expression (Eq. 5.30). However, at this point REDUCE responds with a very depressing and absolutely giant formula. Therefore, we extract at (8) the separate terms that can be greatly simplified by REDUCE and at (9) the terms are printed together with their derivatives [to check Eqs. (5.34) and (5.36]. To make sure no terms were forgotten at (8) we add them together at (10) and compare the result with the initial expression kin.

The memory requirements for this problem were above the capacity of a 640Kb IBM AT, but the IBM 4381 main frame solved the problem

within a minute.

Appendix B: Matrix elements

The matrix elements for the harmonic oscillator basis functions [Eqs. (5.10) and (5.11)]. Let

$$|n>= H_n(\alpha) \tag{5.50}$$

then

$$\begin{aligned}
<m|n> &= \delta_{m,n} \\
<m|\alpha|n> &= [\delta_{m,m+1} + \delta_{m,n-1}]\, 2^{-\frac{1}{2}} b^{-1} \\
<m|\alpha^2|n> &= \Big[\{m(m-1)\}^{\frac{1}{2}}\delta_{m,n+2} + (m+\frac{1}{2})\delta_{m,n} + \\
&\quad \{(m+1)(m+2)\}^{\frac{1}{2}}\delta_{m,n-2}\Big]\, 2^{-1} b^{-2} \\
<m|\frac{\partial}{\partial\alpha}|n> &= -\Big[m^{\frac{1}{2}}\delta_{m,n+1} - (m+1)^{\frac{1}{2}}\delta_{m,n-1}\Big]\, 2^{-\frac{1}{2}} b \\
<m|\frac{\partial^2}{\partial\alpha^2}|n> &= \Big[\{(m(m-1)\}^{\frac{1}{2}}\delta_{m,n+2} + (m+\frac{1}{2})\delta_{m,n} + \\
&\quad \frac{1}{2}\{(m+1)(m+2)\}^{\frac{1}{2}}\delta_{m,n-2}\Big]\, 2^{-1} b^2 \\
<m|\alpha\frac{\partial}{\partial\alpha} + \frac{1}{2}|n> &= -\Big[\{m(m-1)\}^{\frac{1}{2}}\delta_{m,n+2} - \\
&\quad \{(m+1)(m+2)\}^{\frac{1}{2}}\delta_{m,n-2}\Big]\, 2^{-1} \\
<m|\alpha\frac{\partial^2}{\partial\alpha^2} + \frac{\partial}{\partial\alpha}|n> &= \Big[\{m(m-1)(m-2)\}^{\frac{1}{2}}\delta_{m,n+3} \\
&\quad -m(m-1)^{\frac{1}{2}}\delta_{m,n+1} - (m+1)m^{\frac{1}{2}}\delta_{m,n-1} + \\
&\quad \{(m+1)(m+2)(m+3)\}^{\frac{1}{2}}\delta_{m,n-3}\Big]\, 2^{-\frac{3}{2}} b
\end{aligned}$$

Appendix C: REDUCE program for k^{th} derivatives

The following REDUCE [18] program:

```
operator f; let f(0)=1; for all n such that n>0 let f(n)=n*f(n-1);
m:=5; n:=2*m+1; matrix A(n,n),B(n,n);
for i:=1:n do for j:=1:n do A(i,j):=(i-m-1)**(j-1)/f(j-1);
B:=1/A ;end;
```

generates the coefficients $c_j^k = B(k+1, j+m+1)$ that are needed in the symmetric n-points finite difference formula for the k^{th} derivative ($n = 2m+1$):

```
on gcd,ezgcd; for all x let cos(x)**2=1-sin(x)**2;                    % (1)
p:=3; n:=4; array x(n),q(p),m(n); matrix B(n,p),G(p,p),Gi(p,p);      % (2)
q(1):=R; q(2):=alpha; q(3):=theta;
m(1):=mC; m(2):=mH; m(3):=mH; m(4):=mH;
operator Psi; for i:=1:m do depend Psi,q(i);
x(1):=R/2;                                                           % (4)
x(2):=R/2+RCH*cos(alpha);
x(3):=    RCH*sin(alpha)*cos(theta);
x(4):=    RCH*sin(alpha)*sin(theta);

for i:=1:n do for j:=1:m do B(i,j):=df(x(i),q(j));                   % (5)
for i:=1:m do for j:=1:m do G(i,j):=for k:=1:n
                        sum massa(k)*B(k,i)*B(k,j);                  % (6)
Gi:=1/G; d2:=sqrt(det(G)); d4:=1/sqrt(d2);
kin:=-(d4/2)*for i:=1:m sum for j:=1:m
                        sum df(d2*Gi(i,j)*df(d4*Psi,q(j)),q(i));     % (7)

numerator:=num(kin); denominator:=den(kin);                          % (8)
matrix c2(m,m); array c1(m);
for i:=1:m do for j:=1:i do if lterm(numerator,df(Psi,q(i),q(j))) neq 0
          then c2(i,j):=lcof(numerator,df(Psi,q(i),q(j)))/denominator;
for i:=1:m do if lterm(numerator,df(Psi,q(i))) neq 0
          then c1(i):=lcof(numerator,df(Psi,q(i)))/denominator;
if lterm(numerator,Psi) neq 0 then c0:=lcof(numerator,Psi)/denominator;
off exp; for i:=1:m do for j:=1:i do
<< write " term:        ",df(Psi,q(i),q(j));                         % (9)
   write " coefficient: ",c2(i,j);
   write " derivative : ",df(c2(i,j),alpha) >>;
for i:=1:m do << write " term:        ",df(Psi,q(i));
                 write " coefficient: ",c1(i) >>;
on fort;
   write " term:        ",Psi;
   write " coefficient: ",c0;
   write " derivative : ",df(c0,alpha);

on exp; off fort;                                                    % (10)
check:=for i:=1:m sum for j:=1:i sum c2(i,j)*df(Psi,q(i),q(j));
check:=check+c0*Psi+for i:=1:m sum c1(i)*df(Psi,q(i));
if check=kin then write " check OK"  else write " check NOT OK" ;end;
```

Figure 8. Listing of the REDUCE program to evaluate the kinetic energy operator.

$$\frac{\partial^k}{\partial x^k}\psi(x)|_{x=x_i} = \frac{1}{\Delta x^k}\sum_{j=-m}^{m} c_j^k \psi(x_{i+j}) \tag{5.51}$$

The first line of the program defines the factorial function. Note that REDUCE takes $n**0 = 0$, also for $n = 0$. The value of m can be adapted to obtain the desired 2m+1 point formula.

References

[1] J. Stark and P. Lipp, Z. physik. Chem. **86**, 36 (1913).

[2] R. S. Mulliken, Phys. Rev. **41**, 751 (1932).

[3] P. G. Wilkinson and R. S. Mulliken, J. Chem. Phys. **23**, 1895 (1955).

[4] R. McDiarmid and E. Charney, J. Chem. Phys. **47**, 1517 (1967).

[5] R. McDiarmid, J. Chem. Phys. **55**, 4669 (1971).

[6] P. D. Foo and K. K. Innes, J. Chem. Phys. **60**, 4582 (1974).

[7] R. McDiarmid, J. Chem. Phys. **67**, 3835 (1977).

[8] C. Petrongolo, R. J. Buenker, and S. D. Peyerimhoff, J. Chem. Phys., **76**, 3655 (1982).

[9] G. C. Groenenboom and H. M. Buck, J. Chem. Phys. **92**, 4374 (1990).

[10] R. J. Sension and B. S. Hudson, J. Chem. Phys. **90**, 1377 (1989).

[11] K. Kuchitsu, J. Chem. Phys. **44**, 906 (1966).

[12] J. Stoer and R. Burisch, *Introduction to Numerical Analysis* (Springer, New York, 1980).

[13] M. Abramowitz and I. Stegun, *Handbook of Mathematical Functions* (Dover Publications, New York, 1972).

[14] A. J. Merer and J. K. G. Watson, J. Mol. Spectrosc. **47**, 499 (1973).

[15] L. J. Schaad and Jiani Hu, J. Mol. Struct. **185**, 203 (1989).

[16] E. B. Wilson, J. C. Decius, and P. C. Cross, *Molecular Vibrations* (McGraw-Hill, New York, 1955).

[17] N. C. Handy, Mol. Phys. **61**, 207 (1987).

[18] REDUCE Version 3.3 (A. C. Hearn, The Rand Corporation, Santa Monica, California, USA, 1987).

[19] D. Kosloff and R. Kosloff, J. Comput. Phys. **52**, 35 (1983).

[20] *The NAG Fortran Library Manual - Mark 13* (The Numerical Algorithms Group Limited 1988, Oxford, United Kingdom).

[21] C. Petrongolo, R. J. Buenker, and S. D. Peyerimhoff, J. Chem. Phys. **78**, 7284 (1983).

[22] R. Cimiraglia and M. Persico, Mol. Phys. **38**, 1707 (1979).

[23] R. D. Coalson, Adv. Chem. Phys. **73**, 605 (1989).

[24] A. Nauts and R. E. Wyatt, Phys. Rev. Lett. **51**, 2238 (1983).

[25] C. C. Paige and M. A. Saunders, Siam J. Numer. Anal. **12**, 617 (1975).

[26] M. Dupuis, D. Spangler and J. J. Wendoloski, *NRCC Program QG01, GAMESS* (Lawrence Berkeley Laboratory, 1980); M. F. Guest and J. Kendrick, *GAMESS User Manual* (Daresbury Laboratory, Daresbury, 1986); M. F. Guest, F. J. Harrison, J. H. van Lenthe, and L. C. H. van Corler, Theor. Chim. Acta **71**, 117 (1987).

[27] V. R. Saunders and M. F. Guest, *ATMOL3* Part 9, RL-76-106 (1976); M. F. Guest and V. R. Saunders, Mol. Phys. **28**, 819 (1974).

[28] L. E. McMurchie and E. R. Davidson, J. Chem. Phys. **66**, 2959 (1977).

[29] B. R. Brooks and H. F. Schaefer III, J. Chem. Phys. **68**, 4839 (1978).

[30] R. J. Cave, J. Chem. Phys. **92**, 2450 (1990).

[31] J. E. Douglas, B. S. Rabinovitch, and F. S. Looney, J. Chem. Phys. **23**, 315 (1955).

[32] R. McDiarmid, J. Chem. Phys. **50**, 1794 (1969).

[33] W. Siebrand, F. Zerbetto, and M. Z. Zgierski, Chem. Phys. Lett. **174**, 119 (1990).

[34] R. J. Buenker, V. Bonačić-Koutecký, and L. Pogliani, J. Chem. Phys. **73**, 1836 (1980).

[35] A. J. Merer and L. Schoonveld, Can. J. Phys. **47**, 1731 (1969).

[36] see, e.g., A. Anderson, *The Raman effect*, vol. 1 (M. Dekker, New York, 1971). See also references in [10].

[37] N. Moiseyev, R. A. Friesner, and R. E. Wyatt, J. Chem. Phys. **85**, 331 (1986).

Summary

The calculation of the vibrational structure in UV-absorption spectra involves the calculation of ground and excited state potential energy surfaces and the solution of the dynamical problem. This thesis deals with both subjects. Problems are chosen in which the spectra exhibit large-amplitude vibrational motion in an electronically excited state. The rotational structure has been left out of consideration.

The main problem of electronic structure calculations is to assess accurately the electron correlation energy. The multireference Singles and Doubles Configuration Interaction method (MRSDCI) has become a standard tool for the calculation of the electron correlation energy. With the direct CI method and using supercomputers such calculations can routinely involve 10^5 or 10^6 variational parameters. However, the MRSDCI is not size consistent, which means that it becomes progressively worse if the size of the system, i.e., the number of electrons, increases. Therefore, we also employed in this work the Coupled Electron Pair Approximation (CEPA), a size consistent method which is obtained by shifting the diagonal elements of a CI matrix by the estimated interactions between the double and the higher excitations. In a more approximate way, size consistent results can be obtained from a (MR)SDCI calculation by applying for example the Pople correction.

The single reference CEPA is compared with the SDCI and SDCI plus Pople correction in Chapter 2, in an application to the $\tilde{B}\,^1B_u \leftarrow \widetilde{X}$ transition in *trans*-di-imide. The CEPA gives the best results. Furthermore, it is found in that study that the orbitals of the reference configuration should be optimized for a proper single reference description of the $\tilde{B}\,^1B_u$ Rydberg state. Two vibrational modes are involved in these calculations. The semiclassical method of Sorbie is used to obtain the vibrational frequencies and Heller's frozen Gaussian approximation is used to find the intensities.

A much more complicated problem is the calculation of the $V\,^1(\pi,\pi^*) \leftarrow N$ absorption spectrum of ethylene, which is dealt with in Chapter 5. This study involves two nonadiabatically interacting states, the $V\,^1(\pi,\pi^*)$ valence state and the $R\,^1(\pi,3p_y)$ Rydberg state. Three vibrational modes are included; the torsion, the CC stretch and the symmetric scissors. Although the semiclassical methods worked satisfactorily for *trans*-di-imide, it would have been difficult to apply them in this case and therefore the

fully quantum mechanical Lanczos/grid method, developed in Chapter 3, is used. This method is very suitable for one-, two-, or three-dimensional nonseparable vibrational problems, which involve large-amplitude modes.

The calculation of the electronic structure of the V state of ethylene requires a size consistent multireference method and therefore the MRCEPA is used. The MRCEPA is described in Chapter 4, together with some test calculations to check its size consistency and a series of calculations on the ground and V state of ethylene in its planar and perpendicular conformation. It is shown that if the size of the reference space is increased, the MRCEPA tends to converge much faster than the MRSDCI or the Davidson corrected MRSDCI.

In Chapter 5 more convergence checks are done for the MRCEPA, in particular in the avoided crossing region. For the first time it was possible in an *ab initio* calculation to obtain reasonable agreement with experiment for several features of the $V \leftarrow N$ absorption spectrum of ethylene, such as the torsional level spacing, the band origin and the band maximum. Other features of the spectrum such as the intensity distribution and the diffuseness of the torsional bands still demand an explanation.

Samenvatting

Voor de berekening van de vibrationele struktuur in UV-absorptiespectra moeten in de eerste plaats potentiaaloppervlakken berekend worden voor de grondtoestand en de aangeslagen toestanden. Vervolgens moet, uitgaande van deze potentiaaloppervlakken, het dynamische probleem opgelost worden. In dit proefschrift komen beide onderdelen aan de orde. Er zijn problemen gekozen waarbij uit de spectra blijkt dat er in een elektronisch aangeslagen toestand grote-amplitude vibraties voorkomen. De rotatie-struktuur van de spectra is buiten beschouwing gelaten.

Het grootste probleem van de elektronen-struktuur berekeningen is het nauwkeurig bepalen van de elektronen-correlatie energie. Een standaard methode hiervoor is de zogenaamde "multireferentie Configuratie Interactie methode met alle enkele en dubbele excitaties" (MRSDCI). Met de directe-CI methode kunnen, gebruik makend van supercomputers, gemakkelijk MRSDCI berekeningen uitgevoerd worden met 10^5 of 10^6 variationele parameters. Een probleem van de MRSDCI methode is echter dat ze niet "size-consistent" is. Dit betekent dat de methode naar verhouding slechter wordt voor grotere systemen (systemen met meer elektronen). Daarom is er ook gebruik gemaakt van een "size-consistente" methode, de zogenaamde "Coupled Electron Pair Approximation" (CEPA). Bij deze methode wordt, uitgaande van de CI vergelijkingen, een size-consistent resultaat verkregen door de diagonaal elementen van de CI-matrix te corrigeren voor de geschatte interactie-energie tussen de dubbele en de hogere excitaties. Bij benadering size-consistente resultaten kunnen verkregen worden door bijvoorbeeld de Pople-correctie toe te passen op het eindresultaat van een MRSDCI berekening.

In Hoofdstuk 2 wordt de enkele-referentie CEPA vergeleken met de SDCI en de SDCI plus Pople-correctie in een toepassing op de $\tilde{B}\,^1B_u \leftarrow \widetilde{X}$ overgang in *trans*-di-imide. De CEPA methode blijkt het beste resultaat te geven. In dit hoofdstuk wordt verder aangetoond dat voor een goede "enkele-referentie" beschrijving van de $\tilde{B}\,^1B_u$ Rydberg toestand de orbitalen van de referentie configuratie geoptimaliseerd dienen te worden. In de berekeningen worden twee vibratie modes meegenomen. De semiklassieke methode van Sorbie wordt gebruikt voor het verkrijgen van de vibratie-frequenties en Heller's "frozen Gaussian approximation" wordt gebruikt voor de berekening van de intensiteiten.

Een veel moeilijker probleem, dat behandeld wordt in Hoofdstuk 5,

is de berekening van het $V^1(\pi,\pi^\star) \leftarrow N$ absorptiespectrum van etheen. Hierbij spelen twee aangeslagen toestanden een rol die een niet-adiabatische interactie vertonenen, nl. de $V^1(\pi,\pi^\star)$ valentie toestand en de $R^1(\pi,3p_y)$ Rydberg toestand. In deze berekening worden drie vibratiemodes meegenomen; de torsie-, de CC rek- en de symmetrische schaarmode. Hoewel de semi-klassieke methoden goed werkten voor *trans*-diimide, zou het moeilijk geweest zijn om ze in dit geval toe te passen en daarom is hier gebruik gemaakt van de volledig quantummechanische "Lanczos/grid" methode die beschreven wordt in Hoofdstuk 3. Deze methode is erg geschikt voor een-, twee- of drie-dimensionale niet-separabele vibrationele problemen, waarbij grote-amplitude vibraties voorkomen.

Voor de berekening van de elektronenstruktuur van de V toestand van etheen is een size-consistente multi-referentie methode nodig en daarom is er gebruik gemaakt van de MRCEPA methode. Deze methode wordt beschreven in Hoofdstuk 4. In dit hoofdstuk wordt de size-consistentie van de MRCEPA geverifieerd in een aantal test-berekeningen. Verder wordt er een serie berekeningen beschreven aan de grondtoestand en de V toestand, voor de vlakke en de loodrechte conformatie van etheen. Hierbij wordt aangetoond dat het vergroten van de referentie-ruimte bij de MRCEPA veel sneller tot convergentie leidt dan bij de MRSDCI of de Davidson-gecorrigeerde MRSDCI.

In Hoofdstuk 5 worden nog een aantal convergentie testen voor de MRCEPA methode gedaan, in het bijzonder in het gebied van de "avoided crossing". Voor de eerste keer bleek het mogelijk om in een *ab initio* berekening redelijke overeenstemming met het experiment te verkrijgen voor een aantal eigenschappen van het $V \leftarrow N$ absorptiespectrum van etheen, zoals de ligging van de torsie-niveau's en het begin en het maximum van de absorptieband. Andere eigenschappen van het spectrum, zoals de intensiteitsverdeling en de breedte van de torsiebanden vragen nog om een verklaring.

Stellingen

behorende bij het proefschrift

Novel Approaches to the Calculation of the Electronic Structure and Dynamics of Excited States

Application to *Trans*-di-imide and Ethylene

G. C. Groenenboom

1. De opmerking van Hawking dat een planeet op de zon zou storten als de exponent in de gravitatiewet van Newton groter zou zijn dan twee is onjuist. Een planeetbaan is ook stabiel voor alle exponenten tussen twee en drie.

   S. W. Hawking, *A brief history of time*, p. 17 (Bantam, Toronto, 1988).

2. De conclusie van Giroux *et al.* dat de energiebarrière voor een unimoleculaire isomerisatie gewoonlijk lager (en nooit hoger) zal zijn dan de barrière die spectroscopisch bepaald is uit de vibratieniveaus in de normaal-mode die het meest geassocieerd is met de isomerisatie is onjuist.

   L. Giroux, M. H. Back, and R. A. Back, Chem. Phys. Lett. **154**, 610 (1989).

3. Bij de berekening van de grondtoestands-torsie niveaus van etheen gebruikt Wallace een potentiaaloppervlak waarvoor hij zelf heeft aangetoond dat de parametrisering op een vergissing berust.

   R. Wallace, Chem. Phys. Lett. **159**, 35 (1989) en Chem. Phys. **141**, 241 (1990).

4. Voor een goed gelokaliseerde avoided crossing, berekend met het MR-DCI programma van Buenker en Peyerimhoff, zal een schatting van de niet-adiabatische koppeling op basis van de vorm van de potentiaaloppervlakken beter zijn dan de door datzelfde programma berekende waarde.

   P. J. Bruna and S. D. Peyerimhoff, Adv. Chem. Phys. **67**, 1 (1987).

5. In tegenstelling tot de bewering van Killingbeck kunnen de energieniveaus van de "spiked harmonic oscillator" ($H = -\partial^2/\partial r^2 + r^2 + \lambda|r|^{-\alpha}$) wel degelijk variationeel berekend worden met behulp van een harmonische oscillator basisset.

   J. Killingbeck, J. Phys. B. At. Mol. Phys. **15**, 829 (1982).

V. C. Aguilera-Navarro, G. A. Estévez, and R. Guardiola, J. Math. Phys. **31**, 99 (1990).

6. De constructie van de kinetische energie matrix in de Fourier-Grid Hamiltoniaan methode van Marsten en Balint-Kurti kan aanzienlijk versneld worden door op te merken dat het hier een Toeplitz matrix betreft, er hoeft dus slechts één kolom berekend te worden.

   C. C. Marston and G. G. Balint-Kurti, J. Chem. Phys. **91**, 3571 (1989).

7. Werner en Knowles concluderen dat variationele multi-referentie configuratie interactie methoden met interne contractie in de meeste gevallen betere spectroscopische constanten voorspellen dan niet-variationele versies van deze methoden zoals ACPF, QDVPT en LCPMET. Deze conclusie is zorgwekkend, maar waarschijnlijk alleen juist voor berekeningen met grote referentie-sets aan relatief kleine systemen.

   H. J. Werner and P. J. Knowles, Theor. Chim. Acta. **78**, 175 (1990).

8. Heller's formulering van de spectroscopie en misschien ook de term "vertikale excitatie" lijken aanleiding gegeven te hebben tot het wijdverbreide misverstand dat een optische excitatie normaal gesproken aanleiding geeft tot een gelokaliseerd golfpakket in de aangeslagen toestand.

   M. V. Rama Krishna and R. D. Coalson, Chem. Phys. **120**, 327 (1988).

9. Experimenteel blijkt dat de symmetrie van de elektronen-verdeling van de radicaal-anionen van sommige gesubstitueerde difosfine disulfides verbroken wordt voor kleine P-P afstanden, terwijl Hartree-Fock berekeningen hier alleen symmetrische oplossingen lijken te geven. Nader theoretisch onderzoek verdient aanbeveling omdat dit probleem tegengesteld is aan het gebruikelijke symmetrie-verbrekingsprobleem.

   O. M. Aagaard, R. A. J. Janssen, B. F. M. de Waal, J. A. Kanters, A. Schouten, and H. M. Buck, J. Am. Chem. Soc. **112**, 5432 (1990).